

GLIAL SUPPORT OF AXON MAINTENANCE

REQUIRES THE TGF β RECEPTOR *babo*

By

Alexandria Lassetter

A DISSERTATION

Presented to the Neuroscience Graduate Program at the Oregon Health & Science
University, Portland School of Medicine in partial fulfillment of the requirements for the
degree of

DOCTOR OF PHILOSOPHY

CERTIFICATE OF APPROVAL

TABLE OF CONTENTS

CERTIFICATE OF APPROVAL..... ii

TABLE OF CONTENTS..... iii

LIST OF MAIN FIGURES..... vii

LIST OF ABBREVIATIONS..... ix

ACKNOWLEDGEMENTS..... xi

ABSTRACT..... xiv

CHAPTER I:..... 1

INTRODUCTION I..... 2

 Introduction 1.1 – Nervous system architecture 2

 Introduction 1.2 – Neurodegeneration 3

 Introduction 1.3 – Wallerian degeneration 5

 Introduction 1.4 – Axon maintenance..... 8

 Introduction 1.5 – Axon metabolism 10

 Introduction 1.6 – Glial ensheathment of axons in *Drosophila*..... 11

 Introduction 1.7 – Glial support of axons 12

 Introduction 1.8 – Identifying glial genes required for axon maintenance..... 13

 Introduction 1.9 – TGF β signaling in glia 14

 Introduction 1.10 – TGF β signaling beyond development..... 15

 Introduction 1.11 – Dissertation overview..... 16

MATERIALS & METHODS I.....	17
Fly husbandry.....	17
Sensitized RNAi screen	18
Aging assay.....	18
Adult-specific knockdown.....	19
Imaging acutely dissected L1 nerves	19
Quantification of axon degeneration.....	20
Immunofluorescence.....	20
Quantification of iATPsnFR and roGFP in glia	21
Electron microscopy	21
Statistical analysis.....	23
RESULTS I.....	24
Results 1.1 – Ablating wrapping glia causes neurodegeneration	24
Results 1.2 – The role of wrapping glia in axon maintenance.....	28
Results 1.3 – Identifying glial genes required for axon maintenance.....	30
Results 1.4 – Disrupting TGF β superfamily genes in glia results in degeneration of sensitized axons	31
Results 1.5 – TGF β activity in glia is required for long-term axon maintenance.....	32
Results 1.6 – <i>babo</i> is required in mature wrapping glia in the wing	37

Results 1.7 – Disruption of TGF β signaling in glia does not alter axonal ensheathment.....	43
Results 1.8 – Inhibiting Wallerian degeneration rescues age-dependent neurodegeneration caused by glial-knockdown of <i>babo</i>	48
Results 1.9 – Genetic blockade of caspase-mediated cell death rescues neurodegeneration caused by <i>babo</i> knockdown in glia.	51
Results 1.10 – Disrupting glial TGF β activity alters metabolic function of glia.....	53
DISCUSSION I.....	57
Discussion 1.1 – Glial TGF β activity is required for neuron maintenance	57
Discussion 1.2 – Glial ensheathment is critical to long-term axon maintenance	57
Discussion 1.3 – Disruption to glial TGF β does not impair glial ensheathment	58
Discussion 1.4 – Babo and Smox act in mature glia to promote axon maintenance	60
Discussion 1.5 – Babo in glia supports neuron maintenance by directly supporting axons	61
Discussion 1.6 – Blocking caspase activity rescues degeneration caused by loss of <i>babo</i>	64
Discussion 1.7 – Protection of axons by Wld ^S <i>in vivo</i> requires glia.....	65
Discussion 1.8 – Glial metabolism and axon maintenance.....	65
CONCLUSION I	68
CHAPTER II:.....	69
INTRODUCTION II.....	70

Introduction 2.1 – Using the L1 nerve in the wing to study axon degeneration.....	70
Introduction 2.2 – L1 nerve development.....	71
Introduction 2.3 – Glia in the L1 nerve.....	71
Introduction 2.4 – Injury timing and peripheral glia response.....	72
METHODS II.....	73
RESULTS AND DISCUSSION II	79
Results 2.1 – Characterization of the L1 wing nerve makeup	79
Results 2.2 – Axon development with age.....	82
Results 2.3 – Ultrastructural response after injury.....	83
APPENDIX I: Sensitized axon maintenance screen results	87
KEY RESOURCE TABLE.....	136
Fly stocks:	136
Genotypes corresponding to main figures:	136
Antibodies:	140
REFERENCES:	141

LIST OF MAIN FIGURES

<i>Figure 1</i> Peripheral sensory nerve in the <i>Drosophila</i> L1 wing vein.....	24
<i>Figure 2</i> <i>WG split-Gal4</i> expression in the adult wing	25
<i>Figure 3</i> Neurodegeneration in uninjured wings	26
<i>Figure 4</i> Ablating wrapping glia results in neurodegeneration in the peripheral nerve of the wing with age	27
<i>Figure 5</i> <i>Wld^S</i> protects axon after axotomy except when animals lack <i>WG</i>	29
<i>Figure 6</i> Screening for novel regulators of glia support of axons <i>in vivo</i>	30
<i>Figure 7</i> Glial-specific knockdown of <i>TGFβ</i> and <i>BMP</i> pathway components causes axon degeneration in the sensory nerve of the wing.....	32
<i>Figure 8</i> Glial-specific knockdown of <i>TGFβ</i> superfamily members results in age-dependent neurodegeneration in the sensory nerve in the adult wing	34
<i>Figure 9</i> Inhibition of glial <i>TGF</i> signaling results in degeneration of aged neurons	36
<i>Figure 10</i> <i>babo</i> reporter expression in larval peripheral nerves.....	38
<i>Figure 11</i> <i>babo</i> reporter expression in the adult wing L1 nerve.....	40
<i>Figure 12</i> Expression of <i>babo</i> in mature neurons in the wing.....	42
<i>Figure 13</i> Increased number of <i>WG</i> nuclei when <i>TGFβ</i> activity is disrupted.	43
<i>Figure 14</i> Caspase inhibition phenocopies <i>babo</i> knockdown for increased <i>WG</i> numbers but not decreased neuron survival.....	45
<i>Figure 15</i> Glia appear morphologically intact in animals where <i>TGFβ</i> activity is inhibited in glia	46
<i>Figure 16</i> Glial ensheathment of axons appears intact when <i>TGFβ</i> activity is disrupted in glial.	48

<i>Figure 17</i> Wld ^S overexpression in neurons rescues neurodegeneration in <i>babo</i> knockdown animals	50
<i>Figure 18</i> P35 rescues neurodegeneration caused by loss of <i>babo</i> in glia	52
<i>Figure 19</i> Higher levels of ATP present in WG in conditions affecting TGF β activity, mitochondrial, and metabolite transport regulation.	54
<i>Figure 20</i> Mitochondria redox state is altered by disruption to TGF β activity in glia.....	56
<i>Figure 21</i> Diagrams for embedding <i>Drosophila</i> wings in resin.	76
<i>Figure 22</i> Ultrastructure of the <i>Drosophila</i> L1 nerve.....	81
<i>Figure 23</i> Axon caliber growth in the adult wing L1 nerve	83
<i>Figure 24</i> Glial response to injury	86

LIST OF ABBREVIATIONS

- ❖ AD – Alzheimer’s disease
- ❖ ALS – Amyotrophic lateral sclerosis
- ❖ ATP – Adenosine triphosphate
- ❖ *axed* – axundead
- ❖ *babo* – baboon
- ❖ BMP – *bone morphogenic protein*
- ❖ *Bsg* -- *Basigin*
- ❖ CB – cell body
- ❖ *cnc* – *cap-n-collar*
- ❖ *Cox10* – Cytochrome c oxidase assembly factor 10
- ❖ DN – dominant negative
- ❖ dpa – days post axotomy
- ❖ dpe – days post eclosion
- ❖ *Gal80^{ts}* – temperature sensitive Gal80
- ❖ GFP – green fluorescent protein
- ❖ MAPK – mitogen-activated protein kinase
- ❖ NAD⁺ – nicotinamide adenine dinucleotide
- ❖ *NGF* – *neuron growth factor*
- ❖ NMNAT – nicotinamide mononucleotide adenylyltransferase
- ❖ *Nrf2* – *nuclear factory erythroid 2*
- ❖ PD – Parkinson’s disease
- ❖ pmn – progressive motorneuropathy

- ❖ PNS – peripheral nervous system
- ❖ PGC-1 α – peroxisome proliferator-activated receptor gamma co-activator 1 alpha
- ❖ QUAS – Q upstream activating sequence
- ❖ RNAi – ribonucleic acid interference
- ❖ ROI – region of interest
- ❖ SC – Schwann cell
- ❖ *Smox* – *Smad on X*
- ❖ *srl* – *spargle*
- ❖ tdTomato – tandem dimer Tomato
- ❖ TFEB – transcription factor EB
- ❖ TGF β – Transformation growth factor beta
- ❖ UAS – upstream activating sequence
- ❖ WD – Wallerian degeneration
- ❖ WG – Wrapping glia
- ❖ wL3 – wandering 3rd instar larva
- ❖ *Wld^S* – *Wallerian degeneration slow*
- ❖ WT – wildtype

ACKNOWLEDGEMENTS

First and foremost, I would like to acknowledge my supervisor and mentor, Dr. Marc Freeman without whom none of this work would have been possible. Since my very first meeting with Marc, I knew that working in the Freeman lab would be an exciting adventure. His enthusiasm for all the projects in the lab is genuine and has made dealing with the inevitable frustrations that come along with science much more bearable. I appreciate his guidance not only when it comes to designing and interpreting experiments, but also in my professional development. Whether it be writing, presenting, or networking, Marc has always put in the time and effort to support me in achieving my goals. One of the most valuable lessons that Marc has had to repeatedly remind me is to not lose sight of the forest through the trees. It is easy to get lost in the minutia of individual experiments, but the true work of a scientist is to step back and make sense of the collection of data in front of them. This is invaluable advice that I will carry with me in my career. I cannot thank Marc enough for his superb mentorship and I will strive to do the same for my trainees in the future.

Every single member of the Freeman lab has helped me on numerous occasions throughout my time in the lab. I could not have asked for a better group of colleagues to work alongside these past several years. The investment in each other and the shared excitement for new discoveries has made the lab a truly collaborative environment to grow as a scientist. Senior research associates, Amy Sheehan and Romina Barria, put in countless hours towards the screen and I cannot thank them enough for their time and energy. In addition to her work on the screen, I would also like to thank Amy for keeping the lab running smoothly, we are all lucky to have such a wonderful lab manager. Jennifer Beck has been amazing at keeping

the lab organized even though I am sure sometimes it feels like herding cats. I want to thank her for all her help over the years with scheduling, grant submission, and coordinating travel among many other things. Dr. Tobi Stork and Dr. Yunsik Kang have generously shared their expertise with me, and it has been instrumental to the development of my project. My fellow grad students both in the Freeman lab and across the NGP have been wonderful colleagues to tackle graduate school with.

I am incredibly grateful to have had the opportunity to work with Dr. Megan Corty. She has been an extraordinary mentor throughout my time at the Vollum and I have learned so much from her, techniques and otherwise. Together with Jo Hill, they taught me the intricate techniques for transmission electron microscopy and much of this work was supported in part by Dr. Sue Aicher through a P30 grant. I would also like to thank Robert Kayton, Lisa Dirling Vecchiarelli, and Andrea Calhoun for their assistance with the electron microscope.

My advisory committee has provided expert guidance throughout my graduate career. Drs. Kelly Monk, Ben Emery, and Kevin Wright have all been incredibly supportive and enthusiastic about my work. I looked forward to every committee meeting, knowing I would come away with great ideas for where to take my project next. I am so thankful to have had such a remarkable committee to help me grow as a scientist.

I would not have made it to—let alone through—graduate school if it were not for my supportive family and friends. They have always encouraged me to work for my goals, even when it meant moving to another state and not getting to see them as much as we all would have liked. Additionally, I would like to thank Lisa for her support during graduate

school. The continued encouragement from my family and friends has sustained me throughout this journey.

Finally, I want to acknowledge my partner Grant who has been tremendously supportive from day one and uprooted his life to join me in Portland and will be doing so again to go with me to Philadelphia. His unconditional support for me pursuing my passion for science has made navigating graduate school and beyond possible and he has been there for me through all of the highs and lows along the way. I look forward to our next adventure together in Philadelphia.

ABSTRACT

Axons can represent the majority of a neuron's volume and are energetically demanding. Specialized glia ensheath axons to insulate them and are believed to support axon function and maintenance throughout life. The morphology of axon-associated glia is complex and requires massive growth during development. Glial cells must search for and identify the proper axonal targets, sort them from other axons, and ultimately fully ensheath them. Despite their importance, little is known about how glia ensheath axons, what glia do to support neurons, and even less is known about how those functions are regulated throughout the life of an organism. Understanding the mechanisms involved in coordinating this complex process is critical as improper ensheathment can impede the ability of glia to support axons. Human diseases such as multiple sclerosis (MS) or Charcot-Marie-Tooth disease (CMT) are characterized by loss of glia that ensheath axons resulting in functional impairment and progressive degeneration of neurons. In this dissertation I sought to provide new insights into how glia support neurons and in doing so, identified several genes encoding secreted and transmembrane proteins that are required in glia for long-term axon survival *in vivo*. I show that key components of the TGF β superfamily are required cell-autonomously in glia for peripheral nerve maintenance, although their loss does not grossly disrupt glial morphology. I observed age-dependent neurodegeneration in the absence of glial TGF β signaling that was rescued by genetic blockade of Wallerian degeneration. This work identifies the TGF β signaling pathway as a necessary component of glial homeostasis that promotes axon survival and suppresses neurodegeneration.

CHAPTER I:

Glial support of axons in the *Drosophila* peripheral nervous system

In this chapter, I discuss the bulk of my dissertation work examining glial support of axons *in vivo*. Nicky Fox generated the transgenic lines used for the screening assay. Romina Barria and Amy Sheehan conducted much of the visual screening of the collection of RNAi lines for phenotypes of axon disruption. Dr. Megan Corty and Jo Hill provided indispensable guidance and assisted in acquiring electron micrographs from the L1 wing nerve used to evaluate axon ensheathment. I completed all other experiments.

The following data is in revision for publication:

Glial TGF β signaling promotes neuronal survival in peripheral nerves

Alexandria P. Lassetter, Megan M. Corty, Romina Barria, Amy E. Sheehan, Jo Q. Hill,
Sue A. Aicher, A. Nicole Fox and Marc R. Freeman

INTRODUCTION I

Introduction 1.1 – Nervous system architecture

The nervous system is made up of many cell types but by far the most famous of these are neurons. Neurons are a unique class of cells that are highly polarized and come in a variety of complex morphologies. The basic makeup of a neuron includes a dendrite that receives information, the soma that houses the nucleus and many organelles, and an axon that transmits information from the cell body to its target. Both dendrites and axons can be highly complex and connect to multiple synaptic partners. The soma integrates information from multiple synaptic inputs and depending on the timing and polarity of these signals will increase or decrease its own activity on its downstream targets. The transfer of information at the synapse is accomplished by release of neurotransmitters from the axon terminal that activate receptors on the opposing target's membrane.

In addition to neurons, there are a variety of glial cell types that are present throughout the central and peripheral nervous system (CNS, PNS). Just as there are many flavors of neurons, there are multiple types of glial cells that serve distinct functions throughout the nervous system. In the CNS there are astrocytes that have many functions including roles in blood-brain barrier maintenance. Microglia are resident macrophages of the CNS that monitor for pathogens and clear debris following injury or excess synapses during development. Oligodendrocyte precursor cells (OPC) as their name suggests, give rise to oligodendrocytes which form myelin sheathes around axons in the CNS (Allen & Barres, 2009). In the PNS there are two types of Schwann cells (SC) that ensheath the axons that make up nerves: myelinating SCs and non-myelinating Remak SCs (Harty & Monk, 2017; Jessen & Mirsky, 2005). Remak SCs ensheath bundles of small caliber axons and insulate

them from one another whereas each myelinating SC forms a single multi-lamellar myelin sheath around an axon (Harty & Monk, 2017; Jessen & Mirsky, 2005). In between adjacent myelin sheaths is a node of Ranvier where voltage-gated ion channels are concentrated to propagate action potentials down the axon (Black et al., 1990). The insulation provided by myelin allows for this saltatory conduction to accelerate action potential propagation along the axon.

In addition to neurons and glia, the brain is highly vascularized to maintain a constant stream for nutrients and oxygen necessary for its function. The vasculature is made up of endothelial and smooth muscle cells that form the dense arterial and capillary network that shuttle oxygenated blood throughout the brain (Dyrna et al., 2013). Also found along the vasculature are pericytes that wrap their processes around capillaries. Since capillaries lack smooth muscle, pericytes are required to constrict capillaries (Peppiatt et al., 2006). Neuronal activity can be detected by astrocytes that then release vasodilators triggering dilation of blood vessels to divert blood flow to areas of high activity (Attwell et al., 2010; Mishra et al., 2016). Many different cell types are required to maintain the nervous system and disruption to any of them can disrupt neurodevelopment or leave the nervous system susceptible to neurodegenerative disease.

Introduction 1.2– Neurodegeneration

Neurodegeneration is a broad term used to describe loss or damage to the cells that make up the nervous system. This most commonly refers to loss of neurons, but this can be accompanied by loss of glial cells. Several human diseases are characterized by loss or

disruption to the glial cells that ensheath axons both in the CNS and PNS. It has recently been estimated that nearly 1 million Americans are living with multiple sclerosis (MS) (Wallin et al., 2019) a chronic disease resulting from loss of oligodendrocytes in the CNS. Loss of myelin in regions of the brain leads to impaired axonal function and ultimately axons and whole neurons degenerate. Like in MS, when myelinating SCs are lost in the PNS, axon function is impaired and eventually causes degeneration of axons leading to peripheral neuropathies such as Charco-Marie-Tooth disease (CMT)(Brennan et al., 2015). The similarity in disease progression between these families of diseases is suggestive of a role for axon-associated glia in promoting survival of the axon. However, it is notable that glial cell loss does not occur in a vacuum and can be accompanied by inflammation which itself can be damaging to tissue (Compston & Coles, 2008; Niu et al., 2019; Obermeier et al., 2013). For example, in MS microglia and astrocytes respond to the areas of demyelination, releasing inflammatory cytokines and clearing debris (Alvarez et al., 2011; Liddelow et al., 2017). In addition, break down in the blood-brain barrier can occur, allowing peripheral immune cells to enter the brain and exacerbate inflammation (Alvarez et al., 2011). Thus, untangling the role of glial cell loss along an axon from damaging inflammation remains a challenge in understanding the primary cause of the neurodegeneration that follows in demyelinating diseases.

Demyelinating diseases, like MS and CMT, are one category of neurodegenerative disease, however, there are many causes of neurodegeneration that are characterized by different hallmarks. For example, in Alzheimer's Disease (AD) and Parkinson's Disease (PD), aggregation of misfolded or mutated proteins are pervasive and are thought to be toxic to neurons (Baba et al., 1998; Kordower et al., 2008; Li et al., 2008; Toledo et al., 2016).

Other hallmarks common to many neurodegenerative diseases include defects in axon transport (Baldwin et al., 2016; Edgar et al., 2004; Koch et al., 2015; Prior et al., 2017; Sorbara et al., 2014; Young & Crish, 2014) and mitochondrial dysregulation (Baloh, 2008; Dutta et al., 2006; Fernyhough et al., 2010; Niemann et al., 2006; Rocha et al., 2018). Nearly all neurodegenerative diseases in humans are accompanied by changes in glia. In the CNS, astrocytes and microglia dramatically change their morphology and expression profiles in the diseased brain (Colonna & Butovsky, 2017; Liddelw et al., 2017; Prinz et al., 2017). Disentangling the beneficial changes that occur in glia in this context from the detrimental ones, however, proves challenging to study. Examples of beneficial changes include debris clearance of damaged or dying neurons, while detrimental changes include release of inflammatory cytokines (Colonna & Butovsky, 2017; Liddelw et al., 2017; Prinz et al., 2017). It is clear that damage to the nervous system, whether it be disease related or caused by an insult, triggers a cascade of adaptations in both neurons and glia and understanding how these changes influence neurodegeneration is key to improving treatment strategies.

Introduction 1.3 – Wallerian degeneration

Wallerian degeneration describes the process of axon destruction following an insult (Waller, 1850). Augustus Waller, credited for his detailed description of the phenomenon, compared the segmentation of the axon to beads of a necklace (Waller, 1850). Taking advantage of this distinct phenotype, he mapped out nerves by injuring them and following the “beads” to their target (Waller, 1850, 1852). Once thought to be a passive wasting process, is now understood to instead involve a cell-autonomous

molecular signaling cascade within the degenerating axon that actively breaks down the disconnected appendage (Coleman & Freeman, 2010; Coleman & Höke, 2020; Lunn et al., 1989; Osterloh et al., 2012). The serendipitous discovery of the *Wallerian degeneration slow* (*Wld^S*) mutant mouse, whose axons had a significantly protracted degeneration time after injury, was the first indication that Wallerian degeneration was a genetically controlled process (Lunn et al., 1989). This mutant consisted of a coding sequence for a gain of function chimeric protein composed of a portion of a ubiquitin ligase fused to nicotinamide mononucleotide adenylyltransferase (NMNAT)(Coleman et al., 1998; Conforti et al., 2000). Work from our lab established that the NMNAT fragment of *Wld^S* was essential to the protective effects following injury (Avery et al., 2009). Depletion of NAD^+ levels in the axon is a major, albeit not exclusive, contributor in the process of Wallerian degeneration. NMNAT is a relatively short-lived protein in the axon that generates NAD^+ and following injury NMNAT is degraded, and NAD^+ levels drop (Di Stefano et al., 2014). Supplying NMNAT to the axon provides some protection but not to the extent that *Wld^S* does suggesting that NAD^+ levels alone do not necessarily dictate axon destruction (Araki et al., 2004; Avery et al., 2009; Conforti et al., 2007; Sasaki et al., 2009; Wang et al., 2005).

A genetic screen in *Drosophila* in our lab identified an endogenous gene, *Sarm*, that was required for Wallerian degeneration to occur following axotomy (Osterloh et al., 2012). The discovery of *Sarm* and its cell-autonomous role in regulating Wallerian degeneration in *Drosophila* and mice, provided direct evidence for an endogenous signaling mechanism that is required to induce axon destruction following injury. Since, many groups have studied the function of *Sarm* and looked for additional regulators of

Wallerian degeneration. *Sarm* was also found to have endogenous NAD⁺ hydrolase activity when activated, allowing it to further drive down levels of NAD⁺ within the axon (Essuman et al., 2017; Gerdts et al., 2015; Sambashivan & Freeman, 2021). Another screen identified *Drosophila Axed*, encoding a BTB domain-containing protein, that was demonstrated to act genetically downstream of *Sarm* in *Drosophila* (Neukomm et al., 2017). Both *Sarm* and *Axed* mutants have robust protection from injury induced Wallerian degeneration. In addition, there are several other factors that have been shown to participate in Wallerian degeneration, albeit to varying degrees, such as *Highwire* and mitogen-activated protein kinase (MAPK) signaling (Xiong et al., 2012; Yang et al., 2015).

Wallerian degeneration is present in several different neurodegenerative diseases and neurologic injuries. However, the protective effects of *Wld^S* or null *Sarm* alleles do not apply to all types of neurodegeneration. For instance, *Sarm* mutants show reduced degeneration in traumatic brain injury models, or peripheral neuropathies caused by vincristine but does not protect against degeneration in a mouse model of hereditary amyotrophic lateral sclerosis (ALS) (Geisler et al., 2016; Henninger et al., 2016a; Peters et al., 2018). Generally, genetic factors involved in Wallerian degeneration tend to protect better against acute insults to axons, while they are weaker or have no effect on more chronic protracted neurodegenerative diseases. This may be in part due to the axon-specific protection provided by these factors. While *Wld^S* (and null *Sarm* alleles) provide robust protection to axons, they fail to prevent cell death of the neuron soma in many contexts (Adalbert et al., 2006; Beirowski et al., 2008; Fischer et al., 2005; Hoopfer et al., 2006a; Peters et al., 2018). However, in “dying-back” diseases where the axon

degenerates before the cell body does, *Wld^S* does prevent cell death (Ferri et al., 2003; Samsam et al., 2003). This is true for the *progressive motor neuropathy (pmn)* mouse model where normally axons and cell bodies are progressively lost. In this model, protecting the cell body (by blocking programmed cell death) protected the cell body but did not prevent premature death, while *Wld^S* rescued both (Ferri et al., 2003). Taken together, these results indicated that the primary driver of disease progression was the axon loss and cell body loss was secondary. Although it is unclear how loss of the axon drives death of the soma, this model provides a clear example of the axon's status influencing the fate of the soma. However, the factors that communicate the axon's status remain undefined.

Introduction 1.4 – Axon maintenance

Axons are a crucial compartment of neurons responsible for transmitting information from the neuron's cell body to its target. In some cases, the distance between the cell body and the target can be a meter in length such as in the PNS. Alternatively, some axons can have many nearby targets requiring the axon to branch profusely. In both situations, the majority of the neuron's volume is contained within its axon. This creates a situation where the neuron cell body is tasked with supporting an axon many times its own size and whose distal tip can be a meter away. Beyond their sheer size, axons require a significant amount of energy to maintain their membrane potential and conduct action potentials (Ames, 2000; Engl & Attwell, 2015; Harris et al., 2012). It is estimated to require 3.84×10^8 adenosine triphosphate (ATP) molecules to repolarize a single 4 cm long axon following an action potential (Attwell & Laughlin, 2001). Considering an axon in the PNS can be 250 times

this length, the absolute amount of ATP required to repolarize an axon after a single action potential, let alone many thousands in a single day, becomes astronomical. To compound these challenges further, axons must be maintained throughout life in order to maintain proper neural circuitry and function. Together these features pose significant hurdles for the neuron to overcome in maintaining the integrity of its axon.

In addition to meeting energy requirements, replacing damaged proteins and organelles is crucial to sustaining a healthy axon. Many proteins are made in the cell body and can be transported along the axon to replace damaged ones. Slow axon transport is primarily responsible for transporting cytosolic molecules while fast transport utilizes molecular motors, such as kinesins, consume ATP to carry vesicles, mitochondria, and membrane associated proteins along microtubules within the axon (Grafstein & Forman, 1980; Hollenbeck & Saxton, 2005; Vale, 2003). In addition to transporting cargos from the cell body to the axon, dynein is a molecular motor that brings cargos from out in the axon back to the cell body (Vale, 2003). These can include signaling molecules such as nerve growth factor (NGF)-TrkA complexes that are required for axon growth during development in peripheral nerves (Angeletti et al., 1972; Campenot, 2009; Levi-Montalcini et al., 1968, 1969). Retrograde transport is also important for eliminating damaged proteins and organelles from the axon via autophagosomes and lysosomes (Stavoe & Holzbaur, 2019). Together these mechanisms provide an avenue for the cell body to support its axon by turning over proteins and organelles.

Introduction 1.5 – Axon metabolism

Between the ATP consumed through neural transmission and that of homeostatic functions, like transport, the axon requires a steady pool of ATP to function. Several studies indicate that neurons primarily rely on energy produced by mitochondria from aerobic metabolism (Fünfschilling et al., 2012; Pellerin & Magistretti, 1994; Volkenhoff et al., 2015). Mitochondria utilize metabolites such as pyruvate to fuel the tricarboxylic acid (TCA) cycle and produce energy in the form of ATP. Indeed, several studies have shown that genes encoding glycolytic enzymes can be eliminated selectively from neurons with little to no effect while knocking down some proteins required for the TCA cycle just in neurons is lethal (Volkenhoff et al., 2015). Together, these studies indicate that axon energy demands are met primarily by mitochondrial metabolism. Metabolites used to fuel mitochondria can be taken up from local external sources by various monocarboxylate transporters (MCT) in the plasma membrane (Delgado et al., 2018; Pérez-Escuredo et al., 2016). There are several potential sources of metabolites used by axons to support their function. These include the neuron's soma, the extracellular space, and glia that directly ensheath axons. In the PNS the axons are ensheathed by glia, effectively blocking their access to an extracellular supply other than that shuttled via the glia; and the axons in the PNS are so long that relying on diffusion from the distant cell body would be inefficient. Furthermore, myelinating glia in the CNS have been shown to express MCTs on their adaxonal membranes, providing evidence for a transport mechanism between glia and axons (Saab et al., 2016).

Introduction 1.6 – Glial ensheathment of axons in *Drosophila*

Drosophila melanogaster, the model used in these studies, have wrapping glia (WG) that closely resemble Remak SCs in vertebrates (Stork et al., 2008). Like Remak SCs, WG interdigitate between and ensheath multiple axons in peripheral nerves but do not form compact myelin sheaths (Stork et al., 2008). While the role of myelin in accelerating nerve conduction is well characterized, the function of non-myelinating glial ensheathment is not. This represents a significant gap in our collective knowledge, as this non-myelin form of ensheathment is hypothesized to represent the ancestral form and indeed the vast majority of axons in human peripheral nerves are ensheathed in this way (Ochoa & Mair, 1969; Schmalbruch, 1986; Weil et al., 2018).

There are several contributing factors to why the function of these cells remains elusive. First, there is yet to be a robust tool to genetically manipulate Remak SCs in mammalian systems independently from myelinating SCs, making it difficult to attribute mutant phenotypes directly to Remak SCs. During development, both myelinating and Remak SCs are derived from neural crest cells that interdigitate between axons in the peripheral nerves sorting small caliber axons (<1 μm in diameter) into bundles ensheathed by Remaks while larger caliber axons become myelinated in a process called radial sorting (Harty & Monk, 2017; Jessen & Mirsky, 2005). Additionally, because Remak SCs ensheath small caliber axons which are dwarfed in size compared to their myelinated counterparts, they require higher resolution imaging for detailed analysis such as transmission electron microscopy. One of the few observations regarding Remak SCs in the literature is defects in radial sorting where larger caliber axons that should be myelinated are instead ensheathed by Remak SCs. Beyond this, Remak SCs are largely ignored and methods for quantifying their

ensheathment of axons have not been rigorously standardized. These are among the top reasons why Remak SC function remains largely undefined. Filling in this gap in our knowledge about the role of non-myelinating glia is crucial to understanding the fundamental role(s) of this highly conserved glial cell type. Unlike Remak SCs, WG, the *Drosophila* counterpart, are more easily manipulated genetically and provide a tractable model to directly study non-myelinating glia that ensheath axons (Stork et al., 2012). Additionally, work on these cells will likely have a direct impact on understanding human neuropathies, as many of the neurons affected in these diseases are small caliber axons ensheathed by Remak SCs (Beirowski, 2013; Fernyhough et al., 2010; Gonçalves et al., 2020; Niemann et al., 2006; Viader et al., 2011, 2013; Wei et al., 2019).

Introduction 1.7– Glial support of axons

One hypothesized role for this form of ensheathment could be to prevent ephaptic coupling of neighboring axons, where electrical activity of one axon could influence the excitability of neighboring axons. There is also some evidence for a role of WG in improving conduction velocity of peripheral nerves in *Drosophila* (Kottmeier et al., 2020). The most well characterized function of glial ensheathment is a trophic role for glia in supporting axon metabolism. For instance, work on myelinating glia in mice has demonstrated that MCTs that are capable of transporting metabolites that are required in oligodendrocytes for axon survival (Lee et al., 2012). One of these metabolites, lactate, is a product of glycolysis and is thought to be transported to axons to fuel the TCA cycle in the axon (Fünfschilling et al., 2012; Lee et al., 2012; Nave, 2010; Saab et al., 2016). In line with this, inhibiting mitochondrial function by knocking out *Cox10* does not cause

degeneration in myelinated CNS axons, suggesting that TCA cycle activity in mature oligodendrocytes is dispensable (Fünfschilling et al., 2012). Similarly, in *Drosophila*, eliminating glycolytic enzymes from glia, but not neurons, results in axon degeneration (Volkenhoff et al., 2015). In addition to metabolic support, a more recent study has identified a role for glia in protecting axons against iron-mediated toxicity (Mukherjee et al., 2020).

Understanding the depth of glial support of axons requires a broad and unbiased approach to identify new components involved in different facets of glial support. One method to accomplish this is using a genetic approach to identify specific genes whose disruption cause defects in glial support. The genetic tools in *Drosophila* allow one to do just this and specifically disrupt a single gene only in glia while also observing the effect on axon and neuron survival. Using this strategy, I conducted a screen with my colleagues and identified a variety of genes that caused reduced axon survival when eliminated exclusively from glia or caused whole animal lethality. This dataset provides new avenues to study glial support of axons by identifying a host of molecules that are required in glia to support axon survival.

Introduction 1.8 – Identifying glial genes required for axon maintenance

Drosophila melanogaster is a genetically tractable model organism with many tools available to precisely manipulate both glia and neurons independently. In the PNS of *Drosophila*, there are three glial subtypes that ensheath the nerves: perineurial glia (PG) form the outermost layer, subperineurial glia (SPG) create a blood-nerve barrier in the

intermediate layer, and wrapping glia (WG), analogous to Remak Schwann cells, interdigitate between axons, separating them from one another (Stork et al., 2008). There is a peripheral sensory nerve in the L1 vein of the adult wing along the anterior wing margin that can be imaged directly through the wing. Using this tissue as our model, we generated a sensitized screening assay to systematically disrupt glia and evaluate the impact on axon maintenance. Among the hits identified in this screen were several components of the TGF β superfamily. In addition to hits that caused disruption to axon integrity, we also identified 138 genes that when knocked down in glia failed to produce viable adults. Interestingly, a large proportion of these targets are implicated in blood brain barrier function.

Introduction 1.9 – TGF β signaling in glia

The TGF superfamily has two distinct branches, TGF and BMP. Each has a variety of secreted ligands that bind to and activate a heterodimer of type I and type II serine/threonine receptor kinases. Upon activation the type I receptor phosphorylates a cytosolic transcription factor which then binds to a cofactor allowing it to enter the nucleus and modify transcription within the cell (reviewed in Feng & Derynck, 2005; Upadhyay et al., 2017). The superfamily is divided into two based on the types of processes they coordinate. The actions of TGF β signaling are highly context dependent, but it commonly regulates cell proliferation and cell death in many tissues during development (Jang et al., 2001; Perlman et al., 2001; Raftery et al., 2008; Ramesh et al., 2009; Sánchez-Capelo, 2005; Schuster & Krieglstein, 2002a, 2002b; Yoo et al., 2003; J. Yu et al., 2008). Excess Schwann cell precursors are eliminated during nerve

development through activation of the TGF β pathway (D'Antonio et al., 2006; Parkinson et al., 2001). BMP signaling on the other hand is generally involved in coordinating tissue morphogenesis and patterning (Upadhyay et al., 2017; Weiss & Attisano, 2013). During embryogenesis, BMP signaling is crucial to dorsal-ventral patterning of the organism as well as specific tissues (Mullins et al., 1996; Neul & Ferguson, 1998). While many roles for this pathway have been established in developmental contexts, an ongoing role for this signaling pathway in glial support of axons has not been established.

Introduction 1.10– TGF β signaling beyond development

Most of the work studying this superfamily has been done in the context of development. However, as a regulator of cell proliferation and death, TGF β has also been implicated in numerous cancers and is classified as a tumor-suppressor (Massagué, 2008). In addition, TGF β has also been implicated in regulating metabolic activity in the fat body of developing *Drosophila* larvae (Ghosh & O'Connor, 2014). Ghosh & O'Connor, 2014 identified a role for the ligand Dawdle in inhibiting expression of genes involved in mitochondrial biogenesis. They found that loss of this ligand resulted in increased TCA cycle intermediates, and they demonstrated that this phenotype was reliant on the receptor *baboon* (*babo*) and its target *Smad on X* (*Smox*). Similar effects on mitochondrial regulation by TGF β have also been reported in studies on human cancers (Fiz et al., 2021; Slattery et al., 2021). Dysregulation of mitochondria and decreased metabolic activity observed in natural killer cells from breast cancer patients was shown to result from increased TGF β receptor activation (Slattery et al., 2021). Similarly, TGF β was

shown to inhibit PGC-1 α production (a major regulator of mitochondrial biogenesis) resulting in decreased TCA cycle output in renal cancer cells (Nam et al., 2021).

Introduction 1.11 – Dissertation overview

The following work presented here will address the question of how glia support axons *in vivo*. I present the results of a genetic screen identifying numerous genes that negatively impact axon survival when eliminated exclusively from glia. I provide *in vivo* evidence for the requirement of WG to support neuron maintenance in aged animals. In addition, I demonstrate that the protection afforded to axons by *Wld^S* depends on the presence of glia and without glia, axon protection from Wallerian degeneration is compromised *in vivo*. I further demonstrate that TGF β activation within glia is critical for the long-term survival of the peripheral neurons they ensheath identifying this pathway as a regulator of glial support of axons.

MATERIALS & METHODS I

Fly husbandry

Flies (*Drosophila melanogaster*) were grown on standard molasses cornmeal agar with added dry yeast and maintained at 25°C. The following *Drosophila* stocks used in this study were obtained from the following sources. Bloomington: *OK371-QF2* (66473), *10xQUAS-6xGFP*, *UAS-mtdTomato-3xHA* (66479), *Repo-GAL4* (7415), *UAS-Reaper*¹⁴ (5824), *UAS-dronc::GFP* (56759), *UAS-lacZ.NZ*³¹² (3956), *UAS-lacZ.NZ*^{20b} (3955), *Vglut-QF2* (60315), *QUAS-mCD8::GFP* (30002), *UAS-lamin::GFP* (7376), *nrv2-GAL4* (6799), *UAS-babo*^{DN} (64423), *babo*^{RNAi2} (40866), *Smox*^{RNAi2} (41670), *tkv*^{RNAi} (40937), *mav*^{RNAi} (34650), *put*^{RNAi} (39025), *UAS-mCherry.NLS*³ (38424), *babo-Gal4*^{CRIMIC00274} (83164), *tubP-Gal80^{ts-20}* (7019), *UAS-mito-roGFP.Grx1* (67664) (see also KEY RESOURCE TABLE). Vienna *Drosophila* Resource Center RNAi lines are listed in APPENDIX I (Diezle et al. 2007). Additional RNAi lines including *tkv*^{RNAi}, *put*^{RNAi}, and *sax*^{RNAi} were generously provided by Dr. Michael O'Connor. *UAS-dark* was kindly provided by Dr. John M. Abrams (Akdemir et al., 2006). The protein trap *nrv2-GFP* was published in Stork et al., 2008. The ATP sensor was provided by Dr. Baljit Khakh (Lobas et al., 2019). The *WG split-Gal4* line was established using the *nrv2*-DNA binding domain construct previously reported in (Coutinho-Budd et al., 2017) combined with a VP16 activation domain converted from the *IT.0117-Gal4* (BL62647) using methods described in (Gohl et al., 2011). The pQUAST-Wld^S plasmid was sent to BestGene Inc. for injection into *w¹¹¹⁸* embryos to generate the *QUAS-Wld^S(III)* line used in these studies.

Sensitized RNAi screen

RNAi lines were crossed to the w^* ; *Vglut-QF2*, *QUAS-mCD8::GFP/CyO* ; *QUAS-Wld^s*, *Repo-Gal4/TM3* driver line. After 7 days, parents were discarded and progeny returned to 25°C. Adult progeny were later collected, anesthetized on CO₂ fly pads, and sorted for genotype using visible markers. After 4 days at 25°C, flies were anesthetized on CO₂ and one wing was cut between the two cross veins of the wing using spring scissors (F.S.T #15002-08), while the other wing served as an uninjured control. Injured flies were transferred to fresh standard cornmeal agar vials every 3-7 days and then imaged 10 or 14 -days post axotomy (see imaging). For screening of each RNAi line at least 5 wings were evaluated, results are reported in APPENDIX I. RNAi lines were scored as lethal if no viable adult flies of the correct genotype emerged or if all adults died before the imaging timepoint. Both female and male progeny were used except where genetics prohibited use of males.

Aging assay

Animals of the appropriate genotypes were crossed, as described above, selected for markers at eclosion, and adults were aged for the indicated time windows at 25°C. Aging flies were transferred into fresh vials every 3-7 days. The number of dead flies in each vial was recorded during each transfer and these tallies can be found in Figure S3. Subsets of wings from each cohort were imaged at 4, 14, and 28 days after progeny were originally collected. All wings were inspected at 63x for injuries and were excluded if they had any visible tears or scars in the L1 wing vein containing the nerve.

Adult-specific knockdown

Crosses were performed at 18°C and the progeny were allowed to develop at 18°C. Adults of the correct genotype were collected into standard cornmeal agar vials and transferred to 31°C. Flies were maintained at 31°C and transferred to fresh vials every 3-5 days until imaging at 4- and 14-days post eclosion.

Imaging acutely dissected L1 nerves

Imaging of the wing nerve was done as previously described in (Neukomm et al., 2014). Briefly, flies were anesthetized using CO₂ and their wings were removed using spring scissors, mounted on a slide in Halocarbon oil 27 (Sigma #H8773), covered with #1.5 cover glass, and imaged within 15 minutes of mounting. Z-stack images were taken of the nerve on a Zeiss Axio Examiner equipped with a Yokogawa spinning disk and Hamamatsu camera using a 63x1.4NA oil-immersion objective. The same acquisition settings were used across samples for each of the experiments and control samples were imaged in the same imaging session as experimental samples. *VGlut*⁺ neuron cell bodies in the L1 vein were counted under 63x magnification. Cells were counted as intact if they had a clear nucleus and dendrite or were considered dead if they were shrunken and the dendrite or nucleus were not clearly visible (see Figure 3B).

Quantification of axon degeneration

Images were classified into phenotypic categories (intact, mild, or severe degeneration) with the conditions blinded to the scorer (Figure 3A). All genotypes and ages for a given experiment were scored together in one session and later decoded. For experiments in which the wrapping glia were ablated, the channel containing the axons was first extracted from the two-color images before blinding and scoring so that the scorer remained blind to the presence or absence of glia.

Immunofluorescence

Wandering third instar larvae were dissected and pinned open as filets in cold PBS and fixed in 4% paraformaldehyde in PBS for 15 minutes at room temperature. Larvae were then permeabilized in 0.3% PBST (PBS + TritonX-100) for 15 minutes at room temperature with agitation and remaining wash and antibody solutions were made in 0.3% PBST. Antibodies used were: (1°) anti-Repo (Mouse anti-Repo, DSHB #8D12), Alexa Fluor® 647 anti-HRP (Goat anti-HRP, Jackson Labs #123-605-021), anti-oaz (Rabbit anti-oaz, this paper & Corty et al. 2021), anti-GFP (Chicken anti-GFP abcam #ab13970); (2°) DyLight™ 405 Donkey anti-Mouse (Jackson Labs #715-475-150), Alexa Fluor® 488 Donkey anti-Chicken (Jackson Labs #703-545-155), Rhodamine Red™-X Donkey anti-Rabbit (Jackson Labs #711-295-152) (see also KEY RESOURCE TABLE). Samples were incubated in primary antibody solution overnight at 4°C with agitation. Primary antibody solution was removed and the samples were washed 5x15 mins in 0.3% PBST at room temperature with agitation. The same procedure was repeated for the secondary antibody incubation. After staining, larva filets were mounted in Vectashield (Vector Labs #H-1000)

and covered with #1.5 cover glass (Globe scientific #1404-15) and stored at 4°C. Adult wings were stained using the same methods as larvae, however, both primary and secondary antibody incubation steps were extended to 5 overnights at 4°C.

Quantification of iATPsnFR and roGFP in glia

To quantify iATPsnFR intensity, images were acquired as z-stacks and maximum intensity projections were derived for each nerve. Using ZEN 3.4 (blue edition) software, each nerve was then traced, excluding nuclei to control for variability due to differences in nuclei numbers. The average intensity for the traced region for each nerve was then used for statistical analysis. To quantify the roGFP to determine redox state of mitochondria z-stack images were analyzed using Imaris software. First, surfaces were created from the 488 nm signal using the same threshold settings across all images. The average intensity from each channel in the surface was recorded and the ratio was calculated for each image. These ratios were then plotted and used for statistical analysis.

Electron microscopy

Aged flies were maintained as described above. Electron microscopy procedures were modified from a microwave protocol from (Cunningham & Monk, 2018; Czopka & Lyons, 2011). Flies were anesthetized with CO₂ and their wings were removed with spring scissors and immediately put into freshly made fix solution (2% glutaraldehyde, 4% paraformaldehyde, 0.1M sodium cacodylate buffer). Forceps were used to gently submerge the tissue in a 2 mL microcentrifuge tube and microwaved using the following settings: 2x

(100W for 1min, OFF for 1 min), then immediately followed by 5x (450W for 20s, OFF for 20s) before storing the tissue at 4°C overnight in fix solution. The following day samples were washed 3 times in 0.1M sodium cacodylate buffer followed by secondary fixation in 2% osmium tetroxide, 0.1M sodium cacodylate buffer and 0.1M imidazole pH 7.5 and microwaved 2x (100W for 1min, OFF for 1 min), 5x (450W for 20s, OFF for 20s). Following osmium fixation, samples were rinsed in distilled water 3 x 10-minute washes. Samples were stained in saturated uranyl acetate (UA) ~8% in water and microwaved 2x (450W for 1 min, OFF for 1 min). Samples were washed 3 x 10 minutes with distilled water. This was followed by dehydration steps with an escalating ethanol series (25%, 50%, 70%, 80%, 95%) with each step microwaved at 250W for 45s. A final 100% EtOH step was repeated 3 times and each repetition was microwaved for 2x (250W for 1 min, OFF for 1 min). Following EtOH dehydration, samples were dehydrated in 100% acetone and microwaved 2x (250W for 1 min, OFF for 1 min) and repeated 3 times. For all microwave steps, samples were insulated in a cold water bath held at 10°C to prevent overheating. Samples were then transferred to a 50:50 resin:acetone solution and agitated overnight at room temperature in glass scintillation vials. Final resin infiltration was done in 100% resin and agitated at room temperature for at least 1 hour. Tissues were embedded in EMBED-812 resin (EMS #14120) and cured in a 60°C oven overnight. Ultrathin 70 nm sections were cut on a Leica ultramicrotome and transferred to 100mesh Formvar grids (EMS #FCF100-Cu). Grids were counter stained for 20 minutes in 5% uranyl acetate followed by 7 minutes in Reynold's lead citrate. Micrographs were acquired on a FEI Tecnai T12 interfaced to Advanced Microscopy Techniques (AMT) CCD camera.

Statistical analysis

Statistical analyses were done in GraphPad Prism 8. When analyzing the effect of two variables (genotype and age) two-way ANOVA was used with Sidak's multiple comparisons test to analyze the effect of genotype at each age compared to a control group. When comparing multiple experimental groups to the same control group Welch's ANOVA was used with Dunnett's T3 multiple comparisons test to compare experimental groups to the control. When comparing one experimental group to a control a one-tailed Welch's t test was used. Axon classification categorical data was analyzed using either Fisher exact probability test 2x3 (Figures 4, 9, 17 & 18) or Chi-square test (Figure 5B) and the p-values are reported the text. Significance was determined using an α of 0.05. In figures, p-values are represented as follows: ns not significant, * $p < 0.05$, ** $p < 0.01$, *** $p < 0.001$, **** $p < 0.0001$.

RESULTS I

Results 1.1 – Ablating wrapping glia causes neurodegeneration

To explore the mechanisms by which glia support axon function and survival, I used the peripheral nerve in the *Drosophila melanogaster* adult L1 wing vein (Figure 1A). Using this system, it is possible to independently manipulate neurons and glia and examine their morphology with single cell/axon resolution *in vivo* (Figure 1B). This sensory nerve contains roughly 280 sensory neurons (Figure 1C). Their cell bodies are positioned along the anterior wing margin, and they project their axons into the thorax (Figure 1A; (Palka et al., 1983). These are among the longest axons in *Drosophila* (Figure 1A; (Palka et al., 1983) and each is individually ensheathed by wrapping glia (WG) (Figure 1 C). WG cover the entire nerve and interdigitate into the axon bundle separating axons from one another (Figure 1C; (Neukomm et al., 2014). Given their length, and their extensive ensheathment by WG glia, I hypothesized that this nerve would be a suitable model to explore how glia provide essential support for neuronal function and maintenance.

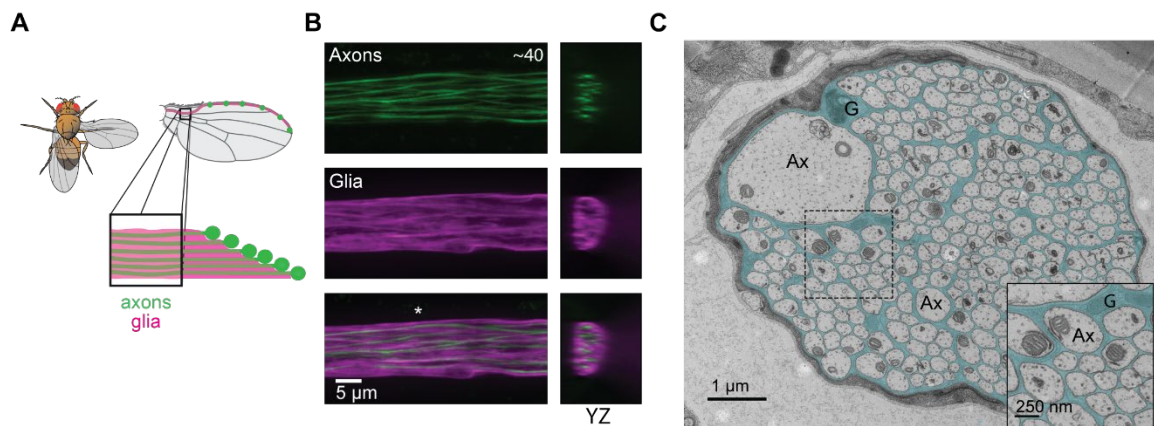


Figure 1 Peripheral sensory nerve in the *Drosophila* L1 wing vein. (A) Diagram of the sensory nerve in the wing of *Drosophila* (B) Images from the area depicted in the box in A. A subset of glutamatergic neurons are genetically labeled with GFP (green) and glia are labeled with tdTomato (magenta). The orthogonal (YZ) fluorescent image corresponds to the location at the asterisk. (C) Electron micrograph of a cross section of the nerve in the wing from the same region as in A. Wrapping glial membrane is pseudocolored in cyan. Example glia (G) and axons (Ax) are labeled.

To assess whether WG were required for maintenance of axons in this model, I selectively ablated WG and measured neuronal integrity as the animals aged. Using the Gal4/UAS binary expression system (Brand & Dormand, 1995), I overexpressed the cell death molecules – Dronc & Dark, or Reaper (Dorstyn et al., 1999; White et al., 1994; Zhou et al., 1999) – along with the fluorescent reporter tdTomato in most of the WG by using a split Gal4 construct (Luan et al., 2006). This split Gal4 was exclusively expressed in WG and is henceforth referred to as *WG split-Gal4*. *WG split-Gal4* labeled 87% of WG in the wing as determined by nuclear reporter expression as compared to *nrv2-Gal4*, which is expressed in all the WG in the wing but is also widely expressed in the central nervous system (Figure 2; (Neukomm et al., 2014).

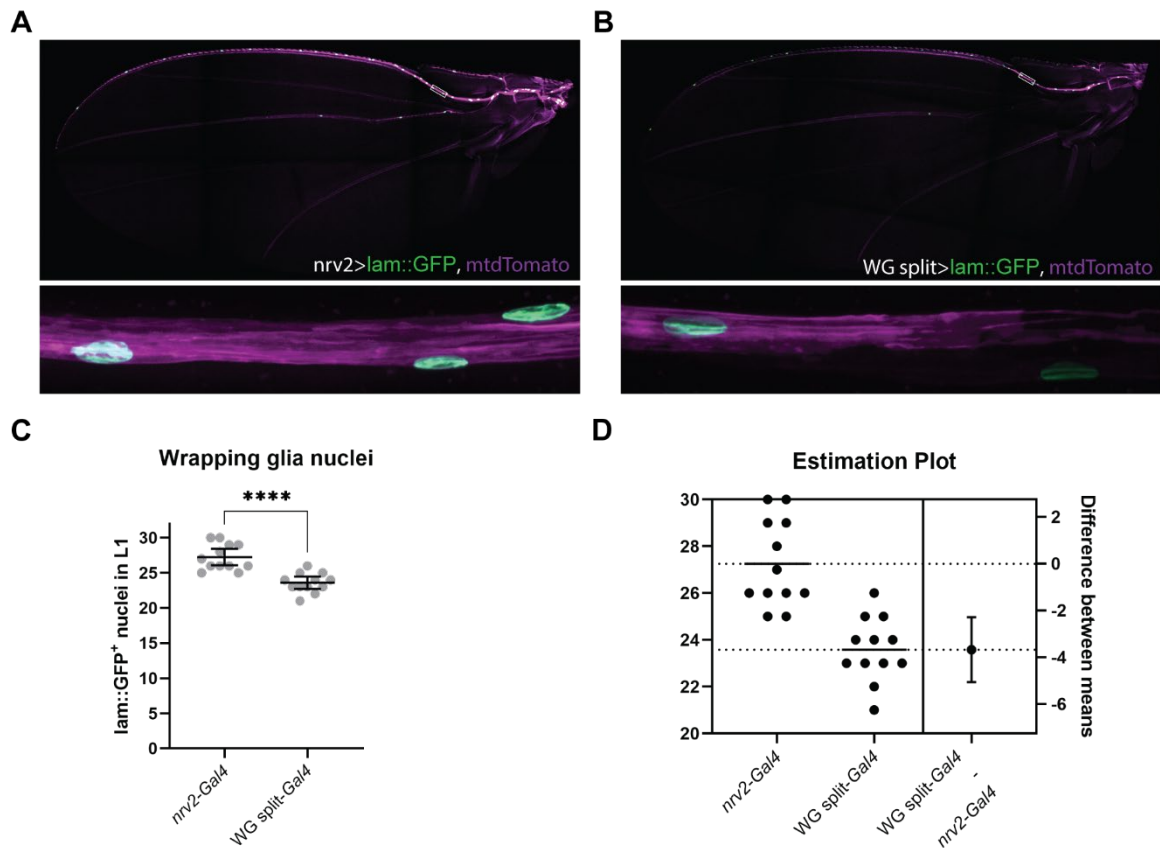


Figure 2 *WG split-Gal4* expression in the adult wing. (A-B) Expression of lamina::GFP and tdTomato under the control of *nrv2-Gal4* (A) or *WG split-Gal4* (B). (C) Quantification of the number of WG nuclei labeled by each driver. (D) Estimation plot of the difference in nuclei labeling between the two drivers.

Using this WG-specific driver, I ablated WG constitutively to measure the effect on sensory neurons in the adult wing. I confirmed ablation of WG by absence of tdTomato expression. Overall, ablation of WG was robust but occasionally faint remnants of tdTomato⁺ WG membrane remained (Figure 3B&C). By combining the *WG split-Gal4* with another independent binary expression system QF2/QUAS (Potter et al., 2010; Riabinina et al., 2015), I fluorescently labeled *VGlut*⁺ neurons (a subset of neurons in the wing ~40) while simultaneously ablating WG. I then examined nerves in the adult wing from 4-, 14-, and 28-day-old animals. I classified blinded images of axons from control and WG-ablated wings into one of three phenotypic categories: intact, mild, or severe degeneration (Figure 3A). In addition to quantifying axon degeneration, I also counted the number of intact neuron cell bodies from each condition, an example of an intact versus cell corpse is shown in Figure 3B. Neurons were counted as intact if they had a clear nucleus and attached dendrite while neuron corpses often appeared shrunken without a clear nucleus or dendrite. Sometimes, corpses appeared dim, other times they appeared much brighter than the surrounding intact cell bodies. This may be due to different type or stages of cell death that could be occurring in these nerves.

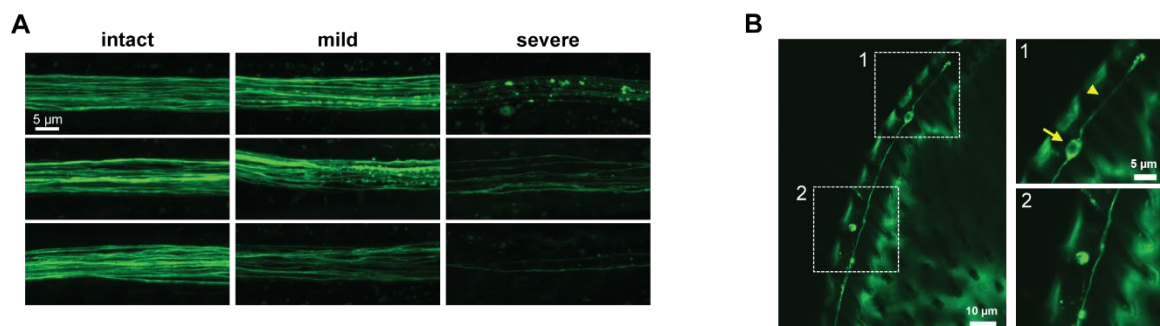


Figure 3 Neurodegeneration in uninjured wings. (A) Examples of nerves classified as intact (left), mild degeneration (middle), or severe degeneration (right). (B) Image from the distal portion of the wing showing an example of an intact (1) cell body with a dendrite (arrowhead) and a nucleus (arrow). A cell corpse is shown in box 2.

Using the aforementioned classification criteria, I quantified the effect of ablating WG in these animals. Eliminating WG caused increased age-dependent degeneration of axons within this peripheral sensory nerve in the wing (Figure 4A-D). A larger proportion of nerves from aged, ablated animals exhibited mild or severe degeneration compared with the control group at 28 days (control: 2/18 animals, Dronc+Dark: 11/18 p=0.0027, Reaper: 10/18 p=0.018; Figure 4D).

In addition to axon degeneration, ablating WG also caused loss of sensory neuron cell bodies (Figure 4A-C box 2 & E). At baseline (4 days post eclosion (dpe)) there were no significant differences in the number of intact GFP⁺ neuron cell bodies per wing between

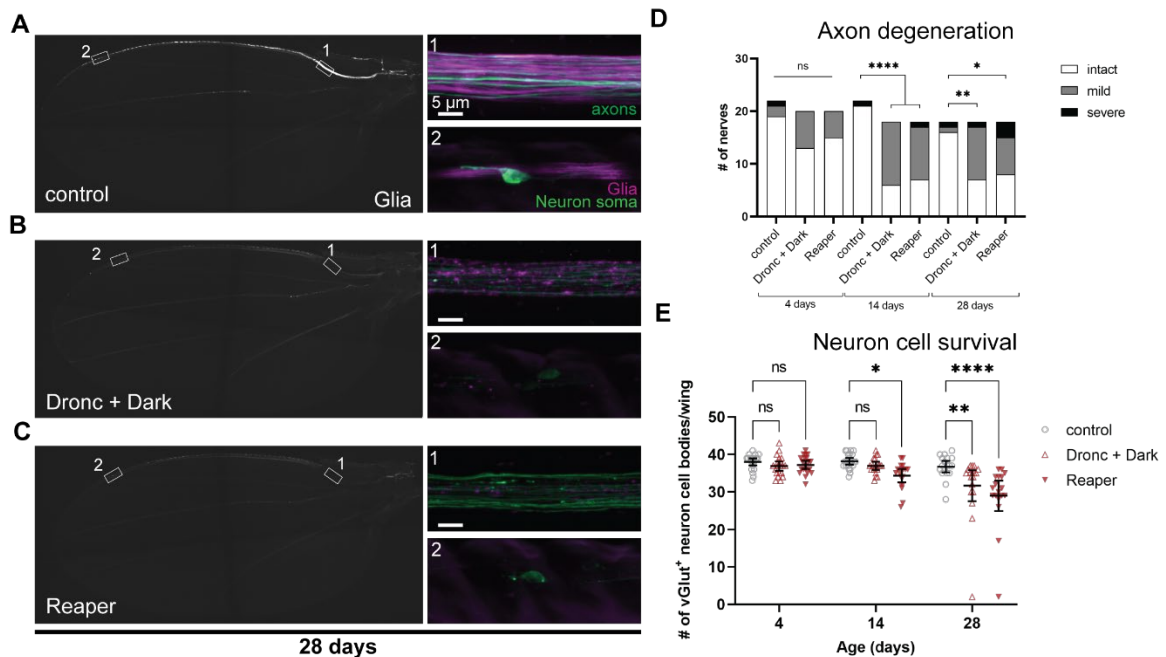


Figure 4 Ablating wrapping glia results in neurodegeneration in the peripheral nerve of the wing with age. (A-C) Representative images of control and glial-ablated wings at 28 days of age with subset of wrapping glia labeled with tdTomato. Boxes 1 & 2 show higher magnification images from ROIs in A-C. (D) Classification of axon phenotype for each nerve categorized into intact, mild, or severe. Fisher exact probability test 2x3. (E) Quantification of the number of intact neuron cell bodies at each time point for nerves from A-C. Example intact and cell corpses are shown in A-C box 2. Data are represented as mean ± 95% CI. Two-way ANOVA with Dunnett's multiple comparisons test. Significance: *, p < 0.05, **, p < 0.01, ***, p < 0.001, ****, p < 0.0001.

genotypes (control: 38.0 ± 2.1 n=21 animals, Dronc+Dark: 36.9 ± 2.7 n=20, Reaper: 37.2 ± 2.4 n=20; Figure 4E). However, at 28 days of age, fewer GFP⁺ neuron cell bodies remained in WG-ablated animals compared to controls (control: 36.7 ± 3.1 n=18 animals, Dronc+Dark: 31.7 ± 8.3 n=18 p=0.0014, Reaper: 29.0 ± 8.1 n=18 p<0.0001; Figure 4E). Together, these data indicate that WG are required for axon and neuronal survival in the sensory nerve of the wing.

Results 1.2 – The role of wrapping glia in axon maintenance

The neuron loss caused by eliminating WG suggested that WG play an important role in axon maintenance in the L1 nerve. Additionally, this result established that this was an appropriate model to investigate glial support of axons. Eliminating WG completely caused neuron loss but to understand why this happened I needed a systematic approach to disrupt specific glial functions and identify key regulators of axon maintenance. To isolate glia→axon support mechanisms specifically (as opposed to the cell body), I severed the axon from its soma thereby creating a situation where all that remains are the axons and the glia that ensheath them (Figure 5A). However, when wild type axons are severed, the portion of the axon distal to the injury site undergoes Wallerian degeneration (WD) and is eliminated (MacDonald et al., 2006). This process involves a signaling cascade in the axon that can be genetically blocked by expressing Wld^S in neurons (Coleman & Freeman, 2010; Conforti et al., 2007; Farley et al., 2018; Neukomm et al., 2014, 2017; Osterloh et al., 2012). Wld^S suppresses WD and allows severed axons to remain intact for weeks after axotomy (Figure 5A; Glass & Griffin, 1991). By expressing Wld^S in neurons in the wing, I was able to remove the neuron cell bodies while allowing the distal axons and the

surrounding glia to remain intact. I hypothesized that this would sensitize the axon to perturbations in glial support by removing its intrinsic support provided by its cell body. The ability of *Wld^S* to protect axons in intact nerves far exceeds its ability to do so in purified neuron cultures (Adalbert et al., 2005; Buckmaster et al., 1995; Conforti et al., 2006; Lunn et al., 1989; Wang et al., 2005). I hypothesized that this greater protection was in part due to presence of glial support to axons *in vivo*. To test this, I ablated WG in animals expressing *Wld^S* in neurons, induced axotomy and measured axon survival at 10 days post axotomy (dpa) (Figure 5A). Nerves lacking WG exhibited decreased axon protection compared to controls (degeneration phenotype: control=7/24 animals, WG-ablated=18/21 p=0.0005; Figure 5B). This suggests that the protection afforded to severed axons by *Wld^S* is contingent upon the presence of support from surrounding glia.

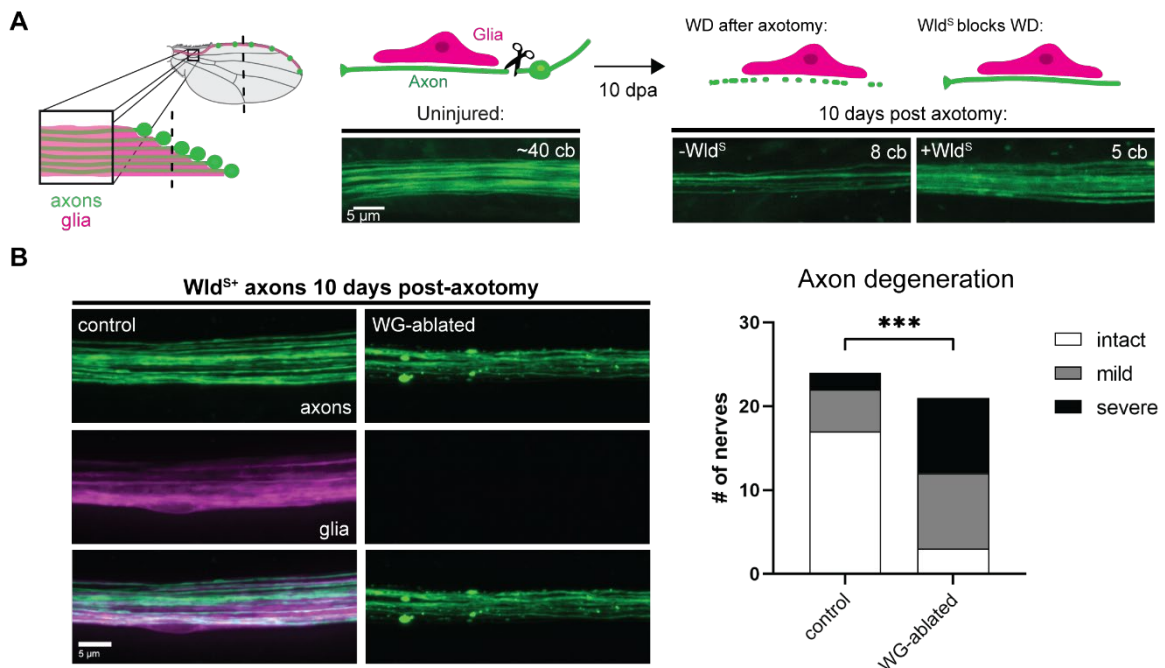


Figure 5 *Wld^S* protects axon after axotomy except when animals lack WG. (A) Diagram illustrating the axotomy induced by removing the distal portion of the wing. 10 days after axotomy (dpa) injured axons are cleared in control nerves while axons with *Wld^S* remain intact. **(B)** Images from control nerves and nerves from WG-ablated animals 10 dpa in animals expressing *Wld^S* in glutamatergic neurons. Right: classification of axon degeneration phenotypes from control and WG-ablated nerves. χ -square test, p=0.0005.

Results 1.3 – Identifying glial genes required for axon maintenance

The next step in furthering our understanding of what glial support of axons means is identifying the relevant cellular processes and the signaling pathways that regulate them. To do this, I used a genetic screening approach to identify glial genes that are necessary for long term axon survival. I severed the L1 nerve in the wing in animals expressing GFP and Wld^{S+} in glutamatergic neurons removing the neuronal cell bodies and leaving behind WD-resistant axons and the surrounding glia (*VGlut-QF2* (Diao et al., 2015), Figure 6A). In the same animals, a single gene was knocked down selectively in glia (*repo-Gal4* Sepp et al., 2001) using genetically encoded RNA interference (RNAi) (Perrimon et al., 2010). Together, my colleagues and I screened >2,000 publicly available *UAS-RNAi* lines targeting a panel of genes enriched for those encoding proteins containing predicted transmembrane domains or signal peptides (Figure 6B).

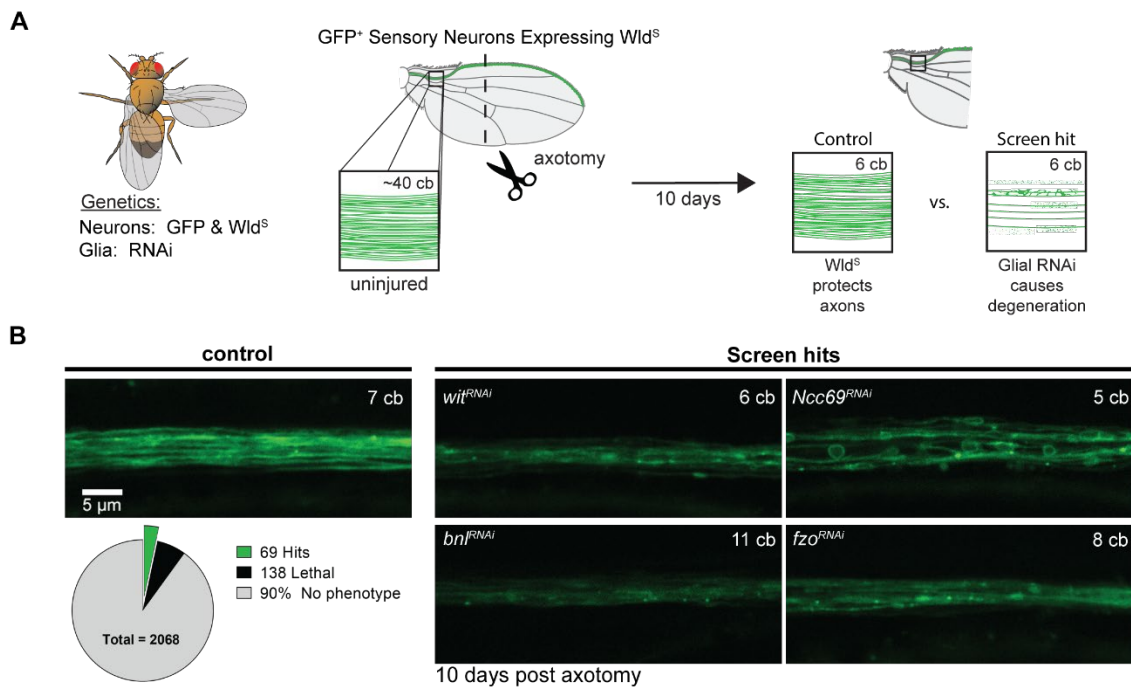


Figure 6 Screening for novel regulators of glia support of axons in vivo. (A) Diagram illustrating screen workflow. **(B)** Examples of control (left) and screen hits (right) Wld^{S+} nerves at 10 dpa. Pie chart summarizing screening results. See also APPENDIX I.

In control animals, *Wld^S* prevented WD and axons remained intact at 10 dpa (Figure 6B). We identified 69 candidate genes whose loss in glia resulted in axon degeneration or defects in axon morphology despite the presence of *Wld^S* (Figure 6B). For instance, depletion of a TGF β receptor (*wit*), a fibroblast growth factor (FGF) (*bnl*), or a mitofusin (*fzo*) led to robust axon loss (Figure 6B). Glial loss of the sodium-chloride co-transporter *Ncc69*, led to an axon blebbing phenotype similar to the neuronal activity-dependent axon disruption observed in zebrafish *slc12a2b* (NKCC1b) mutants (Marshall-Phelps et al., 2020)(Figure 6B. In addition, and consistent with previous work (Mukherjee et al., 2020), we additionally identified 138 genes that caused lethality—defined by absence of viable adult progeny—when selectively knocked down in glia (Figure 6B).

Results 1.4 – Disrupting TGF β superfamily genes in glia results in degeneration of sensitized axons

The TGF β receptor *wit* was one of several members of the TGF β superfamily identified in our screen. The TGF β superfamily is made up of two major branches (TGF β and BMP reviewed in (Upadhyay et al., 2017)(Figure 7A). Our initial screening panel did not include RNAis targeting all members of the TGF β superfamily. I therefore obtained and evaluated additional RNAi lines to test all genes in this pathway using the sensitized screening approach. Most RNAi constructs targeting components of this superfamily caused axon degeneration or lethality when expressed in glia (Figure 7B-C), suggesting a role for TGF β signaling in glial support of axons. Surprisingly, knocking down of both ligands and their receptors—selectively in glia—caused axon defects, suggesting a potential autocrine signaling mechanism in glia.

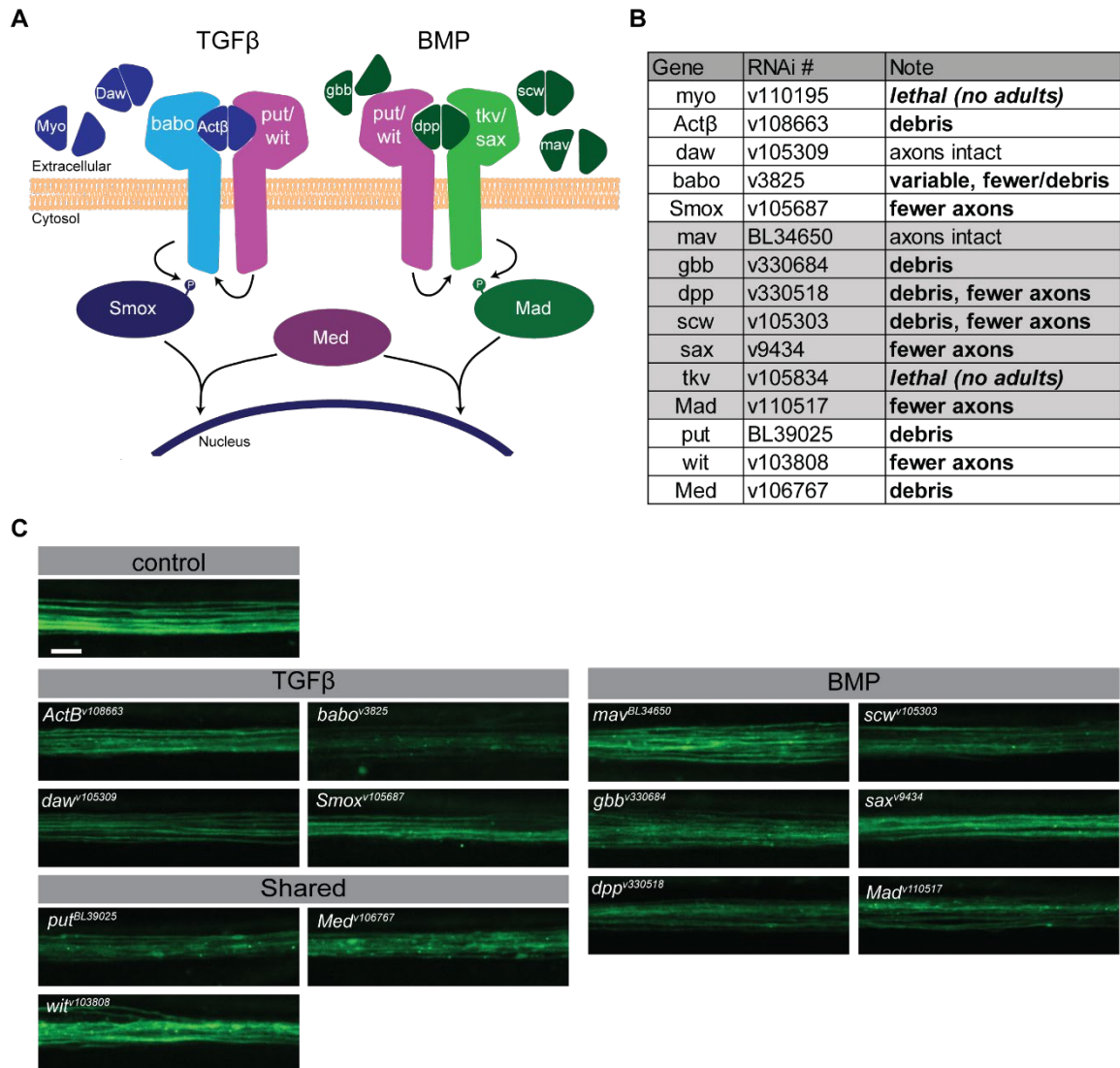


Figure 7 Glial-specific knockdown of TGFβ and BMP pathway components causes axon degeneration in the sensory nerve of the wing. (A) Diagram of the TGFβ superfamily members in the *Drosophila* genome. (B) Table summarizing the phenotypes for the corresponding RNAis targeting the TGFβ superfamily genes. VDRC – ‘v#’, Bloomington – ‘BL#’. (C) Images of Wld^{S+} axons in the sensory nerve of the wing 10 dpa from control and TGFβ knockdown animals. Scale bar 5 μm. Pan-glial knockdown of *myo* or *tkv* were lethal (not shown).

Results 1.5– TGFβ activity in glia is required for long-term axon maintenance

Ablating WG caused age-dependent degeneration in the absence of injury therefore, I next tested whether disruption of TGFβ signaling in glia alone was sufficient to disrupt glial support of uninjured axons. I knocked down each of the TGFβ superfamily genes in glia

using RNAi in animals that *do not* express *Wld^S* in their neurons and evaluated axon integrity and neuron survival as the animals aged (4, 14, and 28 days). As with the sensitized screening approach, this resulted in robust neurodegeneration in several TGF β knockdown conditions as compared to controls (Figure 8A-C). I was specifically interested in the role of WG in promoting axon maintenance, so I next knocked down TGF β genes selectively in WG in the wing using *nrv2-Gal4*. This resulted in a similar pattern of neuron loss as compared to pan-glial knockdown with a few notable differences (Figure 8D). Knockdown of *myo* (*myo^{v110195}*) and *tkv* (*tkv^{v105834}*) was no longer lethal when only knocked down in WG suggesting that the lethality was caused by disruption to other glial cell types (Figure 8D). Another key difference was that knockdown of the TGF β ligand *Dawdle* in WG alone did not cause neuron loss and neither did knockdown of the BMP receptors *sax* or *tkv* (Figure 8D). Together, this data indicates that inhibition of TGF β signaling intracellularly in WG results in neuron loss while inhibition of BMP signaling extracellularly from WG causes neuron loss (Figure 8D). Because knockdown of ligands and receptors for both branches in all glia causes neuron loss, these WG-specific knockdown results suggest crosstalk between glial subtypes via both TGF β and BMP signaling pathways. WG appear to respond to TGF β ligands from other glia and or neurons while they provide BMP ligands to signal to other glia and or neurons.

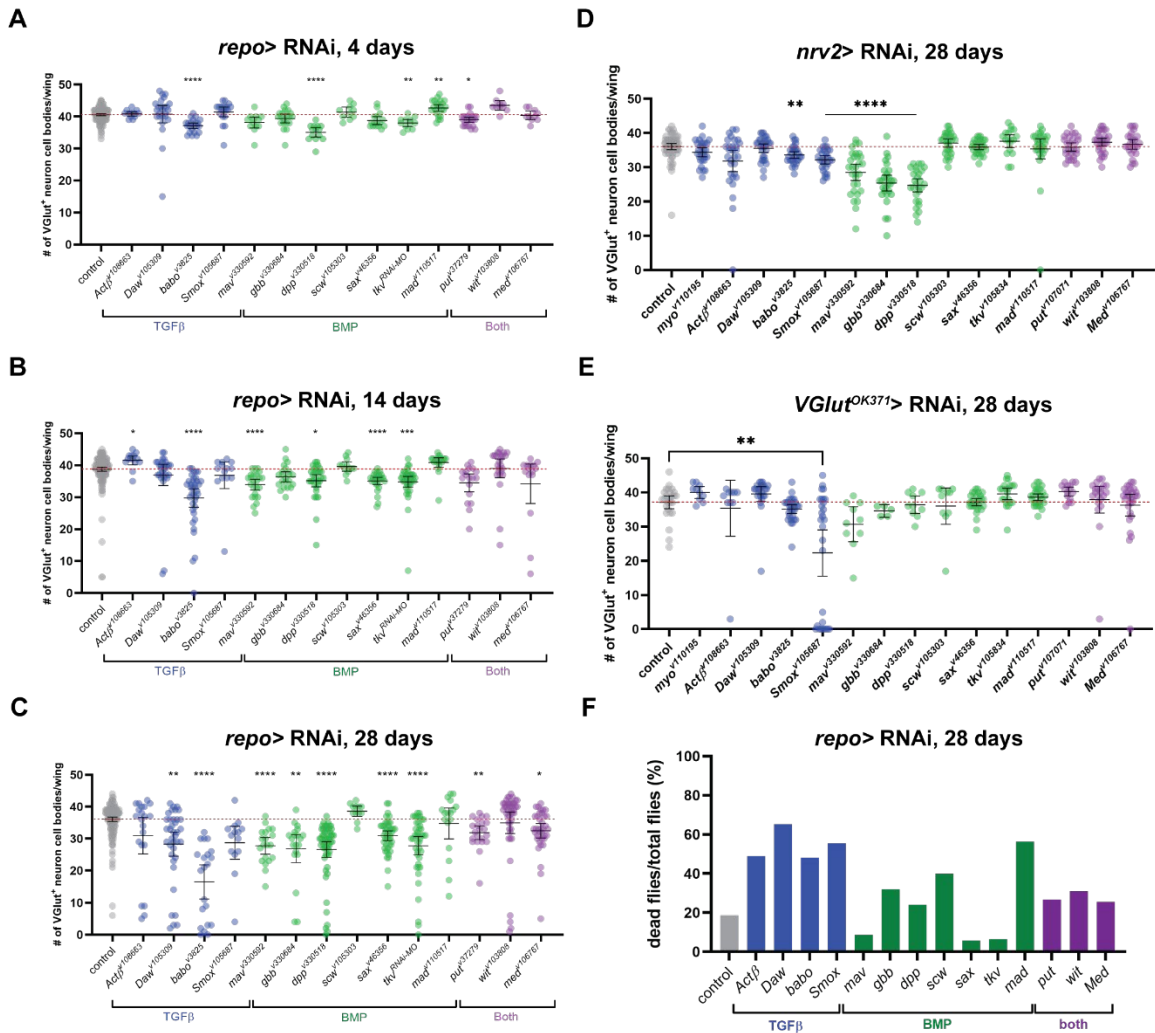


Figure 8 Glial-specific knockdown of TGFβ superfamily members results in age-dependent neurodegeneration in the sensory nerve in the adult wing. (A)

Quantification of the number of intact neuron cell bodies per wing at 28 days for control and TGFβ superfamily knockdown conditions. **(B)** Quantification of the number of intact neuron cell bodies per wing at each time point in control and babo-knockdown animals. **(C)** Images from control and babo-knockdown animals of the axon bundle in the wing at each time point (left) and the classification for each nerve (right) for all conditions. Fisher exact probability test 2x3. **(D)** Quantification of the number of intact neuron cell bodies in control, babo, and Smox knockdown animals using two non-overlapping RNAis each. **(E)** Quantification of the number of intact neuron cell bodies in adult-specific knockdown animals. Data are represented as mean ± 95% CI. Statistics: (B, D, E) Two-way ANOVA with Sidak's multiple comparisons test; (A) One-way ANOVA with Dunnett's T3 multiple comparisons test. Significance: ns, $p > 0.05$, *, $p < 0.05$, **, $p < 0.01$, ***, $p < 0.001$, ****, $p < 0.0001$. (See also Figure S3 & S4)

To examine the role that neurons play via this signaling pathway, I also knocked down each of these components in the glutamatergic neurons. Somewhat to my surprise, only

knock down of the transcription factor *Smox* caused significant neuron loss in aged animals (Figure 8E). Together with the WG-specific knockdown results, this indicates that the BMP ligands from WG are likely signaling to other glial subtypes because loss of these receptors in neurons had no effect on neuron survival while loss of BMP receptors in all glia led to neuron loss (Figure 8A-E). Furthermore, knockdown of TGF β ligands in glutamatergic neurons did not cause neuron loss implying that TGF β receptors in WG respond to ligands from other sources, likely other glial subtypes (Figure 8E). An important caveat to this result however is that because ligands were only knocked down in a small subset of the neurons (~40 out of ~280) it is possible that ligands generated from other neurons in this nerve compensated for this loss thus occluding the effect. While this remains possible, knockdown of *Daw* in all glia resulting in neuron loss suggests that *Daw* from other glial subtypes likely contributes to TGF β activity in WG (Figure 8C). Finally, an additional observation from these experiments was an increased likelihood of premature death in many of the pan-glial knockdown conditions for members of the TGF β superfamily in particular members of the TGF β branch (Figure 8F). This observation further implicates the importance of this signaling pathway in glia.

The strongest phenotype when knocking down components of the TGF β superfamily in all glia was elicited by knocking down the TGF β receptor *babo* causing both axon degeneration and cell body loss (Figure 9A-B, *Note that data shown in Figure 9B is the same data shown in Figure 8A-C where only data for babo and its corresponding control are shown at each timepoint*). To validate this RNAi and control for possible off-target effects, I tested a second, non-overlapping RNAi for both *babo* and its downstream target *Smox*. All four RNAis caused neurodegeneration in the uninjured aged nerve (Figure 9C).

Additionally, I further confirmed this knockdown result using an RNAi-independent method to inhibit TGF β signaling by overexpressing a dominant negative form of the receptor (*babo^{DN}*) in glia (Brummel et al., 1999). Glial expression of *babo^{DN}* also resulted in decreased neuron survival (Figure 9D), indicating that disruption of Babo in glia is sufficient to induce neurodegeneration in aged animals. From these data, I concluded that the TGF β pathway is required in glia for long-term neuron survival.

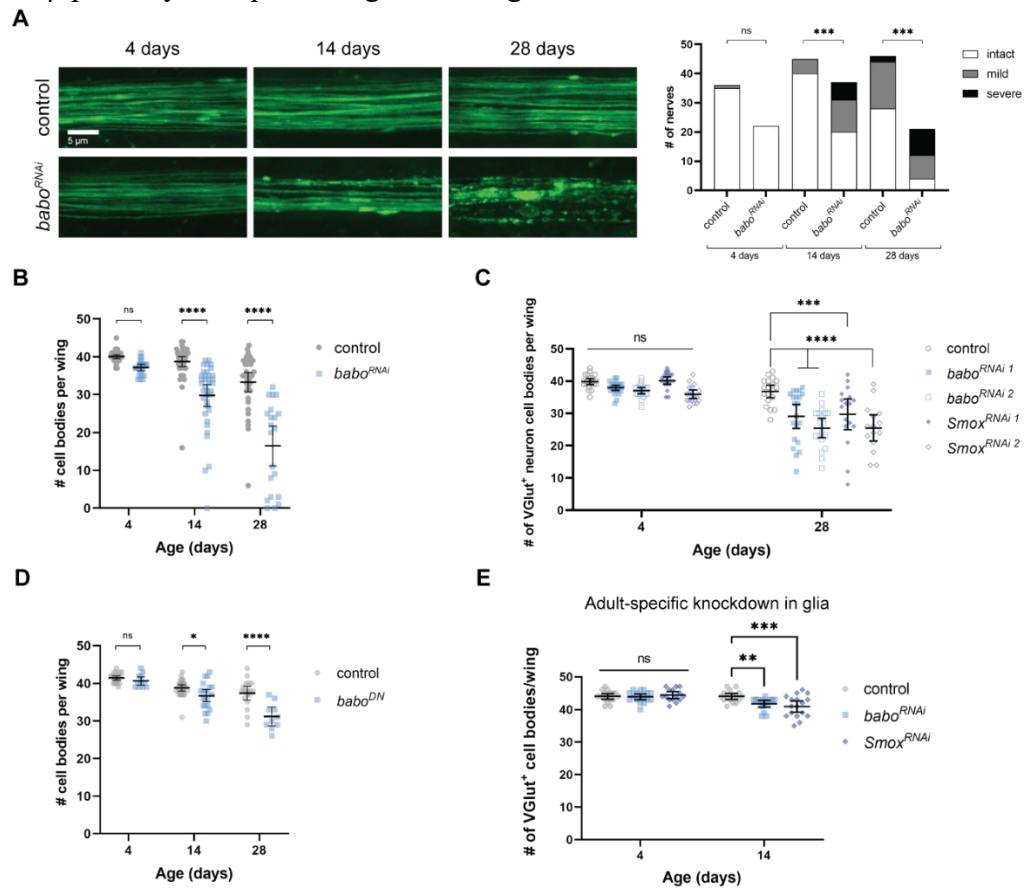


Figure 9 Inhibition of glial TGF signaling results in degeneration of aged neurons.

(A) Images (left) from control and *repo>baboRNAi* animals at 4, 14, and 28 days. Quantification of axon degeneration phenotype (right). Fisher exact probability test. **(B)** Quantification of the number of intact neuron cell bodies from control and *repo>baboRNAi* animals with age. **(C)** Quantification of the number of intact neuron cell bodies from control and *repo>RNAi* aging animals. **(D)** Quantification of the number of intact neuron cell bodies from control and *repo>babo^{Dominant Negative}* animals with age. **(E)** Quantification of intact neuron cell bodies from control animals and those with *babo* or *Smox* knocked down in glia only at the adult stage using temperature sensitive Gal80. (B-E) Two-way ANOVA with Tukey's multiple comparisons test. Significance: *, $p < 0.05$, **, $p < 0.01$, ***, $p < 0.001$, ****, $p < 0.0001$, ns, not significant.

Results 1.6 – *babo* is required in mature wrapping glia in the wing

The effects on neuronal survival could be due to developmental defects that manifest in the mature nerve or it could signify a role for TGF β signaling in mature glia. To begin to delineate these two possibilities, I combined glial-specific knockdown with a temperature-sensitive Gal80 (*Gal80^{ts}*) construct to both spatially and temporally control RNAi expression (McGuire et al., 2003). Using this tool, RNAi expression was inhibited during development until animals eclosed as adults. At 4 days post RNAi induction, there was no significant difference in the number of neuron cell bodies between control and TGF β knockdown animals (control: 44.0 ± 1.65 , *babo*: 43.9 ± 1.65 , *Smox*: 44.4 ± 1.88 ; Figure 9E). However, after 14 days of RNAi-mediated knockdown, both *babo* and *Smox* knockdown animals had fewer intact neuron cell bodies (control: 44.0 ± 1.71 , *babo*: 41.8 ± 1.94 $p=0.0090$, *Smox*: 40.9 ± 3.31 $p=0.0001$; Figure 9E). This phenotype was notably weaker than the constitutive knockdown, however, this was an earlier timepoint (14 days) compared to the 28 days in constitutive knockdown. Due to increased death in these animals when maintained at 31°C (required for *Gal80^{ts}* inhibition) I was unable to evaluate animals aged to 28 days. Nonetheless, the weaker but significant loss of neurons in the adult-specific knockdown condition implicates *babo* and *Smox* as functioning in mature glia and that they are required to support neuron maintenance.

Based on the adult-specific knockdown result, I hypothesized that *babo* would be expressed in mature glia. To test this, I examined the expression pattern of *babo* in developing and mature nerves. I utilized a transgenic fly line where the *Gal4* sequence was inserted into an intron in the *babo* coding region with a splice acceptor, multiple stops, and a minimal promoter sequence. This induces truncation of the *babo* transcript and expression of *Gal4*

in its place and should therefore be expressed wherever *babo* is expressed (Lee et al., 2018). In developing larval nerves, I examined co-localization of a nuclear reporter (*UAS-lamin::GFP*) driven by *babo-Gal4* expression with an antibody that specifically labels WG nuclei within larval peripheral nerves (*Oaz*) as well as the pan-glial nuclear protein Repo (Figure 10). All *Oaz*⁺ nuclei within larval nerves were GFP⁺/Repo⁺ (n=18 *Oaz*⁺ nuclei from n=3 larvae, Figure 10) indicating that *babo* was expressed in WG in peripheral nerves during development. Additionally, all Repo⁺/*Oaz*⁻ nuclei within the nerve were also GFP⁺, indicating that *babo* was also expressed in other nerve glia in addition to WG (n=123 Repo⁺/*Oaz*⁻ nuclei from n=3 larvae, Figure 10).

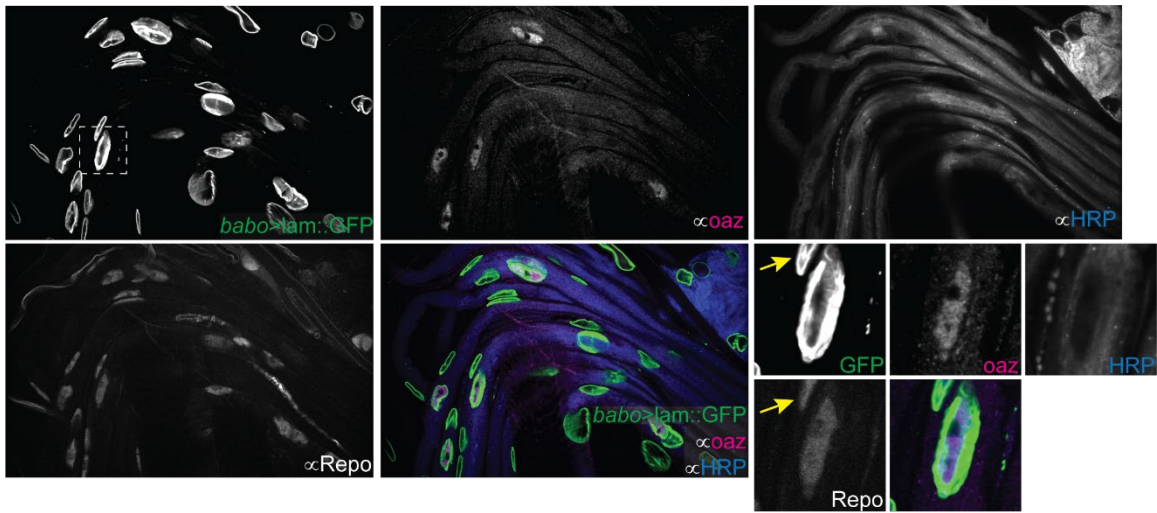


Figure 10 *babo* reporter expression in larval peripheral nerves. Visualization of *babo* reporter expression of nuclear GFP (green) in nerves co-labeled with axon (blue) and glial (magenta & gray) markers. Repo labels all glial nuclei whereas only WG nuclei are *Oaz*⁺ in the nerves. Higher magnification images from the box are shown in the bottom right showing a GFP⁺/*Oaz*⁺/Repo⁺ nucleus. Additionally, a GFP⁺/*Oaz*⁻/Repo⁺ nucleus is also present (arrow).

To test whether *babo* was expressed in adults, I combined the *babo-Gal4* with a nuclear reporter (*UAS-mCherry.NLS*) in a genetic background where WG were labeled independently with GFP (a *nrv2-GFP* protein trap which labels all WG membranes (Stork, Engelen, Krudewig, Silies, Bainton, & Klambt, 2008)). As expected, the positive control (*nrv2-Gal4*) exhibited nuclear reporter expression in nuclei contained within GFP⁺ WG at all timepoints tested (n=12 wings, Figure 11A-B). The experimental *babo-Gal4* wings also labeled nuclei within the GFP⁺ WG at all timepoints tested as well (n=12 wings, Figure 11A-B). Importantly, the only nuclei present within the nerve in this region are glial nuclei (Neukomm et al., 2014), indicating that *babo* is expressed in mature WG within the peripheral sensory nerve in the wing. To further validate that these were glial nuclei, I fixed wings expressing GFP in glutamatergic neurons and nuclear-mCherry under the control of *babo-Gal4* and stained for the pan-glial marker Repo. All mCherry⁺ nuclei within the axon bundle were also Repo⁺, confirming they are glial nuclei (Figure 11C-D).

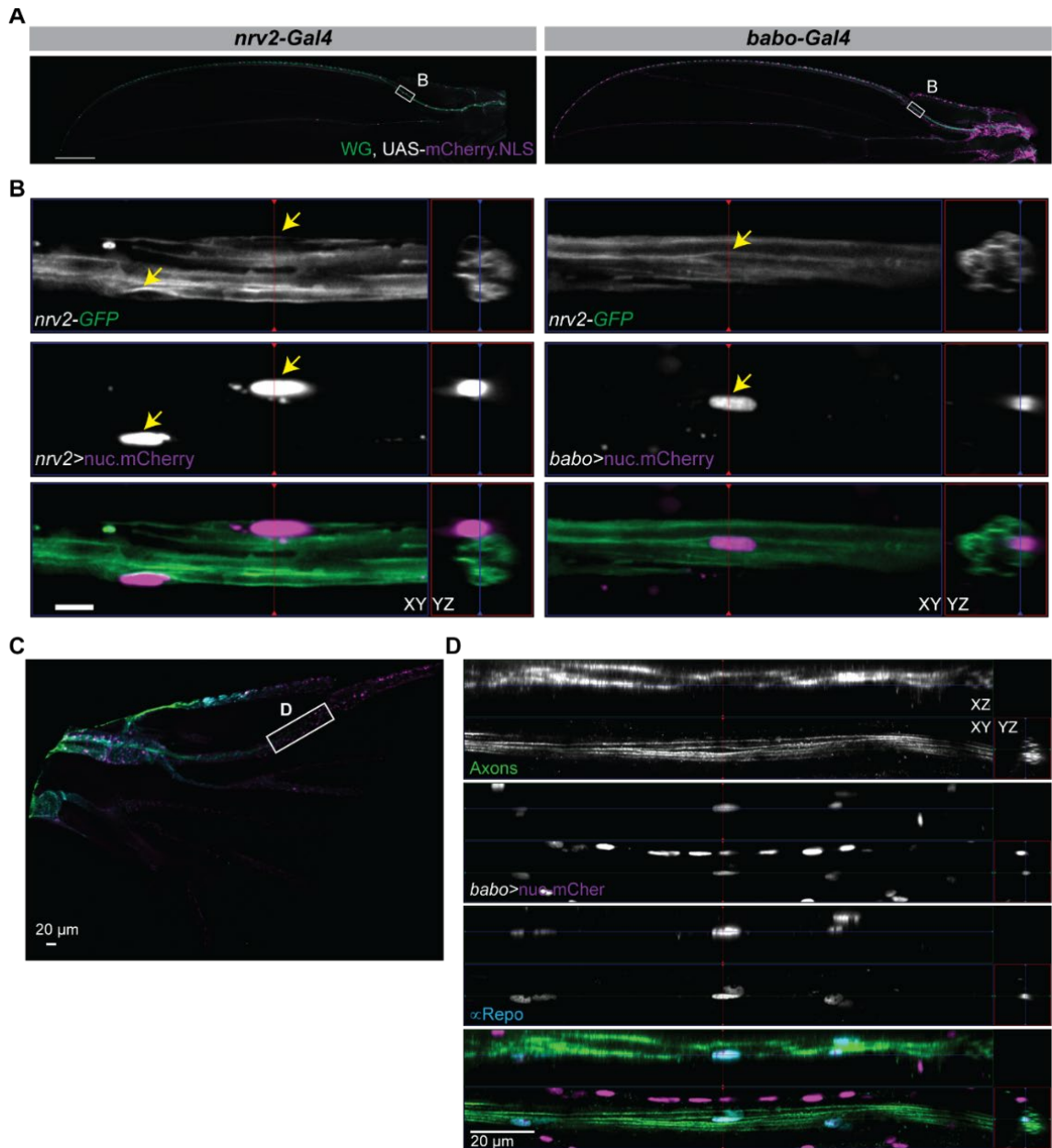


Figure 11 *babo* reporter expression in the adult wing L1 nerve. (A) Low-magnification images of the expression pattern of a nuclear mCherry reporter driven by *nrv2-Gal4* (left) or *babo-Gal4* (right) in combination with *nrv2-GFP* at 28 days scale bar 200 μm . (B) Higher-magnification images from the ROI in A showing mCherry⁺ nuclei surrounded by GFP⁺ WG scale bar 5 μm . (C) Low-magnification image of the proximal region of a fixed wing stained for GFP (axons) and Repo (glial nuclei) scale bar 20 μm . (D) Higher-magnification orthogonal images from ROI in C showing a mCherry⁺/Repo⁺ nucleus with the axon bundle scale bar 20 μm .

I also observed *babo* reporter expression in what appeared to be neurons (Figure 12A-B). To examine this further, I crossed the *babo-Gal4/UAS-mCherry.NLS* to a fly expressing GFP in glutamatergic neurons using the *QF/QUAS* system to independently label neurons. In addition to mCherry⁺ nuclei within the axon bundle (WG), all glutamatergic neurons in the wing examined had mCherry⁺ nuclei at all timepoints tested (Figure 12C-D). The reporter expression pattern of *babo* suggests that the Babo receptor is present in both mature glia and neurons in the wing. This expression in mature glia is consistent with the observation that knockdown of *babo* in mature glia is sufficient to cause neuron loss in aging animals and indicates a role for *babo* in mature glial function.

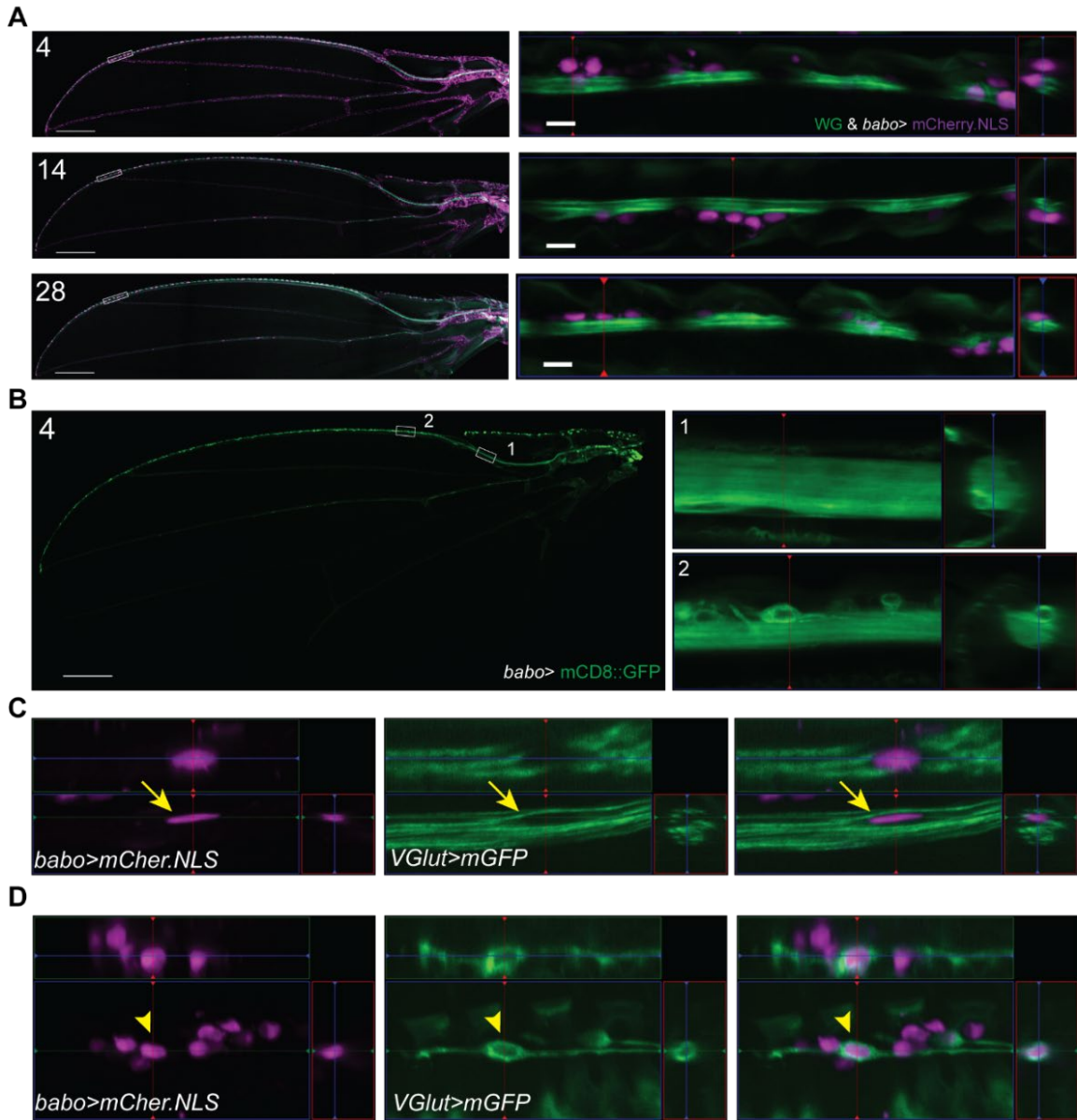


Figure 12 Expression of *babo* in mature neurons in the wing. (A) *babo* nuclear reporter (magenta) expression in the wing at 4 (top), 14 (middle), and 28 (bottom) days. ROIs from boxes shown to the right. *mCherry*⁺ (magenta) nuclei residing outside of *GFP*⁺ *WG* (green) resemble neuronal nuclei. (B) *babo* membrane reporter expression in the adult wing at 4 days. ROIs from boxes shown to the right showing dense labeling throughout the nerve bundle (1) and *GFP*⁺ cells that resemble neurons (2). (C & D) L1 nerve from animals expressing membrane-tethered *GFP* (green) in *VGlut*⁺ neurons along with a nuclear *mCherry* reporter (magenta) driven by *babo-Gal4* expression. (C) A *mCherry*⁺ *WG* nucleus (arrow) is seen within the bundle of axons in the proximal region. (D) The nucleus of a glutamatergic neuron is labeled with the *mCherry* reporter (arrowhead).

Results 1.7– Disruption of TGFβ signaling in glia does not alter axonal ensheathment

TGFβ molecules play crucial roles in tissue development and morphogenesis, so I examined whether loss of this pathway would affect glial development and morphology. I quantified the number of WG present in the nerve in control and WG-knockdown animals by using a genetically encoded nuclear reporter (*UAS-lamin::GFP*) (Figure 13). Knock down of *babo* or *Smox* in WG caused a slight increase in the number of WG in the nerve at 4 days (*nrv2>*: 24.9 ± 3.52 , *nrv2>lacZ*: 26.9 ± 3.37 , *nrv2>babo^{RNAi}*: 30.1 ± 3.54 , *nrv2>Smox^{RNAi}*: 29.0 ± 3.76 ; Figure 13). At 28 days, the number of WG nuclei in *babo* knockdown animals remained elevated compared to controls, but the number of WG nuclei in *Smox* knockdown animals was not significantly different from controls (*nrv2>*: 24.5 ± 3.40 , *nrv2>lacZ*: 26.2 ± 3.39 , *nrv2>babo^{RNAi}*: 29.5 ± 3.38 , *nrv2>Smox^{RNAi}*: 25.4 ± 6.76 ; Figure 13).

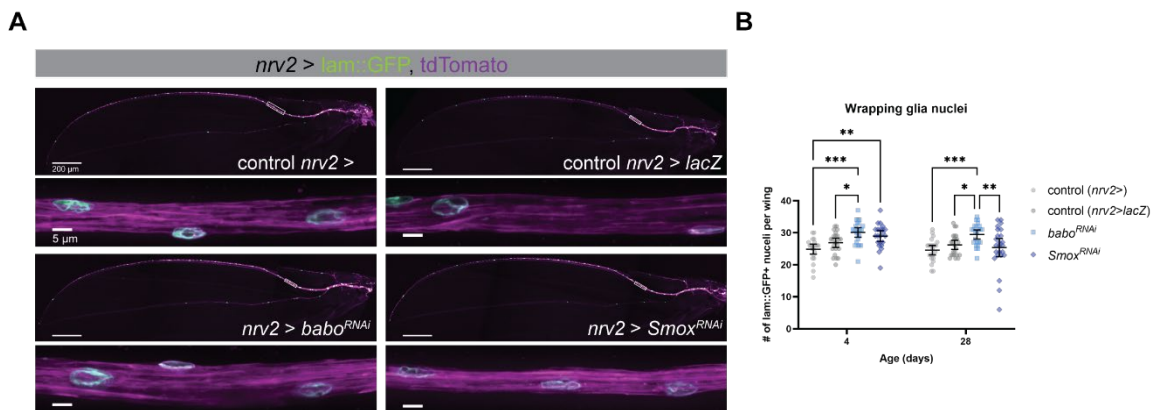


Figure 13 Increased number of WG nuclei when TGFβ activity is disrupted. (A) Low (top) and high (bottom) -magnification images of L1 wing nerves expressing nuclear GFP (green) and tdTomato (magenta) in all WG in the nerve scale bar 200 μm (top) and 5 μm (bottom). **(B)** Quantification of the number of GFP⁺ WG nuclei throughout the L1 nerve for each condition at 4 and 28 dpe. Two-way ANOVA with Tukey’s multiple comparisons test. Significance: p > 0.05, *, p < 0.05, **, p < 0.01, ***, p < 0.001.

I hypothesized that the increase in WG nuclei observed when *babo* or *Smox* was knocked down may be caused by a decrease in developmental apoptosis in these animals. I tested this by overexpressing *p35*, an inhibitor of caspases, to block apoptosis in WG (Hay et al., 1994). Overexpression of *p35* in WG phenocopied the increased WG nuclei observed when *babo* was knocked down in WG (*nrv2>* : 26.13 ± 2.740 , *nrv2>lacZ*: 27.00 ± 3.190 , *nrv2>babo^{RNAi}*: 31.21 ± 1.841 , *nrv2>p35*: 30.79 ± 3.912 ; Figure 14). Next, I evaluated whether increasing the number WG nuclei alone was sufficient to cause degeneration of glutamatergic neurons in aged animals similar to when *babo* is knocked down. Overexpression of *p35* in glia did not cause degeneration of glutamatergic neurons at 28 days (*repo>* : 38.67 ± 1.918 , *repo> babo^{RNAi}*: 35.76 ± 2.066 $p=0.0130$, *repo> p35*: 38.42 ± 1.251 $p=0.965$; Figure 14). This result indicates that increased glial numbers alone is insufficient to cause degeneration of glutamatergic neurons, and this phenotype, at least on its own, is likely not responsible for the degeneration that occurs in glial-*babo*-knockdown animals.

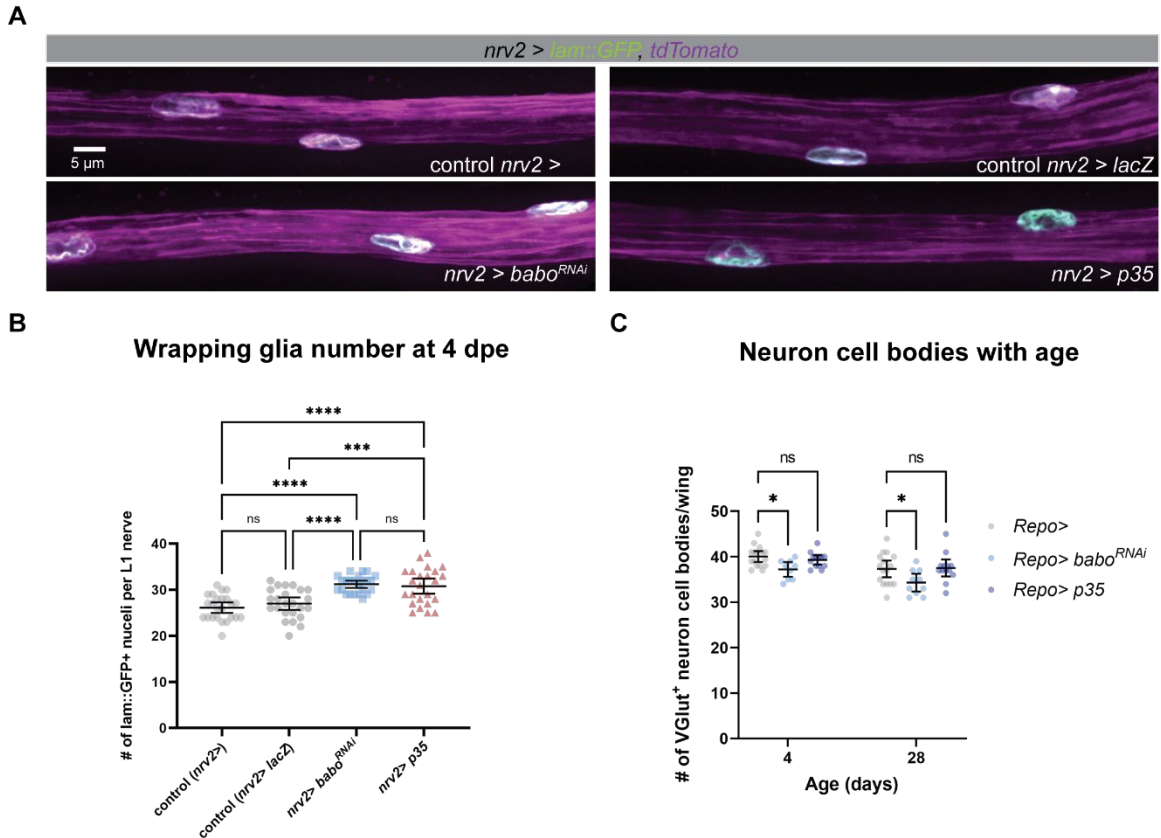


Figure 14 Caspase inhibition phenocopies *babo* knockdown for increased WG numbers but not decreased neuron survival. (A) Images from the L1 nerve showing expression of a nuclear GFP (green) and tdTomato (magenta) in all WG in control, WG-*babo*^{RNAi}, and WG-*p35*^{OE} flies. (B) Quantification of the number of WG nuclei in the L1 nerve from control, WG-*babo*^{RNAi}, and WG-*p35*^{OE} flies at 4 dpe. One-way ANOVA with Tukey's multiple comparisons test. (C) Quantification of the number of intact neuron cell bodies at 4 and 28 dpe from control, glial-*babo*^{RNAi}, and glial-*p35*^{OE} conditions. Two-way ANOVA with Dunnett's multiple comparisons test. Significance: $p > 0.05$, *, $p < 0.05$, **, $p < 0.01$, ***, $p < 0.001$, ****, $p < 0.0001$, ns, not significant.

To examine whether this change in WG numbers negatively impacts ensheathment of the nerve, I imaged glia in the L1 nerve using a genetically encoded fluorescent reporter (*UAS-tdTomato*). Overall coverage of the L1 nerve was not different at 4 and 28 days in *babo*^{RNAi} conditions. Furthermore, there were no obvious defects in glial morphology or coverage of the nerve in knockdown animals compared to controls at either timepoint (4 days: control: n=24 animals, *babo*: n=23, *Smox*: n=21; 28 days: control: n=21, *babo*: n=22, *Smox*: n=16; Figure 15A). Notably even in nerves with evident axonal debris and

significant neuron loss, glial ensheathment appeared intact (Figure 15A-B). Since WG directly ensheath axons in this nerve, I also assessed WG morphology specifically, by examining reporter expression in WG-specific knockdown conditions compared to controls. Similar to pan-glial knockdown, there were no obvious changes in morphology or coverage of the nerve by WG despite the presence of neurodegeneration (4 days:

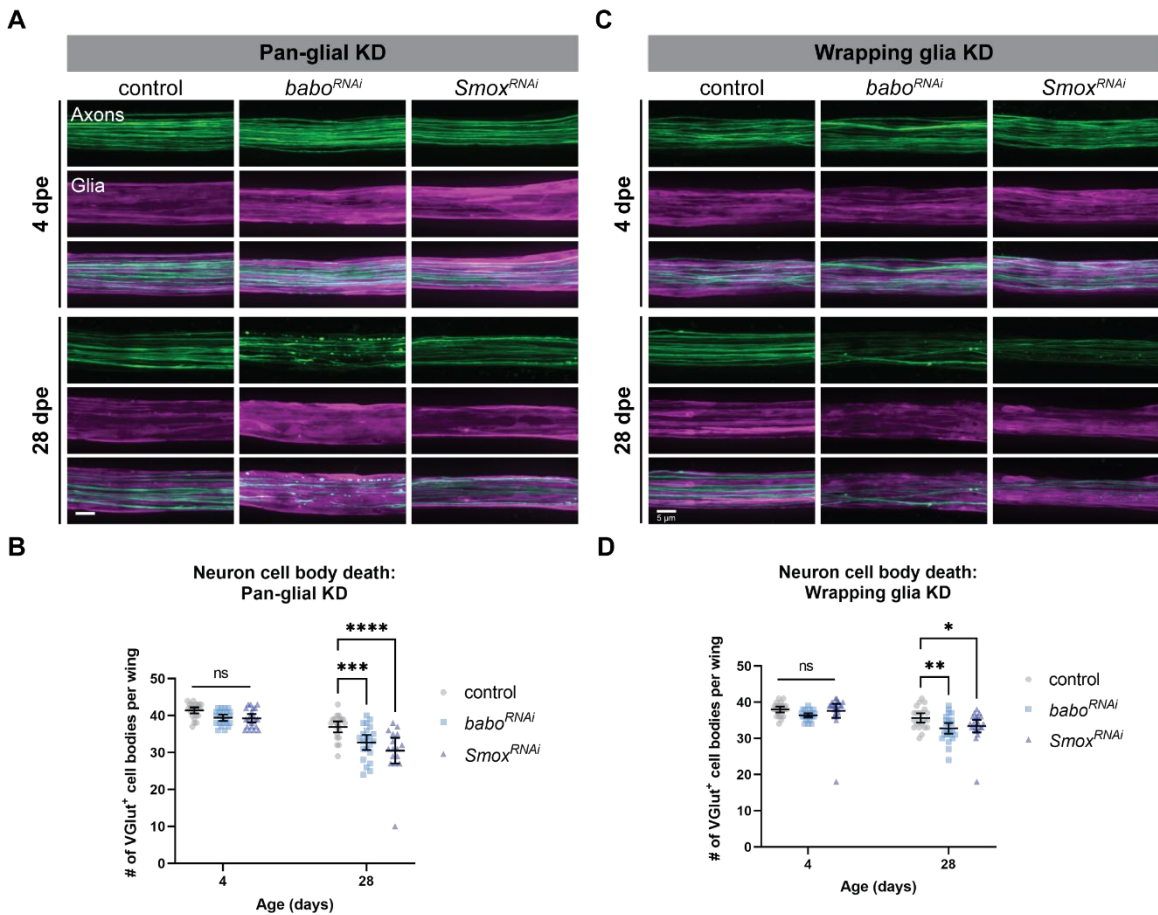


Figure 15 Glia appear morphologically intact in animals where TGFβ activity is inhibited in glia. (A) Image from the L1 nerve showing axon (green) and glia (magenta) morphology at 4 (top) and 28 (bottom) dpe in control and pan-glial knockdown conditions scale bar 5 μm. (B) Quantification of intact neuron cell bodies in control and pan-glial knockdown conditions. (C) Images from the L1 nerve showing axon (green) and glia (magenta) morphology at 4 (top) and 28 (bottom) dpe in control and WG-specific knockdown conditions scale bar 5 μm. (D) Quantification of intact neuron cell bodies in control and WG-specific knockdown conditions. (B&D) Two-way ANOVA with Dunnett's multiple comparisons test. Significance: $p > 0.05$, *, $p < 0.05$, **, $p < 0.01$, ***, $p < 0.001$, ****, $p < 0.0001$, ns, not significant.

control: n=23 animals, *babo*: n=23, *Smox*: n=23; 28 days: control: n=22, *babo*: n=24, *Smox*: n=23; Figure 15C-D).

While these results did not indicate that gross morphology of WG was disrupted upon knockdown of TGF β signaling, to examine whether axonal ensheathment was truly unperturbed required ultrastructural analysis of this nerve using transmission electron microscopy. I examined nerves from control, *babo*, and *Smox* pan-glial knockdown animals and found no evidence of defects in glial ensheathment at 28 days (control: n=3 animals, *babo*: n=5, *Smox*: n=4; Figure 7C-E & Figure S10). To quantify this form of multi-axonal ensheathment, I measured the wrapping index for each nerve using the electron micrographs (Matzat, Sieglitz, Kottmeier, Babatz, Engelen, & Klämbt, 2015). There was no significant difference in the wrapping index between conditions, although one nerve from the *Smox* knockdown condition did appear to have reduced ensheathment (control: 0.88 ± 0.020 n=4, *babo*: 0.84 ± 0.083 n=5, *Smox*: 0.81 ± 0.21 n=4; Figure 7F). Together, this data does not indicate that inhibiting TGF β in glia causes defects in glial ensheathment and would therefore not explain the degeneration observed in TGF β knockdown animals.

In summary, while there was a slight increase in the total number of WG in the adult nerve when TGF β signaling was inhibited, overall glial morphology and axonal ensheathment appeared normal.

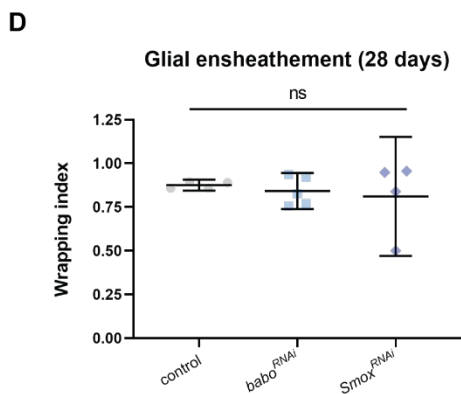
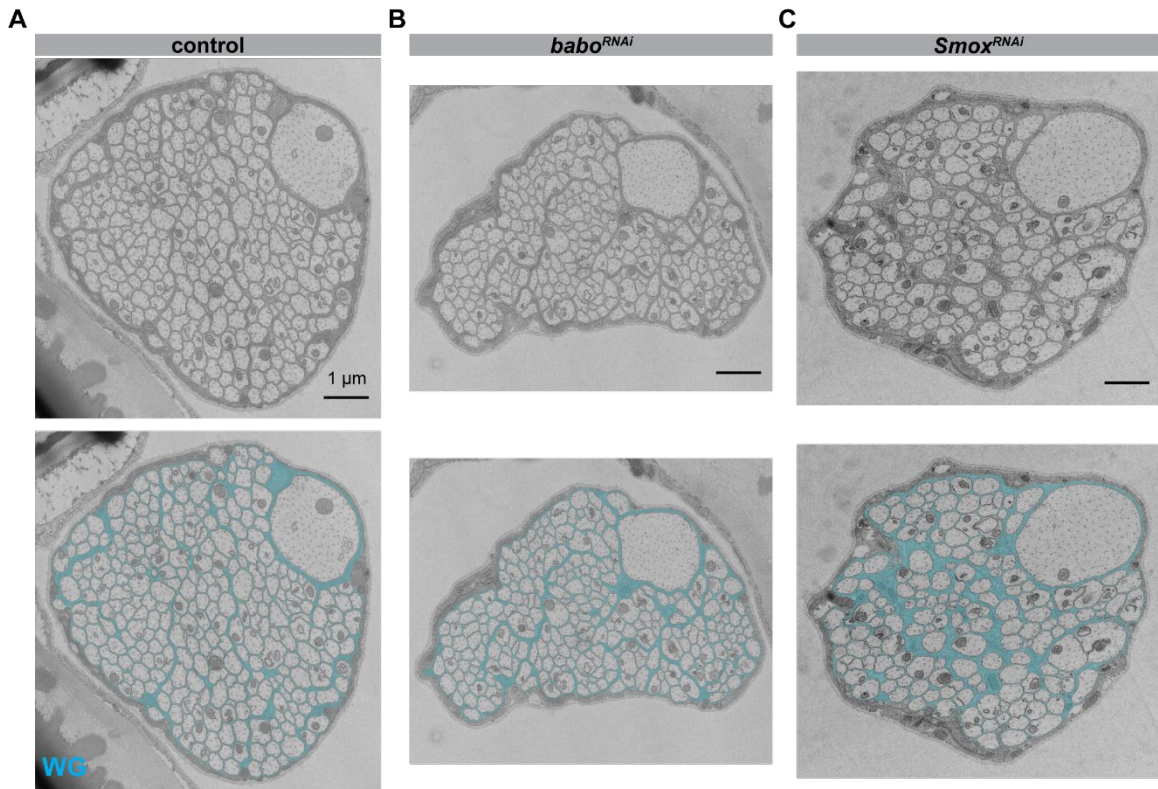


Figure 16 Glial ensheathment of axons appears intact when TGF β activity is disrupted in glial. (A-C) Electron micrographs of cross sections of the proximal region of the L1 nerve at 28 days from control (A), *babo* (B), and *Smox* (C) knockdown animals. WG are pseudocolored in cyan. (D) Quantification of the wrapping index [(individually wrapped axons + bundles of axons) / total axons] from electron micrographs. Data are represented as mean \pm 95% CI. One-way ANOVA with Dunnett's multiple comparisons test. Significance: ns, not significant.

Results 1.8 – Inhibiting Wallerian degeneration rescues age-dependent neurodegeneration caused by glial-knockdown of *babo*

In aging animals both the axons and cell body of the neurons were affected by *babo* knockdown in glia. This could result from a lack of glial support to the neuronal cell bodies, their axons, or both. The neuroprotective effects of Wld^S are known to specifically mediate injury-induced axon degeneration while it fails to block apoptosis in several contexts

(Beirowski et al., 2008; Deckwerth & Johnson, 1994; Hoopfer et al., 2006b). I tested whether promoting axon survival with Wld^S could save axons in aged *babo*^{RNAi} nerves, and possibly the cell body loss as well. I overexpressed *Wld*^S, in glutamatergic neurons to prevent WD in aged, *uninjured* control and *babo* knockdown animals and measured the effect on both axon and cell body integrity. Blocking WD rescued the axon degeneration at 28 days (control - Wld^S n=17, control + Wld^S n=19, *babo*^{RNAi} - Wld^S n=27, *babo*^{RNAi} + Wld^S n=20; Figure 17A-B) indicating that loss of *babo* in glia leads to activation of a Wld^S -sensitive axon degeneration pathway in aged, uninjured axons. Moreover, I found that suppressing axon degeneration with Wld^S also completely rescued neuron cell body loss (Figure 17A & C). These data are consistent with a similar finding that suppressing axon degeneration with Wld^S in a model of motoneuron disease (*pmn* mice) reduced subsequent cell death of neurons (Ferri et al., 2003). The simplest interpretation of this finding is that glial loss of Babo leads to activation of an axon degeneration pathway in neurons that also influences the survival of the cell body.

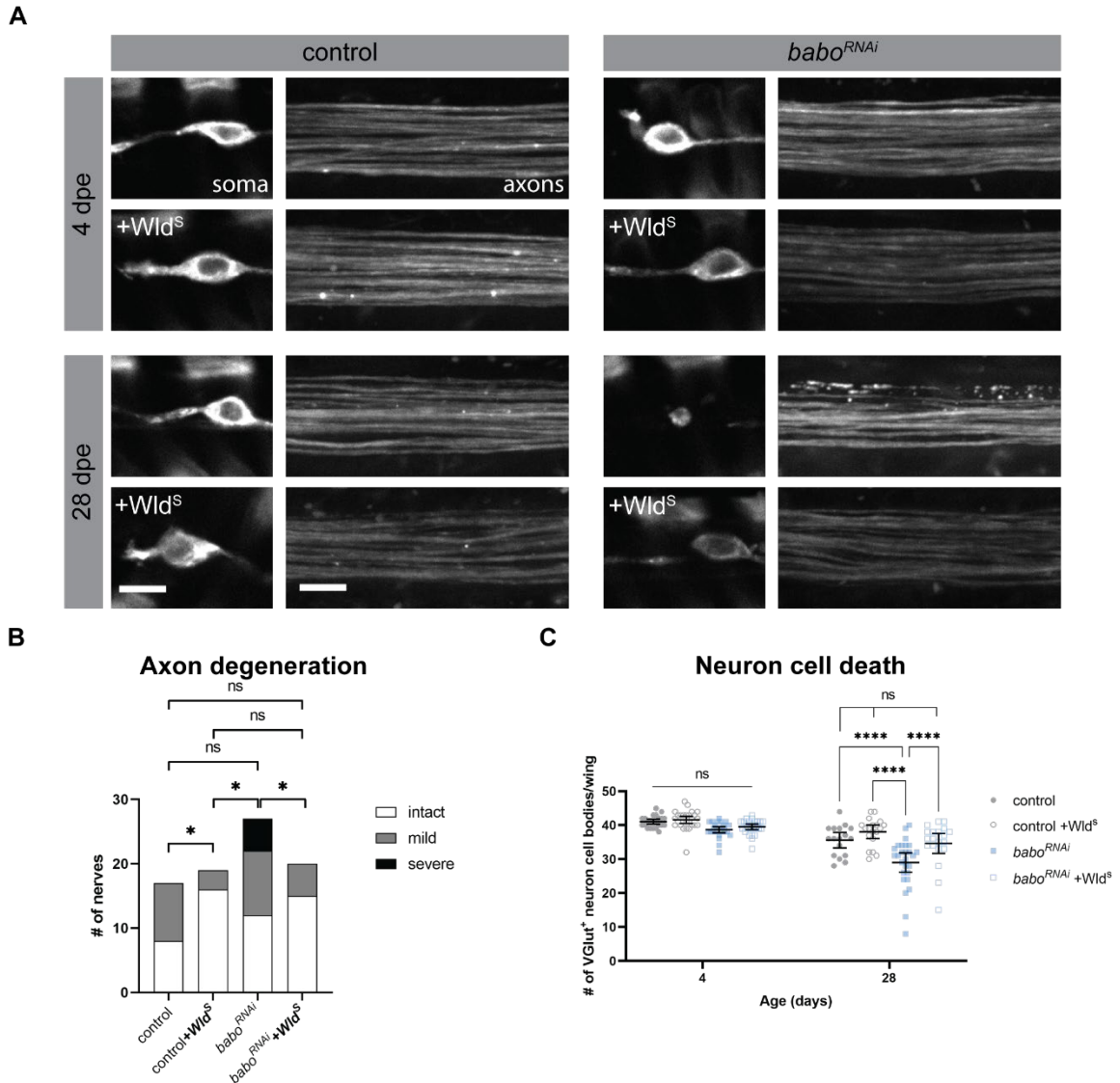


Figure 17 *Wld^S* overexpression in neurons rescues neurodegeneration in *babo* knockdown animals. (A) Representative images of neuron cell bodies and axons within the wing in control and *babo* knockdown animals at 4 (top) and 28 (bottom) days of age with and without *Wld^S* expressed in neurons. Scale bar 5 μ m. **(B)** Classification of axon integrity in control and *babo* knockdown animals at 4 and 28 days with and without *Wld^S*. Fisher exact probability test 2x3. **(C)** Quantification of the number of VGlut⁺ neuron cell bodies in the wing from control and *babo* knockdown animals with and without *Wld^S*. Data are represented as mean \pm 95% CI. Two-Way ANOVA with Tukey's multiple comparisons test. Significance: ns, not significant, *, $p < 0.05$, ****, $p < 0.0001$.

Results 1.9 – Genetic blockade of caspase-mediated cell death rescues neurodegeneration caused by *babo* knockdown in glia.

Since blocking WD rescued degeneration of both the axon and cell body, I next tested whether protecting the cell body could rescue axon degeneration as well. Caspases are part of a signaling cascade required for apoptosis, or programmed cell death. Caspase activity has been shown to be involved in many contexts of neuron cell death but in many cases are not involved in axon degeneration (Finn et al., 2000; Sagot et al., 1995; Whitmore et al., 2003). P35 is a potent inhibitor of a broad range of caspases and can block cell death in *Drosophila* neurons (Hay et al., 1994). To test whether activation of a cell death pathway contributes to neurodegeneration observed in glial-*babo* knockdown animals, I overexpressed *p35* in neurons while simultaneously knocking down *babo* in glia. Significantly more glutamatergic neurons survived when expressing *p35* than those lacking *p35* when *babo* was knocked down in glia (Figure 18). Interestingly, like the cell bodies, overexpression of *p35* in neurons rescued axon degeneration when *babo* was knocked down in glia (Figure 18). This result indicates that knockdown of *babo* in glia also induces caspase-sensitive destruction pathway in neurons. Furthermore, this caspase activity also influences degeneration of the axon in this *uninjured* aged context.

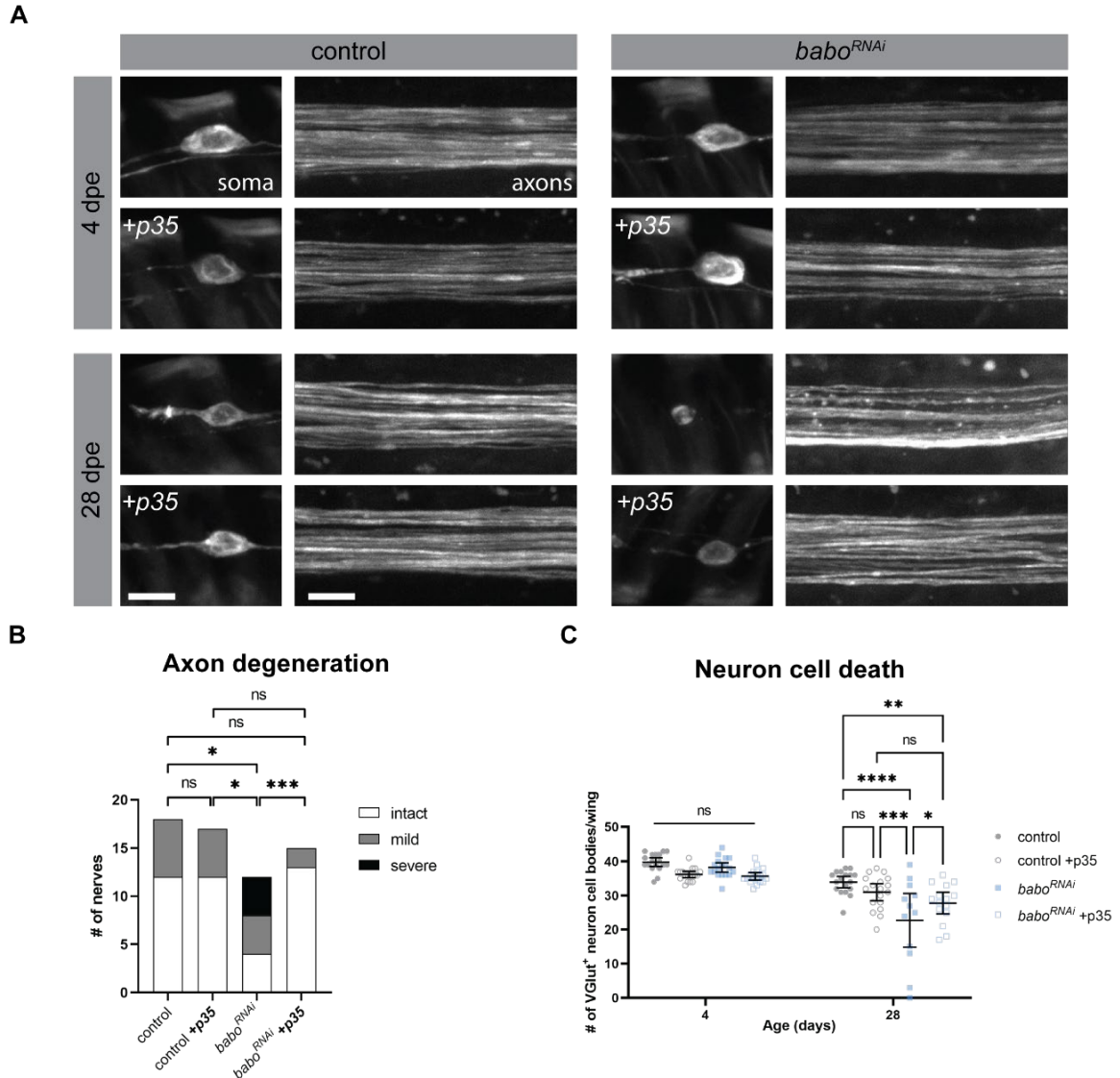


Figure 18 P35 rescues neurodegeneration caused by loss of *babo* in glia. (A) Representative images of neuron cell bodies and axons within the wing in control and *babo* knockdown animals at 4 (top) and 28 (bottom) days of age with and without *p35* expressed in neurons. Scale bar 5 μ m. **(B)** Classification of axon integrity in control and *babo* knockdown animals at 28 days with and without *p35*. Pairwise Fisher Exact Probability Test Shown (two-tailed, 2x3). **(C)** Quantification of the number of VGLut⁺ neuron cell bodies in the wing from control and *babo* knockdown animals with and without *p35*. Graph: mean \pm 95% CI. Statistics: 2-Way ANOVA with Tukey's multiple comparisons test. Significance: ns= not significant, *= p < 0.05, **= p < 0.01, ***= p < 0.001, ****= p < 0.0001.

Results 1.10 – Disrupting glial TGF β activity alters metabolic function of glia

One way that glia support axons is by providing metabolites to fuel energy demands of the axon (Fünfschilling et al., 2012). I hypothesized that reduced TGF β signaling in glia may reduce their metabolite output to neurons. I therefore examined whether metabolism was altered in WG when TGF β signaling was perturbed. Using a genetically encoded ATP sensor, I measured the relative ATP concentrations in control (UAS-lacZ) WG and WG where *babo* or *Smox* were knocked down (Lobas et al., 2019). In both knockdown conditions, ATP levels were increased around 46% and 32% respectively compared to controls (Figure 19). In cells, ATP is primarily produced via glycolysis and mitochondrial respiration. In several contexts it has been shown that glia primarily utilize glycolysis while neurons rely on mitochondrial respiration (Fünfschilling et al., 2012; Volkenhoff et al., 2015). I next artificially increased mitochondrial biogenesis in WG by overexpressing the transcriptional co-activator *srl* (PGC-1 α in mammals)(Dominy & Puigserver, 2013). This caused a similar 36% increase in ATP over control levels compared to *babo*^{RNAi} and *Smox*^{RNAi} conditions and was not significantly different from either (p=0.6206 and p=0.9996 respectively; Figure 19). Interestingly, inhibition of mitochondrial biogenesis in WG by knockdown of *Mitf* (*TFEB* in mammals) or *cnc* (*Nrf2* in mammals), also caused a 110% and 60% increase in ATP respectively (Dominy & Puigserver, 2013)(Figure 19). This increase was significantly greater than that of *srl*^{OE} for both conditions (p<0.0001, p=0.0014) indicating a differential magnitude of affect from increasing versus decreasing mitochondria biogenesis. Finally, I tested whether blocking export of metabolites from WG would impact overall ATP levels by knocking down *Bsg* the adaptor protein required for plasma membrane localization of all monocarboxylate

acid transporters (MCTs) (Besse et al., 2007; Halestrap & Wilson, 2012; Kirk et al., 2000). Inhibiting MCTs did lead to increased ATP levels in WG suggesting they had increased metabolic activity. Together, these results suggest that TGF β signaling participates in regulating metabolic homeostasis of WG.

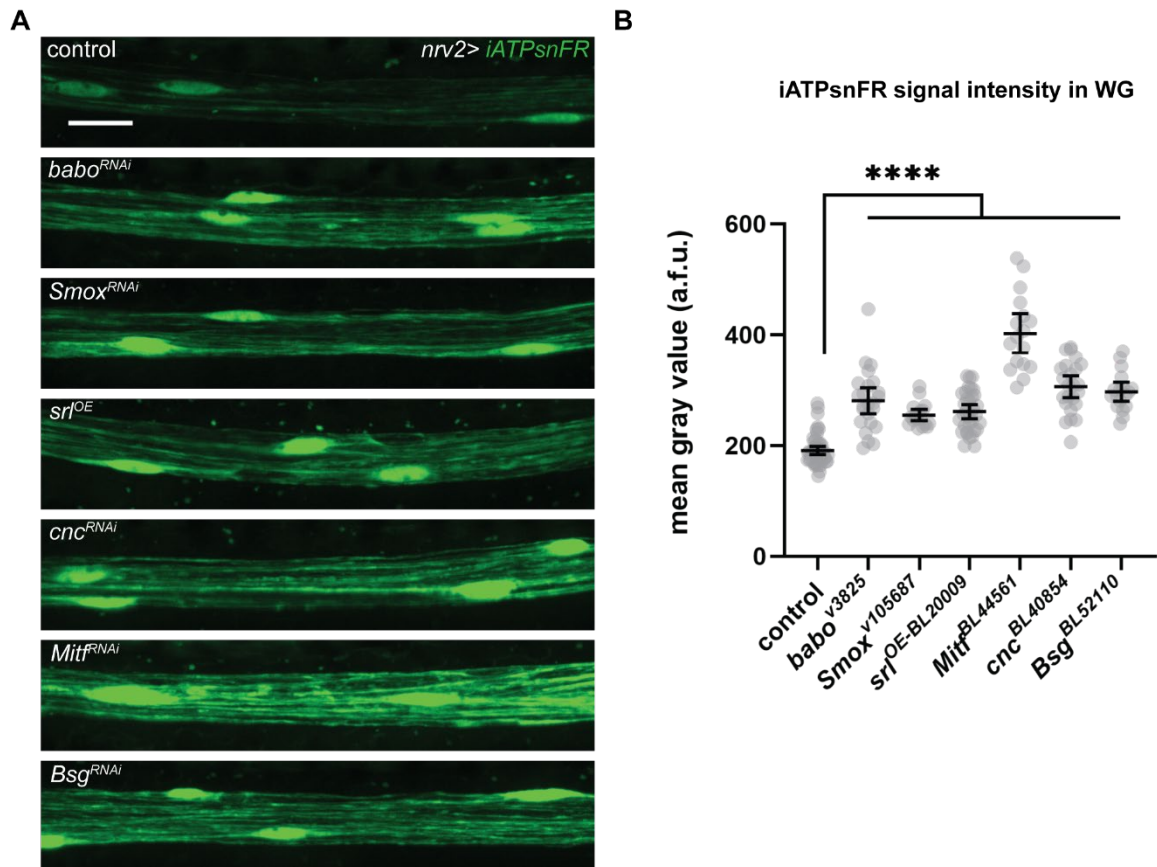


Figure 19 Higher levels of ATP present in WG in conditions affecting TGF β activity, mitochondrial, and metabolite transport regulation. (A) Images from the L1 nerve from animals expressing an ATP sensor (iATPsnFR) in WG in control and experimental conditions at 4dpe. **(B)** Quantification of the mean intensity of the ATP sensor in the nerve (excluding nuclei) across conditions. Data represented as mean \pm 95% CI. One-way ANOVA with Tukey's multiple comparisons test. ****, $p < 0.0001$.

Increases in ATP levels could be caused by increased mitochondrial flux or increase in glycolysis. To examine possible changes to mitochondria in particular I expressed a fluorescent sensor (*roGFP2-Grx1*) and targeted it to mitochondria that responds to different wavelengths of light depending on how reduced or oxidized it is (Albrecht et al.,

2011). Knockdown of *babo* resulted in mitochondria being more reduced, (Figure 20A-B). Similarly, *srl*^{OE} also resulted in more reduced mitochondria (Figure 20). Conversely, inhibition of mitochondria biogenesis (*Mitf*^{RNAi} and *cnc*^{RNAi}) resulted in more oxidized mitochondria (Figure 20A-B). Similarly, blockade of monocarboxylate acid transport (*Bsg*^{RNAi}) also resulted in more oxidized mitochondria (Figure 20A-B). In both increased ATP levels and reduction of mitochondria, loss of *babo* phenocopies *srl* overexpression suggesting a possible role for *babo* in mitochondrial regulation in glia.

I next tested whether the dysregulation of glial mitochondria or metabolism observed in WG when TGF β signaling was disrupted were sufficient to cause degeneration of aged neurons on their own. Using the uninjured aging paradigm, I aged control, glial-knockdown, and glial-overexpression animals and counted the number of intact glutamatergic neurons per nerve at 28 dpe. Blockade of metabolite transport by knockdown of *Bsg* was sufficient to cause neuron loss in aged animals (Figure 20C). Likewise, increasing mitochondria biogenesis (via *srl* overexpression) caused decreased neuron survival (Figure 20C). These results indicate that blocking monocarboxylate acid transport or excessive mitochondrial biogenesis in glia lead to increased intracellular ATP levels in WG and are sufficient to cause decreased survival of sensory neurons in the wing.

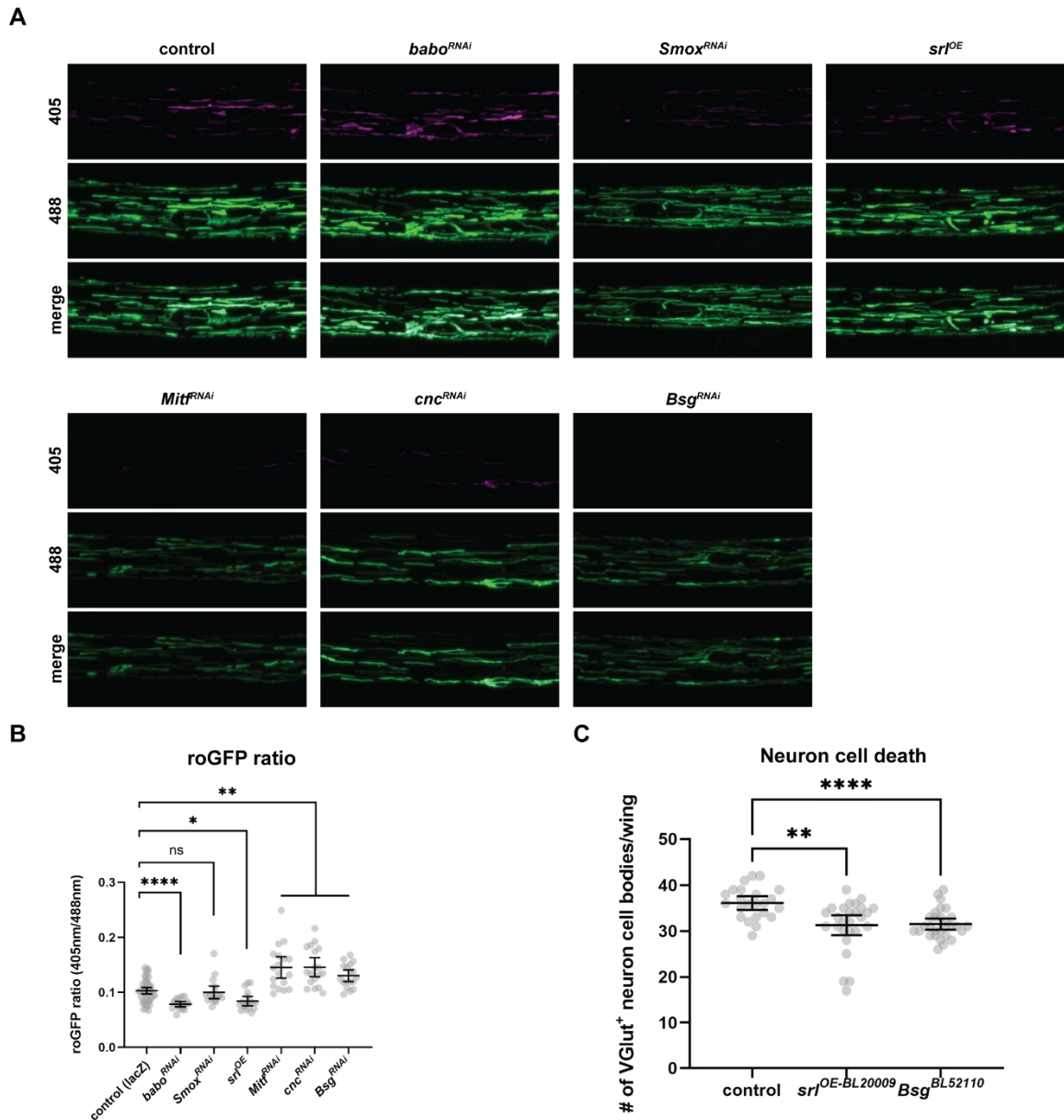


Figure 20 Mitochondria redox state is altered by disruption to TGF β activity in glia. (A) Images from the L1 nerves of 4 dpe animals expressing a mitochondria-targeted RedOx ratio metric sensor (*roGFP2-Grx1*) in glia in control and experimental conditions. The ratio of signal from 405 nm light versus 488 nm light indicates the oxidation state (405:488). The 405 (top), 488 (middle), and merged (bottom) signals are shown for each condition. (B) Quantification of the average 405:488 ratio determined from surfaces created in Imaris. (C) Quantification of the number of intact VGlut⁺ cell bodies in the L1 nerve from aged 28 dpe control and experimental animals where RNAi or OE constructs were expressed in WG. Data represented as mean \pm 95% CI. Brown-Forsythe and Welch ANOVA with Dunnett's T3 multiple comparisons test. Significance: *, $p < 0.05$, **, $p < 0.01$, ***, $p < 0.001$, ****, $p < 0.0001$, ns, not significant.

DISCUSSION I

Discussion 1.1 – Glial TGF β activity is required for neuron maintenance

In this study, I sought to identify genetic pathways that modulate glial support of axons *in vivo*. I focused on the L1 wing nerve of adult *Drosophila*, as it contains some of the longest axons in the fly, and the wrapping glia (WG) that ensheathes them separate axons at the single axon level. Through a genetic screen to identify genes with roles in promoting axon survival, my colleagues and I assayed a library consisting of most of the secreted and transmembrane proteins encoded in the *Drosophila* genome. We identified an array of molecules that, when depleted selectively from glia, lead to axon degeneration. Components of the TGF β superfamily were over-represented in our candidates from this screen, and I have shown that loss of glial TGF β signaling—ligands, receptors, or downstream signaling molecules—leads to age-dependent axon degeneration and neuronal loss. Surprisingly, I found that providing Wld^S to neurons was sufficient to prevent neurodegeneration caused by reduced TGF β signaling in glia as was expressing the caspase inhibitor P35. From these data, I propose that TGF β receptor signaling in glia normally functions to promote axon maintenance, and this support is required to sustain neuronal survival over the animal's lifespan.

Discussion 1.2 – Glial ensheathment is critical to long-term axon maintenance

The intense ensheathment of axons by wrapping glia in the adult L1 wing nerve suggests that isolating individual axons in this tissue is critical for neuronal function, maintenance, or both. It is also worth noting that this ensheathment creates a physical barrier that likely prevents axons from directly accessing metabolites outside the nerve needed to support

their activity. This anatomical arrangement suggests that glia act as the go-between and provide support to the axons they enwrap. Using a new, highly specific split-Gal4 line, I showed that ablating most of the WG in the adult peripheral nerve in the wing caused robust age-dependent neurodegeneration. These results are remarkably similar to what has been seen in vertebrate models of CMT where loss of myelinating glia results in neurodegeneration in peripheral nerves (Adlkofer et al., 1995; Verhamme et al., 2011). Whether the loss of WG in the fly leads to axon degeneration because of a loss of metabolic support, as is observed in mammals (Fünfschilling et al., 2012; Y. Lee et al., 2012), or is a direct result of a lack of survival cues through TGF β receptor activation in glia (or other signaling mechanisms) remains to be fully defined. However, my findings that inhibition of *babo* in glia results in altered ATP levels and changes to the oxidation state of glial mitochondria point to a role for this pathway in regulating mitochondria and metabolic function of glia. Together, this data supports the use of the L1 wing nerve of *Drosophila* as an excellent model to explore how glia support axon maintenance and function.

Discussion 1.3 – Disruption to glial TGF β does not impair glial ensheathment

One could imagine that disruptions in the physical association between axons and glia could indirectly disrupt signaling between them, for instance by impinging on the ability of glia to provide metabolites or survival cues to axons. Conversely, reduced ensheathment could presumably impair the ability of glia to maintain proper extracellular ion concentrations causing disruptions to axon integrity like is seen in the glial *Ncc69^{RNAi}* condition (Figure 6; Leiserson et al., 2011) and the homologous NKCC1b mutant zebrafish (Marshall-Phelps et al., 2020). However, reduced glial ensheathment does not appear to

explain the phenotypes reported here in *babo* and *Smox* knockdown animals. Live imaging and ultrastructural analyses both indicate that glia remain tightly associated with axons in these knockdown animals. Additionally, knockdown of either *babo* or *Smox* did not cause a decrease in WG numbers, but rather an increase. This result is consistent with previous literature on the role of TGF β receptor activation in developmental apoptosis (D'Antonio et al., 2006; Parkinson et al., 2001). Indeed, inhibiting apoptosis in WG phenocopied the increase in WG numbers observed in *babo*^{RNAi} indicating that this phenotype was likely caused by *babo/Smox* signaling during development of the nerve. However, this increase in WG is likely not responsible for the age-dependent neurodegeneration present in *babo*^{RNAi} conditions since adult-specific knockdown was sufficient to induce neurodegeneration. Furthermore, blocking apoptosis in glia did not cause neuron loss at 28 days as was observed when *babo* or *Smox* were knocked down in glia. This indicates that having increased glial numbers alone in the nerve is not sufficient to cause neuron loss and I, therefore, propose that this data instead points to a direct signaling role for glial *babo/Smox* activation in promoting neuron maintenance.

Questions remain as to the precise role of the TGF β pathway in glia→axon support, however, the data presented here points to a possible role in regulating mitochondria biogenesis. Inhibiting members of both branches of the TGF β superfamily (TGF β and BMP) in glia caused neurodegeneration in aged animals. Specifically, the TGF β receptor Babo appears to be required in WG to support axons while BMP ligands produced by WG likely signal to other glial cells and are required for neuron maintenance. This suggests a multi-cellular signaling network between different glial subtypes, as well as glia to neurons, that act together to promote neuron survival. Does Babo signaling in WG regulate

activity-dependent modulation of metabolite production for axons? Is it instead required as a constitutive signal to maintain MCTs at the membrane? Or is it involved in something else entirely? These questions are complex and further studies will be needed to fully define Babo's role. Future studies should focus on this pathway's role in transcriptional regulation as Babo phosphorylates and activates the Smad transcription factor Smox (Upadhyay et al., 2017). Smox has the potential to modify many genetic pathways simultaneously, and given that loss of Smox phenocopies Babo depletion, our data argue that at least part of the ability of TGF β signaling to support axon maintenance involves gene regulation. Identifying the key transcriptional targets for Smox that promote this pro-survival function in axons will be an exciting next step in understanding the full array of molecules involved in glial support of axon maintenance.

Discussion 1.4 – Babo and Smox act in mature glia to promote axon maintenance

Is TGF β signaling required during development or in the adult to support axon survival? Using a genetically encoded reporter, I found that *babo* appears to be expressed in glia in the adult wing, supporting a role for this receptor in mature glia. In line with this observation, conditional knockdown of *babo* or *Smox* specifically in mature glia was sufficient to induce neurodegeneration indicating its requirement in mature glia for neuron survival. The adult-specific knockdown was modest compared to the constitutive knockdown conditions, and this could indicate that *babo/Smox* are required both during development and in the mature nerve. However, there were crucial differences between these experimental approaches that make direct comparison challenging. Most notably, due to lethality of these animals when raised at 31°C (necessary for adult-specific knockdown),

I could only examine animals out to 14 days rather than 28 days used in other experiments. It remains possible, however, that *babo* does play a role in developing glia that contribute to the degeneration of aged neurons. The expression of the *babo* reporter in larval nerves suggests that Babo is expressed in developing WG. Additionally, I found that inhibition of *babo* and *Smox* expression caused a slight increase in WG nuclei numbers in the L1 nerve, directly implicating this signaling in WG development in the L1 wing nerve. Further experiments to separate developmental versus adult roles for this receptor in glia will clarify the context-dependent actions of this pathway. Nevertheless, together this data supports a role for *babo/Smox* activation in mature glia to promote neuron survival.

Discussion 1.5 – Babo in glia supports neuron maintenance by directly supporting axons

The role of the axon in survival of the cell body appears complex, and context dependent. For instance, during development, a lack of trophic support in growing axons leads to death of dorsal root ganglion (DRG) cell bodies (Deckwerth & Johnson, 1994). This allows sensory ganglia to scale DRG numbers according to segment specific changes in the size of the sensory field. Once mature, however, the majority of sensory and peripheral motor axons exhibit robust regenerative capacity when axotomized *in vivo* (Cajal et al., 1991) indicating the requirement for trophic molecules from distal axons in promoting cell body survival is transient. In the context of most neurodegenerative diseases, it remains unclear which part of the cell becomes sick first. Does the axon degenerate, fail to support the neuronal soma, and result in cell death? Alternatively, does the cell body die and axon degeneration follows as a result? In these experiments, I found that axon degeneration and neuronal cell loss was coordinately timed in both glial-ablated and TGF β knockdown

animals. As such, I am unable to determine which compartment of the cell (i.e., axons versus cell body) began to degenerate first.

An alternative approach to determine where neurodegenerative mechanisms impinge on a healthy neuron (axon versus soma) is to block key genetic pathways that drive axonal degeneration versus cell death. Driving expression of the *Wld^S* molecule in neurons is an effective way to suppress axon degeneration without altering apoptotic signaling pathways (Adalbert et al., 2006; Beirowski et al., 2008; Deckwerth & Johnson, 1994) and can be used to probe whether neurodegeneration is driven by primarily the axon versus the cell body. In the case of the *progressive motorneuronopathy (pmn)* mouse, which exhibits age dependent motor axon degeneration followed by motoneuron cell death, simply supplying *Wld^S* was sufficient to block axon loss and suppress motoneuron death (Ferri et al., 2003). These data strongly suggested that axon loss was the primary driver of motoneuron loss in this disease model. Since this initial exciting discovery similar approaches have been used with *Wld^S* and other components of the axon death signaling cascade like *Sarm1* (Osterloh et al., 2012), to probe the molecular programs driving neurodegeneration in a number of disease models (reviewed in (Coleman & Höke, 2020)). In some cases, blocking axon degeneration can profoundly block neurodegeneration (Ferri et al., 2003; Henninger et al., 2016b; Samsam et al., 2003; Turkiew et al., 2017) while in others, it has surprisingly little effect (Adalbert et al., 2006; Beirowski et al., 2008; Fernandes et al., 2018; Fischer et al., 2005; Peters et al., 2018). The latter observation does not rule out a role for *Wld^S* or *Sarm1* in these diseases, it only reveals that blockade of the axon death pathway alone is not sufficient to alleviate neurodegeneration in these models of human disease.

Applying this strategy to my work, I found that preventing Wallerian degeneration in *uninjured*, normally aging animals rescued axon and neuron cell loss caused by *babo* knockdown in glia. This suggests that loss of *babo/Smox* signaling in glia results in activation of a Wld^S-sensitive axon death signaling cascade to drive axon loss and increased neuron cell loss. It is notable that Wld^S was able to rescue age-dependent degeneration in glial-*babo* knockdown conditions, but not in the sensitized injury paradigm where axons expressing Wld^S were severed *and* TGF β genes were knocked down in glia. One could imagine that an aged axon that remains attached to its cell body is healthier than an axon completely devoid of support from its own cell body. Therefore, the ability of Wld^S to prevent spontaneous axon degeneration in an intact aged neuron is likely to be different than its potency at preventing degeneration of a severed axon when glial support is also impeded. The difference in these two sensitizing conditions likely explains the difference in the ability (or lack thereof) of Wld^S to rescue axon degeneration when *babo* is also knocked down in glia. I would speculate that loss of *dSarm* in axons would result in a similar phenotype (i.e., rescue of axons), but technical limitations precluded my doing this experiment. In line with this, I found that Wld^{S+} injured axons did not survive as well when WG were ablated. This exciting result provides evidence that severed Wallerian degeneration-resistant axons rely on glial ensheathment in order to maintain their integrity *in vivo*. While it remains possible that Wld^S directly protects the neuron cell bodies, this would depart from the body of data supporting an axon-specific role for Wld^S in suppressing neurodegeneration. Therefore, the simplest interpretation of my data is that *babo* is required in glia to support axon maintenance and its loss results in progressive axon degeneration that can culminate in neuron cell death.

Discussion 1.6 – Blocking caspase activity rescues degeneration caused by loss of *babo*

Just as Wld^S rescued both axon and somatic death in neurons, inhibiting caspases in neurons prevented degeneration of both compartments as well. This result was somewhat unexpected as in several studies examining neurodegeneration, unlike Wld^S, inhibiting apoptosis fails to prevent Wallerian degeneration (Beirowski et al., 2008; Hoopfer et al., 2006a). However, P35, the tool used in this study, broadly suppresses caspases and there are examples of caspase involvement in axon and neurite degeneration (Kuo et al., 2006; Nikolaev et al., 2009; Simon et al., 2012; Williams et al., 2006). It therefore remains possible that P35 could be acting within the axon to suppress axon degeneration in aged *babo* knockdown animals. Further experiments to target specific caspase activity selectively within the neuron soma would provide further insights to clarify these results.

Together, rescue of neurodegeneration in *babo* knockdown animals by either Wld^S or P35 indicates that both Wallerian degeneration and caspase-dependent cell death pathways are activated in neurons in this context. Because blocking either of these pathways is sufficient to protect the whole neuron, this suggests that there is reciprocal signaling between the axon and the soma within these neurons such that the survival of each compartment is influenced by the status of the other. If the axon undergoes Wallerian degeneration this somehow activates cell death of the soma in these neurons while if the soma degenerates, the axon would also degenerate.

Discussion 1.7 – Protection of axons by Wld^S *in vivo* requires glia

A yet-to-be explained phenomenon in the study of axon degeneration is the observation that Wld^S is a much more potent suppressor of Wallerian degeneration *in vivo* as compared to *in vitro*. Severed Wld^{S+} axons survive for many weeks *in vivo* (Adalbert et al., 2005; Lunn et al., 1989), yet in purified neuron cultures, protection persists for a matter of days (Buckmaster et al., 1995; Wang et al., 2005). While there are many differences between these environments, one striking difference is the presence or absence of a glial sheath around axons. I found that ablating WG significantly impaired the ability of Wld^S to protect injured axons *in vivo* suggesting that when axons lack a neuronal cell body their survival is highly dependent upon glial support.

Discussion 1.8 – Glial metabolism and axon maintenance

It has previously been shown that glia that ensheath axons can provide metabolic support to the axon (Fünfschilling et al., 2012; Lee et al., 2012; Nave, 2010; Saab et al., 2016). The nature of this support, particularly whether it is dynamic and can respond to changes in neural activity, remains to be defined for all glial subtypes that ensheath axons. However, work from Saab et al. 2016, provided evidence for activity-dependent regulation of metabolic support by glia. This group found that a glucose transporter GLUT1 was regulated by activation of NMDA receptors on glia both by expression and insertion of the transporter into the membrane. This provides a mechanism for glia to detect axonal activity via glutamate-NMDA receptor signaling and uptake their glucose in response and produce more lactate that can be released for axonal consumption. The authors put forth that calcium entry drives insertion of GLUT1 into the membrane, but it is still unknown how

changes to its expression are regulated by NMDA activity. It is possible that TGF β signaling (or another pathway) could be involved in this process.

The coupling of glia-axon metabolic activity suggests that glial metabolism is tightly regulated to optimize axon support. Previous work illustrates that glycolysis is preferential used by glia and mitochondrial respiration by neurons (Fünfschilling et al., 2012; Y. Lee et al., 2012; Nave, 2010; Volkenhoff et al., 2015). However, it is notable that the glia in the peripheral L1 wing nerve have an extensive mitochondrial network that runs throughout their processes. Furthermore, mitochondria are indispensable in peripheral nerve glia in mice and their dysfunction causes demyelination and axon degeneration of both small and large caliber axons (Viader et al., 2011, 2013). Consequently, disrupting mitochondria function in SCs shifts the balance of lipid metabolism away from synthesis in favor of oxidation and this shift produces toxic species that cause axons to degenerate (Viader et al., 2013). Considering these observations, it is reasonable to surmise that WG in *Drosophila* peripheral nerves balance similar metabolic processes and disruption to one would likely impact the efficiency of the others.

I found that disrupting *babo* in glia led to changes in oxidation state of mitochondria that mimicked those caused by forced overexpression of mitochondrial genes (*sr1^{OE}*). This was the opposite of what happened when mitochondrial biogenesis genes were knocked down (*Mitf^{RNAi}* & *cnc^{RNAi}*). This could indicate a role for *babo* in inhibiting mitochondria biogenesis in glia. It has been shown in the larval fat body that loss of *Daw* signaling through *babo* and *Smox* results in increased mitochondrial respiration and expression of nuclear-encoded mitochondrial genes (Ghosh & O'Connor, 2014). Similar transcriptional control may be present in WG such that *babo* acts to limit mitochondria biogenesis, constitutively

or dynamically, to maintain a proper balance between metabolic pathways. Therefore, disruption to *babo* signaling would cause this balance to be lost resulting in increased mitochondrial biogenesis and respiration. Consistent with this prediction, both *babo* knockdown and ectopic mitochondria biogenesis resulted in similar changes to both intracellular ATP levels and mitochondria oxidation state. Further studies are required to assess the link between *babo* activation, mitochondria biogenesis, and neurodegeneration to determine the direct versus indirect nature of these observations. For instance, increased mitochondria activity could cause a decreased pool of metabolites available to the axons, or alternatively it could cause an increase in toxic species that directly damage neurons. Future studies should address both of these possibilities. Nonetheless, these results provide a causative link between *babo*, metabolic activity of glia, and degeneration of neurons.

Given the known roles of glia in providing metabolic support to axons, one could imagine that disrupting metabolite transport would also negatively impact axon survival. Indeed, disrupting metabolite transport did cause degeneration of neurons in aged animals. One might argue that blocking transporters could also prevent import to the glia in the first place, however, both the increased ATP levels and oxidation state of the mitochondria observed in these animals would indicate that the glia have generally higher levels of metabolic flux supporting the conclusion that metabolite output to neurons is impaired in this condition. These results support a role for WG in providing metabolic support to neurons in this peripheral nerve, making it a suitable model for studying the regulation of metabolic supply of axons by glia.

While inhibiting MCTs phenocopied the neuron loss observed in *babo* knockdown conditions, the changes to mitochondria oxidation state were markedly different. ATP

levels were similarly high when transport was blocked, but blocking transport had the opposite effect on mitochondria oxidation state as compared to *babo* knockdown. This suggests that directly regulating metabolite export at the membrane is likely not the primary

CONCLUSION I

In summary, this work provides direct *in vivo* evidence that WG are crucial for supporting long axons. When these glia are eliminated, axons show increased age-dependent degeneration that even *Wld^S* is unable to protect against. My colleagues and I have identified several candidate genes required for this glial support of axon integrity and neuronal survival *in vivo*. Among these genes, I showed that the TGF β signaling pathway in glia plays a crucial role in suppressing axon degeneration, even in uninjured nerves, and its loss leads to activation of both *Wld^S*- and P35-sensitive destruction. Finally, I identified significant changes to glial metabolism when *babo* is disrupted. In particular, changes consistent with increased mitochondria biogenesis pointing to a role for *babo* in regulating glial metabolic function.

CHAPTER II:

Ultrastructural analysis of the *Drosophila* peripheral L1 nerve

In this chapter I discuss the ultrastructural analysis of the *Drosophila* L1 nerve in the wing. Dr. Megan Corty and Jo Hill pioneered the method for processing the wing tissue for imaging via electron microscopy. With their help, we obtained electron micrographs from various conditions including different regions of the nerve, different ages, following injury in both wildtype and mutant animals as well as other genetic conditions discussed elsewhere. These results are summarized in the following chapter.

INTRODUCTION II

Introduction 2.1 – Using the L1 nerve in the wing to study axon degeneration

Neukomm et al. 2014 established the L1 peripheral nerve in the wing as a suitable model to study axon degeneration and identify novel genes involved in Wallerian degeneration. Since then, this nerve has continued to be used by several groups to study Wallerian degeneration as well as other biological processes. This includes my work described herein examining glial support of axons.

There are several features of the L1 nerve that make it a desirable nerve to study. First, it is optically accessible with minimal dissection. One can directly image fluorescently labeled cells in the nerve through the cuticle using a confocal microscope. This feature makes morphological screening highly efficient by not requiring time-consuming dissections or staining protocols. The anatomy of this nerve is particularly advantageous for studying Wallerian degeneration since the cell bodies of the neurons reside distally and are easily removed to leave behind the severed axons. From a glial biologist's perspective, this nerve is especially interesting as the wrapping glia (WG) individually ensheath the axons in the proximal region of this nerve similar to vertebrate Remak SCs.

The usefulness of this nerve to study multiple aspects of neurobiology warrants its detailed characterization to provide context for interpreting experimental results derived from its use.

Introduction 2.2 – L1 nerve development

The nerve in the L1 vein in the anterior wing margin houses sensory neurons that respond to chemical or mechanical stimuli (Raad et al., 2016). The sensory neurons, glia, and supporting cells develop from sensory organ precursors (Giangrande, 1994). The neuron cell bodies are in the L1 vein, project their single dendrite into the shaft of the bristles and project their axon medially into the thorax (Hartenstein & Posakony, 1989). The glial cells ensheath the axons starting at the base of the soma at the axon initial segment such that the cell bodies are just outside of the nerve while the axons are contained within it (Giangrande, 1994; Hartenstein & Posakony, 1989). In addition to chemical and mechanoreceptors the wing also has campaniform sensilla, two of which are some of the closest cell bodies in the L1 vein (Cole & Palka, 1982). Campaniform sensilla detect deflections in the curvature of the wing likely feeding into proprioception in flight (Cole & Palka, 1982). The largest axon present in the L1 nerve, belongs to one of the campaniform sensilla neurons that is substantially larger than any other axon in the nerve and is recognizable in every wing (Corty et al., 2021).

Introduction 2.3 – Glia in the L1 nerve

In developing larval nerves there are three layers of glia that ensheath the axons forming a nerve. These are: WG, the innermost cells that directly ensheath axons; subperineurial glia (SPG), that surround the bundled axons and WG and form the blood-brain barrier; and the outermost perineurial glia (PG) that have yet to be functionally defined (Stork et al., 2008, 2012). In the adult wing, both WG and SPG are present, but PG are not detectable by either reporter expression using PG drivers or by electron microscopy

(EM). It is possible that reporter lines for PG do not express in wing PG, however, we also do not see a third glial layer in cross sections of the L1 nerve by EM suggesting that PG are not present in the peripheral wing nerve.

Introduction 2.4 – Injury timing and peripheral glia response

In the *Drosophila* wing, axons rapidly degenerate following injury and the debris is cleared by the glia in the nerve. By 3 hours after injury, axon transport in the nerve is halted both in the injured and bystander neurons (Hsu et al., 2021). By 6 hours severed axons in the L1 nerve begin to fragment and nearly all of the axonal debris is cleared by 7 days following injury (Neukomm et al., 2014). The glial receptor required for debris clearance throughout the *Drosophila* nervous system is Draper (MEGF10 in mammals) (MacDonald et al., 2006). Selective knockdown of Draper in WG results in significantly reduced debris clearance in the wing while its elimination from SPG had a weaker impact on debris clearance (Neukomm et al., 2014). These results indicate that WG are primarily responsible for debris clearance in the L1 nerve, however, SPG do participate to a lesser extent. How do WG juggle debris clearance with axonal ensheathment? Phagocytosing debris requires substantial and dynamic changes to the membrane to engulf debris and recycle membrane. Are these dynamics isolated to just the areas directly in the vicinity of the debris, or does the whole cell respond? If so, are there disruptions to the support mechanisms of glia provided to the axon and for how long?

METHODS II

Detailed stepwise protocol for microwave tissue processing for the ultrastructural analysis of the *Drosophila* L1 nerve. Adapted from (Cunningham & Monk, 2018; Czopka & Lyons, 2011).

Solutions:

- Primary fix: 2% glutaraldehyde, 4% paraformaldehyde, 0.1M sodium cacodylate buffer (final concentrations)
- Buffer: 0.1M sodium cacodylate buffer (final concentration)
- Osmium fix: 2% osmium tetroxide, 0.1M sodium cacodylate buffer and 0.1M imidazole pH 7.5 (final concentration)
- UA: saturated (~8%) uranyl acetate in distilled water
- Ethanol series: ethanol:water: 25%:75%, 50%:50%, 70%:30%, 80%:20%, 95%:5%, 100%:0%.
- Acetone, Glass distilled (EMS #10015)
- Resin: EMbed-812 (EMS #14120) (EMbed-812, DDSA (specially distilled), NMA, DMP-30)
- Acetone:Resin: 50% acetone (100%), 50% EMbed-812 (made fresh)

For all microwave steps insulate samples in a cold-water bath held at 10°C to prevent overheating.

Dissection and Primary Fixation:

Flies were anesthetized with CO₂ and their wings were removed with spring scissors and immediately put into freshly made fix solution. Forceps were used to gently submerge the tissue into approximately 500-1,000 µL of fix in a 2 mL round-bottom microcentrifuge tube and microwaved using the following settings: 2x (100W for 1min, OFF for 1 min), then immediately followed by 5x (450W for 20s, OFF for 20s) before storing the tissue at 4°C overnight in fix solution. For best results, do not crowd the microcentrifuge tubes and put <15 wings per tube. Otherwise, solution changes become more difficult throughout.

Washes and Secondary Fixation:

The next day, wash samples 3 times in 0.1M sodium cacodylate buffer followed by secondary fixation and microwaved 2x (100W for 1min, OFF for 1 min), 5x (450W for 20s, OFF for 20s). For all solution changes use disposable plastic pipettes with fine tips. Avoid sucking up the wings when removing solutions or getting them stuck to the tip. The wings will be floating on top of the solution until the dehydration steps. Following osmium fixation, wash using distilled water 3 x 10-minute washes.

UA Staining and Dehydration Series:

Remove water and replace with enough UA to cover samples. Then microwave 2x (450W for 1 min, OFF for 1 min). Following microwave, wash samples 3 times with water. This is followed by dehydration with an escalating ethanol series (25%, 50%,

70%, 80%, 95%, 100%) where each step is microwaved at 250W for 45s. The final 100% EtOH step is repeated 3 times with each step microwaved for 2x (250W for 1 min, OFF for 1 min). Following EtOH dehydration, samples are dehydrated in 100% acetone and microwaved 2x (250W for 1 min, OFF for 1 min) and repeated 3 times.

Resin Infiltration:

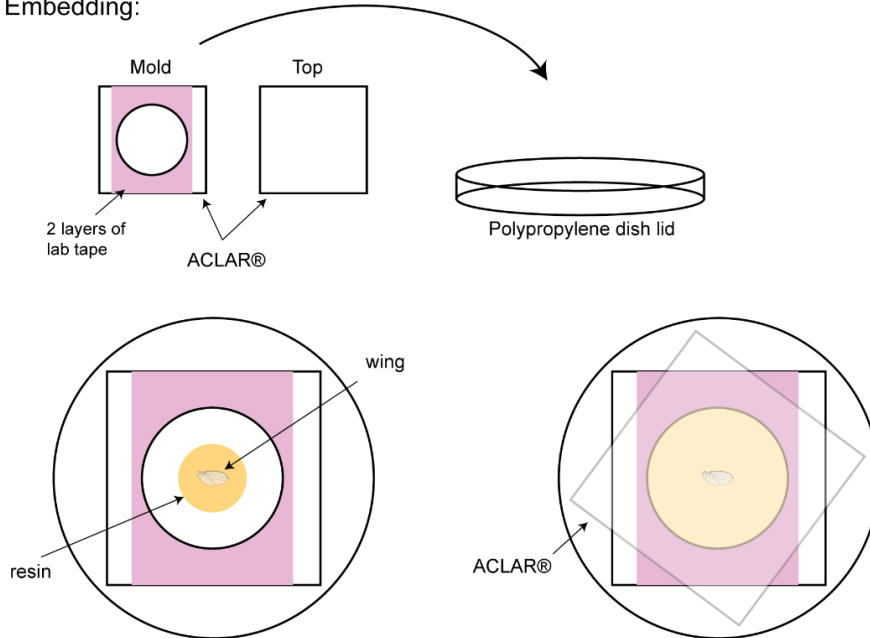
Prepare glass scintillation vials containing a 50:50 acetone:resin solution and transfer wings from final acetone change into the glass scintillation vial of acetone:resin mixture using a wide plastic pipette. Agitate samples overnight at room temperature in glass scintillation vials. The next day, replace the acetone:resin solution with 100% resin at room temperature and agitate at room temperature for at least 1 hour.

Flat Embedding:

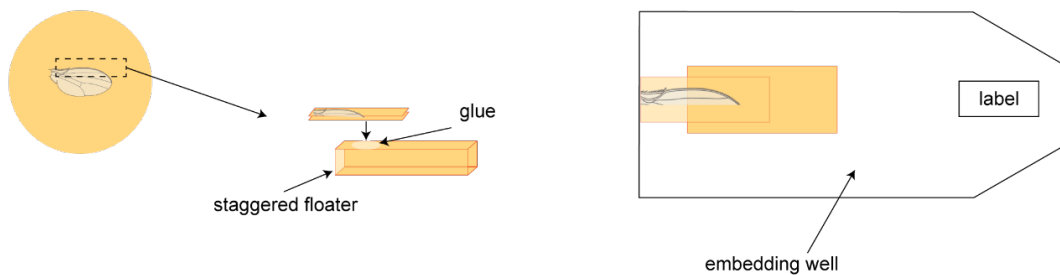
Using ACLAR® (EMS # 50425) add two layers of lab tape to create a thicker mold. Cut squares large enough to punch an approximately ½ of an inch circle out of the tape/ACLAR® piece. Also cut squares of ACLAR® alone, these will sit on top of the sample to flatten the resin (Figure 21). Aliquot room temperature resin into 2 mL microcentrifuge tubes and use a benchtop centrifuge to spin the tubes for 10 minutes two times at ~10,000 rpm to reduce air bubbles in the resin. Insert the mold into a lid of a polypropylene dish (Ted Pella #36135). Using a 1 mL syringe without a needle, add a drop of resin at room temperature to the center of the hole filling approximately half of the area of the hole. Using a broken wood stick with a flat edge, scoop wings out of the

glass scintillation vials one at a time and place them into the center of the drop of resin in the mold. Slowly place a square piece of ACLAR® on top of the resin to flatten the resin and sample (Figure 21). Repeat for each wing. The wing will likely move when adding the top piece of ACLAR® but lowering the cover slowly will help reduce introducing bubbles and movement. Cure flat embed samples in a 60°C oven overnight.

Flat Embedding:



Trimming Flat Embed for Second Embedding:



Trimming and Facing into Block-face:

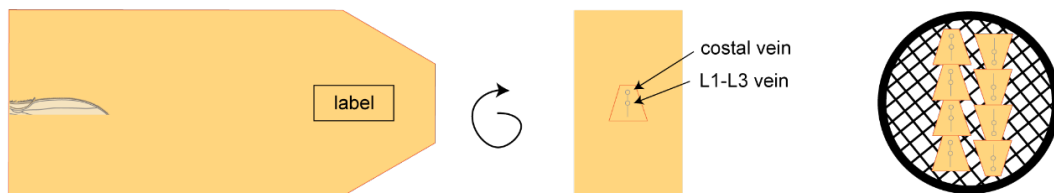


Figure 21 Diagrams for embedding *Drosophila* wings in resin.

Second Embedding:

Following flat embedding, trim the wing to isolate the region of interest using a razor blade. Depending on the hardness of the resin, this may require doing this on a glass slide on a hot plate at about 55-60°C. Leave extra tissue/resin on the opposite side of the region of interest for gluing (Figure 21). Make staggered floaters by cutting small blocks of flat cured resin pieces. The goal is to lift the sample towards the middle of a coffin mold so that it is not at the very bottom of the block after curing. Glue (EMS #12646-06) the back part of the trimmed flat-embedded wing to one side of the staggered floater such that the region of interest sticks out past the base piece (Figure 21). This will allow the second embedding resin to support the flat embedded wing. Insert the staggered floater into the smaller cavities of a LDPE mold (EMS #70918) with the ROI up against the flat side of the mold being careful to keep the wing as parallel to the bottom of the mold as possible (Figure 21). Add a label of choice to each well. Carefully add resin to the mold and use a pointed wooden stick to push any air bubbles to the surface and away from the ROI checking that the wing is pushed against the edge of the well and is parallel to the bottom. Cure molds in the oven overnight at 60°C. Samples may move while curing.

Block Trimming and Sectioning:

Using a sharp razor blade (EMS #71980), trim the block face into a trapezoid around the cross section of the wing such that the costal vein is near narrow (top) edge of the trapezoid and the posterior wing blade is towards the thicker (bottom) edge (Figure 21). Be sure that the top and bottom edges are as parallel as possible. Use the perfect loop to hover over the block face to estimate how many sections will fit on a single grid and

reduce the size of the trapezoid to aim for 5-15 sections per grid. Cut thicker sections (500 or 200 nm, 1mm/s or 0.4 mm/s) either on a glass knife or a histology knife to face into the sample until reaching the region of interest. Take sections and stain with toluidine blue to check the angle of the sections and make sure that the L1 and L3 veins are separated before proceeding. Toluidine blue sections can be preserved with CytoSeal 60 (EMS #18006) and a coverslip for archiving. For obtaining micrographs, ultrathin 70 nm sections are cut on a DiATOME® ultra 45° diamond knife (0.2 mm/s) and transferred to 100mesh Formvar-coated grids (EMS #FCF100-Cu) using a perfect loop (EMS #70944).

Counter Staining:

Counterstain grids for 20 minutes face down on drops of 5% uranyl acetate. Rinse grids with double distilled water 5 times followed by 7 minutes face up in Reynold's lead citrate. 5 washes in double distilled water then dry section side up on filter paper for at least 30 minutes. Store in grid boxes (EMS #71147-12) until imaging.

Imaging Grids:

Micrographs were acquired on a FEI Tecnai T12 interfaced to Advanced Microscopy Techniques (AMT) CCD camera.

RESULTS AND DISCUSSION II

Results 2.1– Characterization of the L1 wing nerve makeup

Remak SCs in mammals individually ensheath axons whereas in larval nerves some axons are individually ensheathed while others are grouped in small bundles (Harty & Monk, 2017; Stork et al., 2008). We wanted to examine whether this was also the case for the L1 nerve in the adult or if the WG instead more closely resembled Remak SCs and ensheath every axon individually. From fluorescent live imaging experiments, it appears that the L1 nerve is densely ensheathed by glia. However, confocal imaging approaches lacked sufficient resolution to determine the degree to which individual axons are ensheathed. To overcome this limitation, my colleagues and I used transmission electron microscopy to assess the ultrastructure of the L1 nerve and determine the nature of glial ensheathment of axons at the single axon level. Unlike larval nerves, the axons in the L1 nerve are all individually ensheathed on average in the proximal region even as early as 1 dpe (Figure 22A-B, (Stork et al. 2008)). This arrangement of axons is strikingly similar to Remak bundles in mammalian nerves and is suggestive of a conserved function. In addition, work from our lab and others has shown that genes regulating mammalian myelinating and non-myelinating ensheathing glia have conserved function in WG (Corty et al., 2021; Matzat et al., 2015; Petley-Ragan et al., 2016; Yu et al., 2009). Finding individual axonal ensheathment in this nerve furthers the notion that Remak SCs and myelinating glia and WG descend from a common ancestor. The genetic tools available in *Drosophila* to manipulate WG make this a promising model to study the function of non-myelinating glia in peripheral nerves.

In contrast to the proximal region of the L1 nerve, cross sections from more distal regions, did not maintain this degree of separation of individual axons (Figure 22A, C & D). This was an unexpected result given the robust ensheathment observed in the proximal region. One contributing factor that may explain this difference is that density of WG nuclei in the proximal region is higher and gets progressively sparser as one looks more distally. Therefore, it is possible this region of the nerve is more robustly ensheathed than distal regions due to increased density of WG. However, axon numbers show a similar pattern of density because the neuron cell bodies reside in the periphery along the wing margin and send their axons medially to the thorax. This means that distal regions will have fewer axons for WG to ensheath. The ratio between axon number and size to total area of WG membrane in a given cross section will require further investigation to determine the precise relationship between axon and WG density along this nerve.

One challenge in assessing axonal ensheathment in distal regions is caused by axons entering the nerve at every point in the anterior margin (the cell bodies are outside of the nerve). Thus, many axons in these cross sections appear to be cut at an angle unlike in the proximal region where all the axons are arranged near parallel to one another and are cut orthogonally. Despite these observations, WG membrane is nonetheless pervasive throughout the axon bundle (Figure 22C & D). Finally, because these samples came from animals that were only 1 dpe, it is also possible that what is shown here represents incomplete ensheathment that has not fully developed. The robust ensheathment observed in the proximal region at the same age would suggest that this is not the case, however, we cannot rule out that there could be differences in timing of wrapping between

different regions of the nerve. Future studies will be needed to examine ensheathment in lateral regions at later timepoints to address this question. If axonal ensheathment is indeed different in these two regions, it will be of interest to determine the functional consequences of this difference on neural transmission throughout the nerve. In addition, assuming differential ensheathment is a feature of this nerve, this could provide a unique model to study genetic regulation of both hyper- and hypo-ensheathment due to the graded degree of ensheathment.

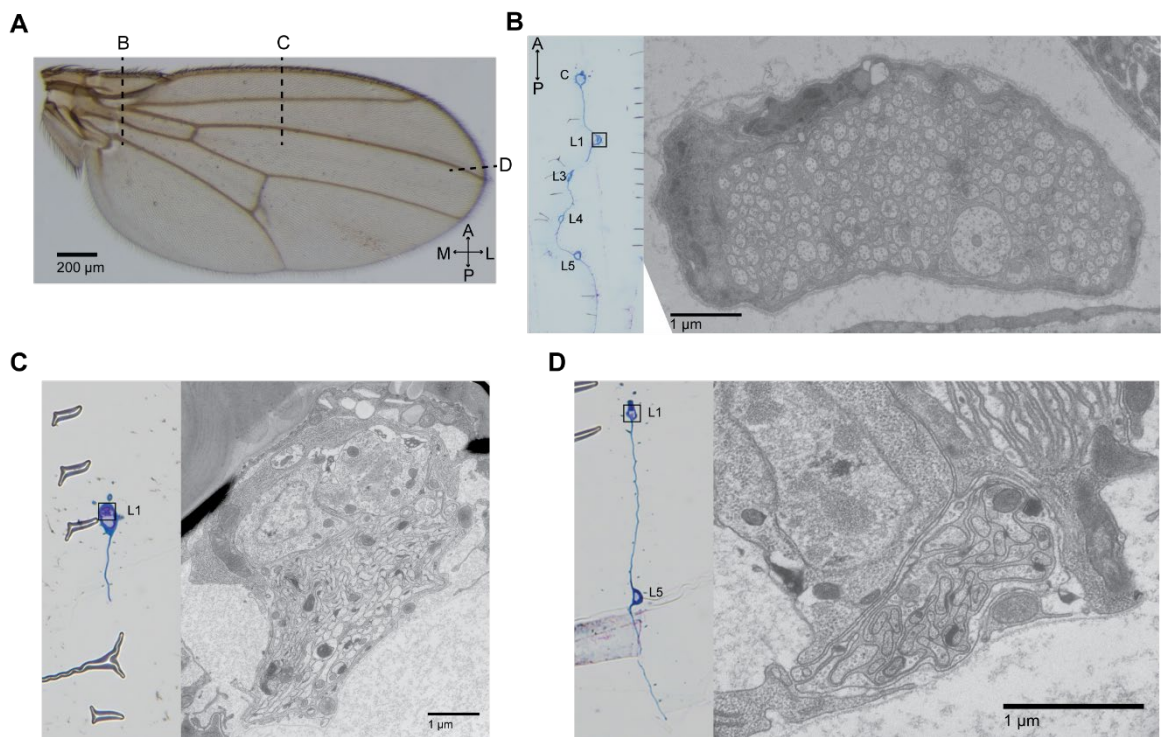


Figure 22 Ultrastructure of the *Drosophila* L1 nerve. (A) A processed wing from a 1-day post eclosion (dpe) female embedded in resin. Dashed lines indicate approximate location of cross sections shown in B-D. (B) Low magnification cross section of the wing stained with toluidine blue (left) and the corresponding electron micrograph (right) of a cross section of the L1 nerve distal to where the L1 and L3 veins separate. (C) Low magnification cross section of the wing stained with toluidine blue (left) and the corresponding electron micrograph (right) of a cross section of the L1 nerve approximately midway along the nerve. (D) Low magnification cross section of the wing stained with toluidine blue (left) and the corresponding electron micrograph (right) of a cross section of the L1 nerve near the distal end of the L1 nerve.

Results 2.2 – Axon development with age

The process of axon diameter growth is not well understood. In mammalian systems, axon caliber increases at the onset of myelination and without myelination there is a shift towards smaller caliber axons (Martini, 2001; Sánchez et al., 1996; Windebank et al., 1985; Yin et al., 1998). This would suggest that glial ensheathment influences axon caliber growth. However, how glia non-cell autonomously regulate axon growth is poorly understood. (Corty et al., 2021) showed that loss of the receptor Ddr from glia caused a significant decrease in axon caliber in the wing. The dorsal twin sensillum of the margin (dTSM) is the largest axon in the L1 nerve bundle (Figure 23; (Corty et al., 2021)). We found that this axon undergoes robust caliber growth early after eclosion and remains largely stable in size after 5 dpe (Figure 23). The stereotypic nature of this axon in the L1 nerve provides a useful system to study axon caliber growth in a genetically tractable model. Furthermore, the demonstrated impact of manipulating glia on axon caliber growth suggests a conserved function between fly and mammalian glia in promoting axon growth (Corty et al., 2021).

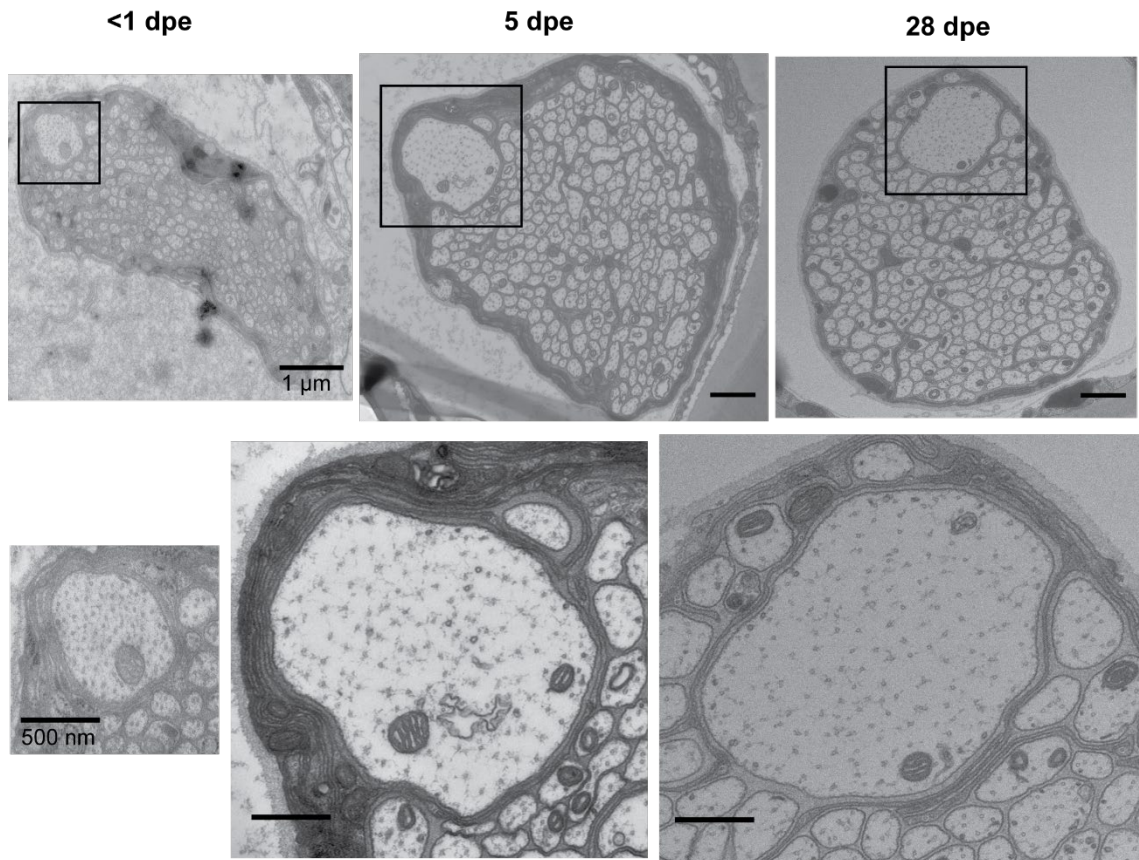


Figure 23 Axon caliber growth in the adult wing L1 nerve. Top: electron micrographs of the entire L1 nerve cross section in young and aged animals. Bottom: higher magnification micrographs of the dTSM axon from the nerves imaged above.

Results 2.3– Ultrastructural response after injury

The use of the L1 nerve to study axon degeneration prompted us to evaluate nerve ultrastructure following injury. We found that at 12 hpa, signs of axonal debris were evident in regions of the nerve (Figure 24A). Debris were darker compared to intact axons. In addition, remnants of axons lacked defined microtubules and most appeared smaller in size compared to intact axons (Figure 24A). 24 hpa, regions of axonal debris appeared similar to those observed at 12 hpa, however, at 10 dpa (when debris is no longer visible by fluorescent reporter (Neukomm et al., 2014)) the regions of axonal

debris appear smaller in wildtype animals (Figure 24A). Since Draper is required for glia to clear debris in the wing, we examined debris clearance in *draper* null mutants (*drpr^{Δ5}*) (Neukomm et al., 2014). Similar debris was present in *drpr^{Δ5}*, however, at 10 dpa when wildtype nerves had less debris present, *drpr^{Δ5}* animals still had similar levels of debris as compared to 24 hpa (Figure 24B). This is consistent with data from fluorescent reporter expression and provides further confidence that what we concluded to be debris in the wildtype nerves was indeed axonal debris (Neukomm et al., 2014).

In addition, to increased residual debris present in the *drpr^{Δ5}* nerves, we also noticed that the debris cross sections appeared generally lighter compared to wildtype but still lacked distinct microtubules (Figure 24A-B). This could indicate that darker profiles represent debris that has been engulfed by glia but not yet metabolized or it could represent a change that occurs within the axonal debris following injury that is dependent on the glial response. Because these were whole animal mutants as opposed to glial-specific knockdown of *draper*, it is also possible that *draper* acts within the axon itself causing this darkening phenotype. Experiments using glial-specific knockdown strategies will address this possibility. Furthermore, inhibition of phagocytosis downstream of engulfment in glia would provide further clarity into the cause of darkened debris.

A fascinating feature of glia within this nerve is their ability to clear debris while also maintaining axonal ensheathment. To address the behavior of WG as it relates to axonal ensheathment following injury, we measured the wrapping index for each nerve. We found that following injury, single axon ensheathment decreased at 10 dpa in wildtype nerves but not in *drpr^{Δ5}* (Figure 24C). At 10 dpa nearly all of the debris is cleared by the glia and this result suggests that glial processes throughout the nerve are changed in

response to injury and not just those directly opposed to the debris. One of the *drpr^{A5}* mutants had severe degeneration across the entire nerve with only 3 axons that appeared to remain intact (Figure 24D). This outlier was not included in the wrapping index analysis due to the presence of just a few axons. The maintained single axon ensheathment in *drpr^{A5}* nerves suggests that this rearrangement of glial processes throughout the nerve is dependent on Draper. Going forward, it will be interesting to investigate how this reduced ensheathment impacts axon maintenance and function in the short a long term. We only examined out to 10 dpa but determining the timeframe for if and when single axon ensheathment recovers after injury will be informative as to how the nerve as a whole copes with an injury of a subset of its axons.

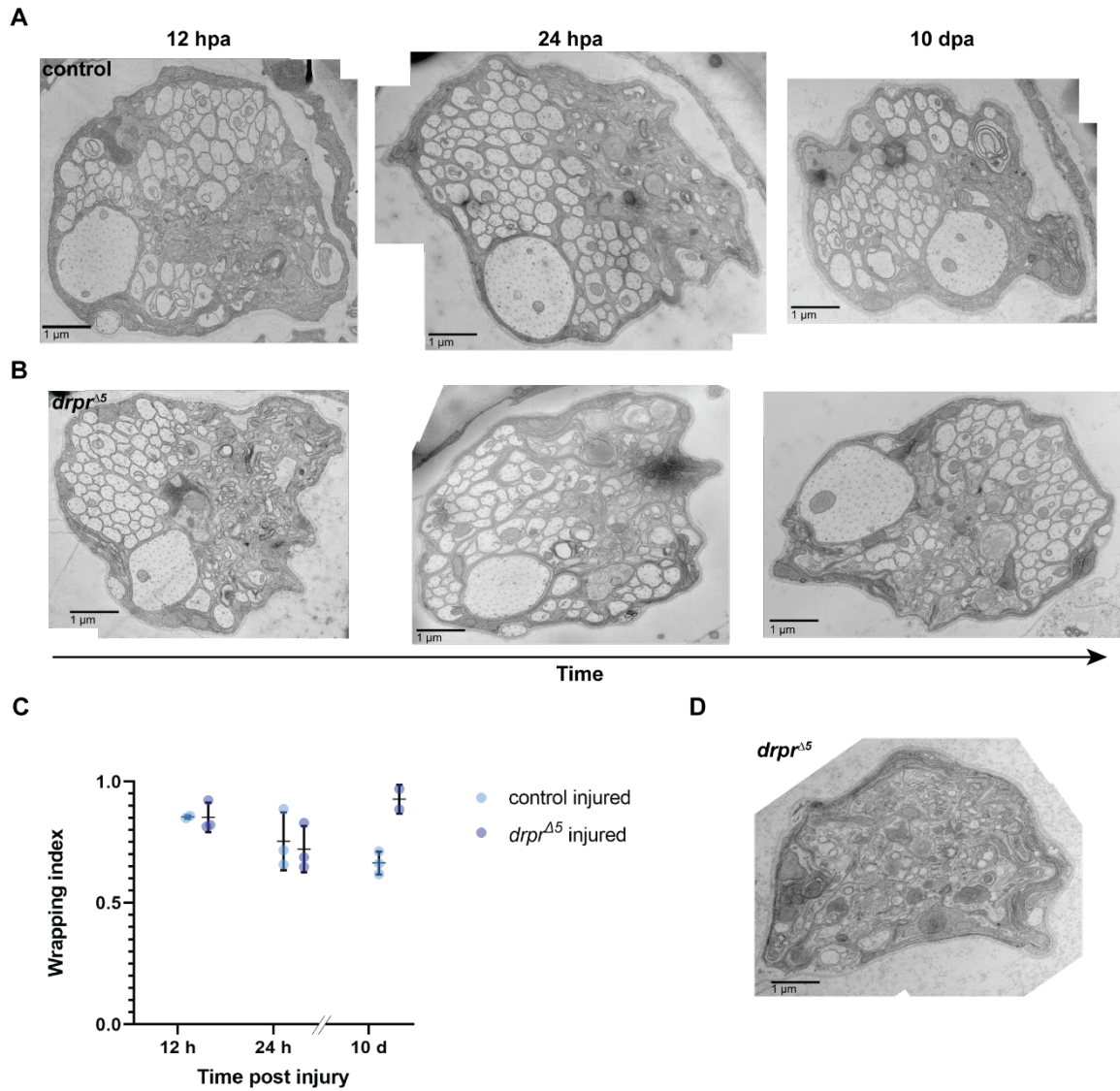


Figure 24 Glial response to injury. (A-B) L1 nerve from *w¹¹¹⁸* (A) or *drpr^{Δ5}* (B) females at increasing time post injury. (C) Quantification of the wrapping index of remaining intact axons in the nerve at each time point. Wrapping index = (# of wrapped units)/(# of axons). (D) Outlier nerve from a 10 dpi *drpr^{Δ5}* wing.

APPENDIX I: Sensitized axon maintenance screen results

VDRG Stock #	Gene (CG)	Gene Symbol	Phenotype
1050	CG9138	uif	lethal
1385	CG9753	AdoR	lethal
2660	CG9261	nrv2	lethal
3040	CG15658	CG15658	lethal
3306	CG1517	na	lethal
3962	CG1298	kune	lethal
5236	CG10620	Tsf2	lethal
6229	CG9985	sktl	lethal
6719	CG6668	atl	lethal
6860	CG9702	CG9702	lethal
7296	CG3702	CG3702	lethal
8010	CG1817	Ptp10D	lethal
9073	CG9637	Task6	lethal
10102	CG6817	foi	lethal
10424	CG31240	repo	lethal
10598	CG4797	CG4797	lethal
12330	CG5670	Atpalpha	lethal
12763	CG17117	CG17117	lethal
13324	CG4692	CG4692	lethal
13359	CG1732	CG1732	lethal
14874	CG2145	CG2145	lethal
15580	CG3246	CG3246	lethal
16696	CG11395	CG11395	lethal
19555	CG13333	link	lethal
20909	CG2845	Raf	lethal
21317	CG31317	stumps	lethal
21594	CG11098	Tango1	lethal
22209	CG5838	Dref	lethal
22210	CG5838	Dref	lethal
23620	CG8745	CG8745	lethal
26850	CG5803	Fas3	lethal
27180	CG7223	htl	lethal
29689	CG33110	CG33110	lethal
30730	CG9364	Treh	lethal
33012	CG17838	Syp	lethal
33112	CG31136	Syx1A	lethal
33166	CG13393	l(2)k12914	lethal
37217	CG9128	Sac1	lethal
40975	CG13743	CG13743	lethal
40987	CG2893	zyd	lethal

40988	CG2893	CG2893	lethal
41749	CG31366	Hsp70Aa	lethal
42467	CG9664	CG9664	lethal
42549	CG14181	Use1	lethal
44929	CG10624	sinu	lethal
45775	CG4166	not	lethal
47449	CG14224	Ubqn	lethal
49547	CG31201	GluRIIE	lethal
50156	CG2979	Yp2	lethal
50306	CG14779	pck	lethal
51491	CG4894	Ca-alpha1D	lethal
100095	CG10449	Catsup	lethal
100197	CG7586	Mcr	lethal
100198	CG31976	ovm	lethal
100234	CG13078	CG13078	lethal
100386	CG33189	CG33189	lethal
100619	CG5670	Atpalpha	lethal
100630	CG17117	HTH	lethal
100644	CG12525	Ir67a	lethal
100693	CG11901	eEF1gamma	lethal
100844	CG14958	CG14958	lethal
100927	CG8795	CG8795	lethal
101312	CG9053	opm	lethal
101319	CG3500	CG3500	lethal
101339	CG6058	Ald1	lethal
101400	CG5484	CG5484	lethal
101404	CG1903	sno	lethal
101485	CG7708	CG7708	lethal
101495	CG14792	sta	lethal
101559	CG18000	sw	lethal
101766	CG4147	Hsc70-3	lethal
101847	CG17664	CG17664	lethal
101978	CG44838	CG44838	lethal
101980	CG1856	ttk	lethal
102054	CG8367	cg	lethal
102194	CG4590	Inx2	lethal
102223	CG7713	CG7713	lethal
102333	CG15658	Lapsyn	lethal
102406	CG2216	Fer1HCH	lethal
102444	CG3638	CG3638	lethal
102636	CG4294	CG4294	lethal
102922	CG12210	Syb	lethal
103641	CG5876	heix	lethal

103704	CG1560	mys	lethal
103753	CG5802	CG5802	lethal
104038	CG10789	ng4	lethal
104210	CG7000	Snmp1	lethal
104287	CG12763	Dpt	lethal
104322	CG15532	hdc	lethal
104390	CG18389	Eip93F	lethal
104421	CG10693	slo	lethal
104490	CG3161	Vha16-1	lethal
104502	CG8280	eEF1alpha1	lethal
104673	CG6901	CG6901	lethal
105113	CG13626	Syx18	lethal
105181	CG7398	Trn	lethal
105353	CG8222	Pvr	lethal
105635	CG4501	bgm	lethal
105732	CG34412	tlk	lethal
105806	CG8121	CG8121	lethal
105834	CG14026	tkv	lethal
106260	CG4500	hll	lethal
106466	CG2163	Pabp2	lethal
106660	CG8034	CG8034	lethal
106680	CG10275	kon	lethal
106891	CG10374	Lsd-1	lethal
106920	CG6230	CG6230	lethal
107000	CG42321	CG42321	lethal
107014	CG4109	Syx8	lethal
107186	CG7654	Tom20	lethal
107264	CG5081	Syx7	lethal
107446	CG3725	Ca-P60A	lethal
107450	CG12369	Lac	lethal
107937	CG15304	Neb-cGP	lethal
108128	CG6827	Nrx-IV	lethal
108184	CG6906	CAH2	lethal
108297	CG31004	CG31004	lethal
108341	CG4775	Tango14	lethal
108352	CG3954	csw	lethal
108690	CG16884	Vajk3	lethal
108928	CG4214	Syx5	lethal
108952	CG3171	Tre1	lethal
108962	CG45186	Svil	lethal
109300	CG11325	GRHR	lethal
109464	CG8271	Sln	lethal
109499	CG5320	Gdh	lethal

109630	CG5651	pix	lethal
109633	CG31634	Oatp26F	lethal
109660	CG9539	Sec61alpha	lethal
109855	CG14239	CG14239	lethal
110014	CG4099	Sr-CI	lethal
110103	CG8628	Acbp3	lethal
110394	CG31116	CIC-a	lethal
110708	CG8422	Dh44-R1	lethal
110760	CG33162	SrpRbeta	lethal
3162	CG5847	zye	hit
3825	CG8224	babo	hit
4312	CG17941	ds	hit
18873	CG10236	LanA	hit
25666	CG31058	CG31058	hit
30315	CG1724	CG1724	hit
30329	CG12832	Tsp42Eq	hit
30363	CG13288	CG13288	hit
30379	CG6038	crim	hit
34708	CG3764	CG3764	hit
36164	CG3389	Cad88C	hit
36355	CG14226	dome	hit
37123	CG10234	Hs2st	hit
38010	CG4698	Wnt4	hit
39218	CG8116	CG8116	hit
39474	CG42678	ReepA	hit
44197	CG2813	cold	hit
46757	CG3977	Ctr1A	hit
47506	CG10617	Syt12	hit
47537	CG11010	Ent3	hit
100002	CG3936	N	hit
100153	CG42674	CG42674	hit
100260	CG10952	eag	hit
100384	CG34120	CG34120	hit
100789	CG10808	Syngt	hit
101377	CG4608	bnl	hit
101407	CG4356	mAChR-A	hit
101504	CG8732	Acsl	hit
101601	CG11147	CG11147	hit
102178	CG12844	Tsp42Eh	hit
102240	CG33207	pxb	hit
102266	CG30269	CG30269	hit
102432	CG11278	Syx13	hit
102642	CG18241	Toll-4	hit

102776	CG7075	Ntl	hit
102784	CG14957	CG14957	hit
103808	CG10776	wit	hit
103982	CG5550	CG5550	hit
104122	CG13948	Gr21a	hit
104345	CG6927	CG6927	hit
104975	CG1148	Osi2	hit
105096	CG43867	CG43867	hit
105189	CG2467	pot	hit
105303	CG31695	scw	hit
105387	CG42611	mgl	hit
105475	CG30272	CG30272	hit
105637	CG6750	CG6750	hit
105650	CG13189	CG13189	hit
106072	CG4568	fzo	hit
106499	CG4357	Ncc69	hit
106616	CG43225	axo	hit
106897	CG33233	CG33233	hit
107168	CG16961	Or33b	hit
107301	CG3074	Swim	hit
107423	CG31284	wtrw	hit
107993	CG11895	stan	hit
108619	CG6293	CG6293	hit
108861	CG43128	Shab	hit
108913	CG1448	Inx3	hit
108991	CG10978	jagn	hit
109143	CG10781	ng1	hit
109582	CG11621	Pi3K68D	hit
109665	CG7638	CG7638	hit
109898	CG11440	laza	hit
110331	CG8583	sec63	hit
110549	CG43444	Tet	hit
848	CG7904	put	no phenotype
939	CG5803	Fas3	no phenotype
940	CG5803	Fas3	no phenotype
965	CG8896	18w	no phenotype
1038	CG32179	Krn	no phenotype
1089	CG10244	Cad96Ca	no phenotype
1092	CG7100	CadN	no phenotype
1112	CG3936	N	no phenotype
1162	CG10221	Hrd3	no phenotype
1172	CG6178	CG6178	no phenotype
1194	CG6844	nAcRalpha-96Ab	no phenotype

1204	CG5789	CG5789	no phenotype
1262	CG6070	gb	no phenotype
1316	CG5508	mino	no phenotype
1364	CG7816	CG7816	no phenotype
1366	CG7875	trp	no phenotype
1378	CG7912	CG7912	no phenotype
1571	CG13646	CG13646	no phenotype
1684	CG13223	CG13223	no phenotype
1698	CG5348	CG5348	no phenotype
1706	CG12490	CG12490	no phenotype
1783	CG10823	SIFaR	no phenotype
1793	CG11144	mGluR	no phenotype
1794	CG11144	mGluR	no phenotype
2472	CG2657	Ir21a	no phenotype
2507	CG2789	Tspo	no phenotype
2548	CG31668	CG31668	no phenotype
2575	CG9964	Cyp309a1	no phenotype
2593	CG3131	Duox	no phenotype
2656	CG6863	tok	no phenotype
2657	CG31103	CG31103	no phenotype
2673	CG14238	CG14238	no phenotype
2703	CG10810	Drs	no phenotype
2756	CG5853	CG5853	no phenotype
2793	CG43394	CG43394	no phenotype
2804	CG7806	CG7806	no phenotype
2980	CG4717	kni	no phenotype
2981	CG4717	kni	no phenotype
3005	CG11614	nkd	no phenotype
3091	CG5803	Fas3	no phenotype
3116	CG18243	Ptp52F	no phenotype
3120	CG18146	nimC2	no phenotype
3226	CG7734	shn	no phenotype
3231	CG4847	CG4847	no phenotype
3282	CG5993	os	no phenotype
3295	CG12127	amx	no phenotype
3324	CG10593	Acer	no phenotype
3329	CG10697	Ddc	no phenotype
3339	CG15162	MESR3	no phenotype
3392	CG18741	Dop1R2	no phenotype
3470	CG30394	CG30394	no phenotype
3621	CG3394	Fatp3	no phenotype
3720	CG3619	DI	no phenotype
3749	CG7749	kug	no phenotype

3775	CG10021	bowl	no phenotype
3837	CG15257	Tim17b2	no phenotype
3875	CG31783	ninaD	no phenotype
3909	CG10165	CG10165	no phenotype
3912	CG10337	CG10337	no phenotype
4138	CG11387	ct	no phenotype
4142	CG14743	CG14743	no phenotype
4158	CG8008	CG8008	no phenotype
4301	CG6124	eater	no phenotype
4341	CG4370	Irk2	no phenotype
4365	CG8285	boss	no phenotype
4402	CG5646	CG5646	no phenotype
4482	CG1232	tipE	no phenotype
4544	CG4846	beat-Ia	no phenotype
4637	CG8824	fdl	no phenotype
4650	CG8785	CG8785	no phenotype
4671	CG3814	CG3814	no phenotype
4848	CG33478	Or46a	no phenotype
4861	CG8323	CG8323	no phenotype
4871	CG10117	ttv	no phenotype
5038	CG33717	PGRP-LD	no phenotype
5198	CG14173	Ilp1	no phenotype
5203	CG42825	CG42825	no phenotype
5229	CG6928	CG6928	no phenotype
5247	CG11281	snky	no phenotype
5271	CG6869	FucTA	no phenotype
5294	CG6456	Mip	no phenotype
5329	CG7446	Grd	no phenotype
5341	CG5485	Prestin	no phenotype
5551	CG43368	CG43368	no phenotype
5594	CG11709	PGRP-SA	no phenotype
5606	CG11937	amn	no phenotype
5608	CG17131	tyn	no phenotype
5738	CG15585	Osi1	no phenotype
5776	CG14605	CG14605	no phenotype
5805	CG7459	CtrlB	no phenotype
5820	CG11775	Ir85a	no phenotype
5838	CG18802	alpha-Man-II	no phenotype
6031	CG6666	SdhC	no phenotype
6065	CG14723	HisCl1	no phenotype
6112	CG15904	Ir56d	no phenotype
6137	CG9703	Axs	no phenotype
6178	CG33253	CG33253	no phenotype

6183	CG14194	CG14194	no phenotype
6205	CG42269	CG42269	no phenotype
6372	CG31787	CG31787	no phenotype
6375	CG10373	Jwa	no phenotype
6452	CG8468	CG8468	no phenotype
6459	CG11495	rasp	no phenotype
6487	CG1213	CG1213	no phenotype
6498	CG12116	CG12116	no phenotype
6586	CG34396	CG34396	no phenotype
6685	CG31190	Dscam3	no phenotype
6708	CG5912	arr	no phenotype
6762	CG12943	CG12943	no phenotype
6774	CG10917	fj	no phenotype
6782	CG6331	Orct	no phenotype
6800	CG5802	CG5802	no phenotype
6838	CG17244	CG17244	no phenotype
6872	CG2003	CG2003	no phenotype
6938	CG5304	dmGlut	no phenotype
6950	CG7537	Inx5	no phenotype
7031	CG2930	CG2930	no phenotype
7035	CG2938	CG2938	no phenotype
7042	CG42594	CG42594	no phenotype
7126	CG4536	iav	no phenotype
7136	CG3039	ogre	no phenotype
7254	CG32463	Tengl2	no phenotype
7274	CG33281	CG33281	no phenotype
7291	CG10019	CG10019	no phenotype
7303	CG15438	MFS18	no phenotype
7309	CG3305	Lamp1	no phenotype
7326	CG6126	CG6126	no phenotype
7363	CG11210	CG11210	no phenotype
7380	CG8046	CG8046	no phenotype
7391	CG12341	CG12341	no phenotype
7434	CG33166	stet	no phenotype
7524	CG10035	CG10035	no phenotype
7679	CG14928	spz4	no phenotype
7705	CG18507	CG18507	no phenotype
7930	CG31741	CG31741	no phenotype
7934	CG10106	Tsp42Ee	no phenotype
7944	CG8791	CG8791	no phenotype
8034	CG11715	Cyp4g15	no phenotype
8036	CG9369	m	no phenotype
8064	CG10178	CG10178	no phenotype

8069	CG31793	CG31793	no phenotype
8124	CG7777	CG7777	no phenotype
8169	CG42292	Ir7f	no phenotype
8222	CG5549	CG5549	no phenotype
8249	CG11703	CG11703	no phenotype
8269	CG5123	W	no phenotype
8329	CG9518	CG9518	no phenotype
8357	CG6906	CAH2	no phenotype
8359	CG10960	CG10960	no phenotype
8373	CG7255	CG7255	no phenotype
8380	CG4672	TMS1	no phenotype
8382	CG17245	plexB	no phenotype
8393	CG3665	Fas2	no phenotype
8405	CG14900	Cad89D	no phenotype
8408	CG3389	Cad88C	no phenotype
8424	CG9472	brv1	no phenotype
8439	CG18281	CG18281	no phenotype
8442	CG5078	CG5078	no phenotype
8450	CG7442	SLC22A	no phenotype
8549	CG1058	rpk	no phenotype
8628	CG13409	CG13409	no phenotype
8655	CG1801	CG1801	no phenotype
8677	CG17167	CG17167	no phenotype
8681	CG12061	CG12061	no phenotype
8712	CG12845	Tsp42Ef	no phenotype
8759	CG9035	Tapdelta	no phenotype
8875	CG3139	Syt1	no phenotype
8880	CG15444	ine	no phenotype
8913	CG14969	CG14969	no phenotype
8963	CG30464	Ir52d	no phenotype
8976	CG8389	CG8389	no phenotype
9011	CG10633	Ir64a	no phenotype
9131	CG11655	CG11655	no phenotype
9152	CG6531	wgn	no phenotype
9206	CG32072	Elo68alpha	no phenotype
9235	CG5183	KdelR	no phenotype
9285	CG2328	eve	no phenotype
9340	CG11767	Or24a	no phenotype
9354	CG13206	Or47b	no phenotype
9406	CG7400	Fatp	no phenotype
9417	CG2988	ems	no phenotype
9429	CG5661	Sema-5c	no phenotype
9434	CG1891	sax	no phenotype

9437	CG5227	sdk	no phenotype
9452	CG11437	CG11437	no phenotype
9455	CG1158	Tim17b1	no phenotype
9517	CG14069	CG14069	no phenotype
9542	CG11561	smo	no phenotype
9559	CG15113	5-HT1B	no phenotype
9673	CG6982	CG6982	no phenotype
9737	CG14777	CG14777	no phenotype
9795	CG7005	Esp	no phenotype
9981	CG3979	Indy	no phenotype
10004	CG2019	disp	no phenotype
10045	CG3615	Atg9	no phenotype
10140	CG10742	Tsp3A	no phenotype
10268	CG42732	CG42732	no phenotype
11037	CG9778	Syt14	no phenotype
11117	CG15095	l(2)08717	no phenotype
11142	CG9304	CG9304	no phenotype
11346	CG4545	SerT	no phenotype
11570	CG5488	B-H2	no phenotype
11812	CG12900	Ir47a	no phenotype
11823	CG5481	lea	no phenotype
11925	CG11760	CG11760	no phenotype
12101	CG5474	SsRbeta	no phenotype
12189	CG33513	Nmdar2	no phenotype
12233	CG2727	emp	no phenotype
12352	CG10211	CG10211	no phenotype
12413	CG5888	CG5888	no phenotype
12416	CG4472	Idgf1	no phenotype
12423	CG4559	Idgf3	no phenotype
12441	CG12414	nAcRalpha-80B	no phenotype
12573	CG12052	lola	no phenotype
12692	CG9310	Hnf4	no phenotype
12764	CG17117	CG17117	no phenotype
12975	CG6440	Dms	no phenotype
13164	CG5966	CG5966	no phenotype
13249	CG11066	scaf	no phenotype
13343	CG2985	Yp1	no phenotype
13352	CG4889	wg	no phenotype
13386	CG10609	Orco	no phenotype
13392	CG6515	Takr86C	no phenotype
13407	CG9254	CG9254	no phenotype
13463	CG12517	CG12517	no phenotype
13769	CG6723	CG6723	no phenotype

13807	CG3940	CAH7	no phenotype
13864	CG7225	wbl	no phenotype
14063	CG13676	CG13676	no phenotype
14091	CG13480	Lk	no phenotype
14109	CG14153	CG14153	no phenotype
14136	CG4974	dally	no phenotype
14201	CG18090	Dsk	no phenotype
14429	CG6705	tsl	no phenotype
14624	CG1780	Idgf4	no phenotype
14704	CG6173	Kal1	no phenotype
14803	CG3135	shf	no phenotype
14853	CG11842	CG11842	no phenotype
14892	CG1505	gd	no phenotype
15204	CG7047	Vdup1	no phenotype
15305	CG11051	Nplp2	no phenotype
15387	CG4604	Glaz	no phenotype
15428	CG9280	Glt	no phenotype
15466	CG32209	serp	no phenotype
15541	CG13095	Bace	no phenotype
15810	CG4700	Sema-2a	no phenotype
15975	CG42230	bbg	no phenotype
16037	CG10365	CG10365	no phenotype
16063	CG10514	CG10514	no phenotype
16136	CG10970	CG10970	no phenotype
16390	CG12090	Iml1	no phenotype
16403	CG2723	ImpE3	no phenotype
16416	CG3953	Invadolysin	no phenotype
16643	CG9345	Adgf-C	no phenotype
16677	CG6378	SPARC	no phenotype
16813	CG31332	Unc-115b	no phenotype
16820	CG2855	aph-1	no phenotype
17349	CG14039	qtc	no phenotype
17657	CG14489	olf186-M	no phenotype
17860	CG33543	CG33543	no phenotype
17898	CG7503	Con	no phenotype
18054	CG11320	CG11320	no phenotype
18121	CG34127	CG34127	no phenotype
18825	CG18105	ETH	no phenotype
18977	CG32372	ltl	no phenotype
19022	CG11153	Sox102F	no phenotype
19291	CG15105	tn	no phenotype
19512	CG33956	kay	no phenotype
19594	CG32635	Neto	no phenotype

19603	CG42264	CG42264	no phenotype
20099	CG18445	oys	no phenotype
20321	CG1691	Imp	no phenotype
20874	CG34321	inaF-C	no phenotype
20926	CG2867	Prat	no phenotype
21114	CG42678	ReepA	no phenotype
21206	CG3047	Sgs1	no phenotype
21401	CG31712	CG31712	no phenotype
22061	CG5321	CG5321	no phenotype
22082	CG5344	wkd	no phenotype
22254	CG6148	Past1	no phenotype
22667	CG8010	CG8010	no phenotype
22853	CG10772	Fur1	no phenotype
22879	CG12376	CG12376	no phenotype
22944	CG2198	Ama	no phenotype
22975	CG32451	SpoCk	no phenotype
22989	CG34059	ppk16	no phenotype
23153	CG34413	NKAIN	no phenotype
23158	CG9095	CG9095	no phenotype
23206	CG13873	Obp56g	no phenotype
23316	CG33531	Ddr	no phenotype
23358	CG6988	Pdi	no phenotype
23526	CG6132	Sgs8	no phenotype
23587	CG5804	Acbp5	no phenotype
23720	CG9665	Cpr73D	no phenotype
23725	CG9391	CG9391	no phenotype
24106	CG8464	HtrA2	no phenotype
24189	CG9424	bocks	no phenotype
24540	CG12449	Gfat1	no phenotype
24578	CG34358	shakB	no phenotype
24988	CG2381	Syt7	no phenotype
24998	CG5973	CG5973	no phenotype
25020	CG3083	Prx6005	no phenotype
25365	CG42330	Dscam4	no phenotype
25586	CG30159	CG30159	no phenotype
25740	CG31253	CG31253	no phenotype
26758	CG10680	CG10680	no phenotype
26783	CG1090	CG1090	no phenotype
26815	CG17795	mthl2	no phenotype
26817	CG30469	Ir52b	no phenotype
26852	CG5803	Fas3	no phenotype
26876	CG7485	Oct-TyrR	no phenotype
27097	CG11282	caps	no phenotype

27099	CG6890	Tollo	no phenotype
27202	CG1634	Nrg	no phenotype
27207	CG11516	Ptp99A	no phenotype
27215	CG31009	Cad99C	no phenotype
27220	CG17245	plexB	no phenotype
27225	CG4125	rst	no phenotype
27229	CG3936	N	no phenotype
27232	CG6899	Ptp4E	no phenotype
27290	CG10618	CHKov1	no phenotype
28059	CG7549	mtg	no phenotype
28155	CG10706	SK	no phenotype
28206	CG17975	sut2	no phenotype
28294	CG1084	Cont	no phenotype
28359	CG3690	CG3690	no phenotype
28413	CG6508	CG6508	no phenotype
28471	CG30092	jbug	no phenotype
28667	CG9559	fog	no phenotype
28941	CG8725	CG8725	no phenotype
28942	CG8725	CG8725	no phenotype
29155	CG31999	CG31999	no phenotype
29257	CG13707	CG13707	no phenotype
29385	CG30404	Tango11	no phenotype
29720	CG33531	Ddr	no phenotype
29799	CG32169	Rbp6	no phenotype
29910	CG8581	fra	no phenotype
29917	CG32704	Ir8a	no phenotype
29930	CG4926	Ror	no phenotype
29985	CG30081	Ir51b	no phenotype
30033	CG2759	w	no phenotype
30038	CG8721	Odc1	no phenotype
30072	CG43079	nrm	no phenotype
30240	CG3774	Efr	no phenotype
30269	CG1688	CG1688	no phenotype
30273	CG6308	CG6308	no phenotype
30320	CG1494	CG1494	no phenotype
30567	CG11172	NFAT	no phenotype
30678	CG7596	Sgs5	no phenotype
30935	CG7447	slow	no phenotype
31298	CG10627	nst	no phenotype
31364	CG10837	eIF4B	no phenotype
32257	CG6407	Wnt5	no phenotype
32263	CG15002	mas	no phenotype
32395	CG16901	sqd	no phenotype

32945	CG17523	GstE2	no phenotype
33123	CG4356	mAChR-A	no phenotype
33217	CG1506	Ac3	no phenotype
33262	CG5687	CG5687	no phenotype
33277	CG10125	zpg	no phenotype
33317	CG10047	Syt4	no phenotype
33787	CG31211	CG31211	no phenotype
33817	CG13439	dpr	no phenotype
33909	CG9019	dsf	no phenotype
34082	CG42679	CG42679	no phenotype
34412	CG32138	Frl	no phenotype
34444	CG32203	Spn75F	no phenotype
34836	CG4394	Traf-like	no phenotype
35177	CG7139	CG3139	no phenotype
35499	CG11205	phr	no phenotype
35584	CG4178	Lsp1beta	no phenotype
36219	CG17941	ds	no phenotype
36269	CG10443	Lar	no phenotype
36320	CG6445	Cad74A	no phenotype
36328	CG7050	Nrx-1	no phenotype
36348	CG11059	Cals	no phenotype
36350	CG3665	Fas2	no phenotype
36523	CG13194	pyr	no phenotype
36557	CG6701	CG6701	no phenotype
36563	CG30084	Zasp52	no phenotype
36659	CG7577	ppk20	no phenotype
36665	CG2841	CG2841	no phenotype
37141	CG3409	CG3409	no phenotype
37165	CG12344	CG12344	no phenotype
37173	CG12960	Ir52a	no phenotype
37208	CG3413	wdp	no phenotype
37209	CG3413	wdp	no phenotype
37249	CG5751	TrpA1	no phenotype
37263	CG7888	CG7888	no phenotype
37264	CG7888	CG7888	no phenotype
37288	CG3619	DI	no phenotype
37295	CG7571	Oatp74D	no phenotype
37297	CG14585	Ir75a	no phenotype
37305	CG3961	CG3961	no phenotype
37329	CG31522	CG31522	no phenotype
37358	CG6898	Zip3	no phenotype
37376	CG15549	CG15549	no phenotype
37435	CG2679	CG2679	no phenotype

37458	CG15598	Osi17	no phenotype
37865	CG1106	Gel	no phenotype
37917	CG10701	Moe	no phenotype
37968	CG8808	Pdk	no phenotype
37988	CG6453	GCS2beta	no phenotype
38003	CG13983	CG13983	no phenotype
38008	CG42369	CG42369	no phenotype
38020	CG5867	CG5867	no phenotype
38188	CG42543	mp	no phenotype
38787	CG34383	kmr	no phenotype
38852	CG42260	CG42260	no phenotype
39176	CG8595	Toll-7	no phenotype
39177	CG6383	crb	no phenotype
39446	CG34380	CG34380	no phenotype
39470	CG3380	Oatp58Dc	no phenotype
39478	CG15860	pain	no phenotype
39596	CG6151	fwe	no phenotype
39690	CG1483	Map205	no phenotype
40223	CG31274	CG31274	no phenotype
40577	CG5072	Cdk4	no phenotype
40631	CG10975	Ptp69D	no phenotype
40686	CG17691	CG17691	no phenotype
40803	CG8776	nemy	no phenotype
40906	CG14855	CG14855	no phenotype
40918	CG32848	VACHT	no phenotype
40929	CG18039	GluRIID	no phenotype
40993	CG34405	NaCP60E	no phenotype
41103	CG10537	Rdl	no phenotype
41162	CG10433	CG10433	no phenotype
41186	CG11347	CG11347	no phenotype
41194	CG8982	Acp26Aa	no phenotype
41479	CG1212	p130CAS	no phenotype
42172	CG8978	Arpc1	no phenotype
42231	CG5803	Fas3	no phenotype
42235	CG1762	betaInt-nu	no phenotype
42236	CG17716	fas	no phenotype
42321	CG31158	Efa6	no phenotype
42326	CG13648	tnc	no phenotype
42391	CG3443	pcx	no phenotype
42397	CG11958	Cnx99A	no phenotype
42450	CG4977	kek2	no phenotype
42485	CG3297	mnd	no phenotype
42566	CG8967	otk	no phenotype

42613	CG1150	Osi3	no phenotype
42620	CG31284	wtrw	no phenotype
42630	CG31100	CG31100	no phenotype
42658	CG4451	Hs6st	no phenotype
42669	CG9717	CG9717	no phenotype
42689	CG9903	CG9903	no phenotype
42742	CG11822	nAcRbeta-21C	no phenotype
42776	CG33298	CG33298	no phenotype
42805	CG6417	Oatp33Eb	no phenotype
42856	CG1322	zfh1	no phenotype
42857	CG1322	zfh1	no phenotype
42862	CG4445	pgant3	no phenotype
42872	CG3829	CG3829	no phenotype
42892	CG42679	Lmpt	no phenotype
42911	CG6788	CG6788	no phenotype
43018	CG14141	nkt	no phenotype
43101	CG17715	CG17715	no phenotype
43201	CG14746	PGRP-SC1a	no phenotype
43210	CG1124	CG1124	no phenotype
43288	CG5959	MCO3	no phenotype
43307	CG31605	Bsg	no phenotype
43329	CG7887	Takr99D	no phenotype
43368	CG43368	CG43368	no phenotype
43473	CG14815	Pex5	no phenotype
43534	CG12847	Tsp42Ec	no phenotype
43702	CG1847	CG1847	no phenotype
43784	CG4527	Slik	no phenotype
43848	CG13586	itp	no phenotype
43928	CG32227	gogo	no phenotype
43955	CG1412	RhoGAP19D	no phenotype
44029	CG33196	dpy	no phenotype
44045	CG12366	O-fut1	no phenotype
44092	CG10076	spir	no phenotype
44117	CG11967	CAHbeta	no phenotype
44178	CG4550	ninaE	no phenotype
44271	CG11891	CG11891	no phenotype
44288	CG9033	Tsp47F	no phenotype
44438	CG8442	GluRIA	no phenotype
44532	CG34368	Fili	no phenotype
44536	CG3424	path	no phenotype
44545	CG1151	Osi6	no phenotype
44562	CG11739	CG11739	no phenotype
44663	CG9389	CG9389	no phenotype

44687	CG9528	retm	no phenotype
44702	CG5423	robo3	no phenotype
44895	CG5099	msi	no phenotype
44934	CG1380	sut4	no phenotype
44940	CG31321	CG31321	no phenotype
44967	CG5400	Eh	no phenotype
45160	CG9659	egh	no phenotype
45188	CG16700	CG16700	no phenotype
45198	CG5076	elk	no phenotype
45226	CG31523	CG31523	no phenotype
45232	CG4821	Tequila	no phenotype
45457	CG4934	brn	no phenotype
45486	CG6199	Plod	no phenotype
45590	CG11128	slif	no phenotype
45643	CG42514	CG42514	no phenotype
45696	CG12444	Ir48c	no phenotype
45718	CG9564	Try29F	no phenotype
45739	CG4690	Tsp5D	no phenotype
45740	CG4690	Tsp5D	no phenotype
45807	CG9467	CG9467	no phenotype
45809	CG9485	CG9485	no phenotype
45883	CG4280	crq	no phenotype
45912	CG13195	Ir48b	no phenotype
45921	CG8178	Nach	no phenotype
45989	CG8743	trpml	no phenotype
46253	CG32019	bt	no phenotype
46367	CG5250	CG5250	no phenotype
46398	CG17063	Inx6	no phenotype
46538	CG17292	CG17292	no phenotype
46920	CG9668	Rh4	no phenotype
47047	CG32792	CG32792	no phenotype
47074	CG9126	Stim	no phenotype
47112	CG33494	CG33494	no phenotype
47181	CG4531	aos	no phenotype
47269	CG17514	l(3)80Fj	no phenotype
47543	CG3874	frc	no phenotype
47550	CG5621	CG5621	no phenotype
47552	CG31424	Ir94b	no phenotype
47768	CG12199	kek5	no phenotype
47832	CG33321	CheB38b	no phenotype
47896	CG6919	Octbeta1R	no phenotype
47972	CG9127	Pfas	no phenotype
47977	CG8713	CG8713	no phenotype

48008	CG15899	Ca-alpha1T	no phenotype
48010	CG3168	CG3168	no phenotype
48011	CG3168	CG3168	no phenotype
48092	CG43368	CG43368	no phenotype
48093	CG43368	CG43368	no phenotype
48159	CG5610	nAcRalpha-96Aa	no phenotype
48184	CG4404	CG4404	no phenotype
48324	CG12420	CG12420	no phenotype
48410	CG33052	Gorab	no phenotype
48478	CG33688	CG33688	no phenotype
48551	CG1552	CG1552	no phenotype
48562	CG42235	CG42235	no phenotype
48786	CG11637	CG11637	no phenotype
48830	CG7026	VhaPPA1-2	no phenotype
49200	CG17026	CG17026	no phenotype
49217	CG33229	CG33229	no phenotype
49320	CG1742	Mgstl	no phenotype
49464	CG33178	CG33178	no phenotype
49565	CG17029	CG17029	no phenotype
49692	CG18816	Tsp42Eb	no phenotype
49782	CG33720	Pif1B	no phenotype
49835	CG12193	Or22a	no phenotype
49889	CG8234	Tret1-2	no phenotype
49925	CG18085	sev	no phenotype
49973	CG42575	CG42575	no phenotype
50099	CG18853	CG18853	no phenotype
50200	CG43067	FoxP	no phenotype
50295	CG13094	Dh31	no phenotype
50319	CG10146	AttA	no phenotype
50352	CG11889	CG11889	no phenotype
50426	CG5992	Adgf-A	no phenotype
50469	CG17751	CG17751	no phenotype
50586	CG31447	MESK4	no phenotype
50637	CG5493	CG5493	no phenotype
50699	CG33934	CG33934	no phenotype
50749	CG6496	Pdf	no phenotype
50772	CG12405	Prx2540-1	no phenotype
51018	CG33670	stg1	no phenotype
51043	CG33932	CG33932	no phenotype
51048	CG33933	Indy-2	no phenotype
51060	CG3285	CG3285	no phenotype
51083	CG2177	CG2177	no phenotype
51090	CG8804	wun	no phenotype

51129	CG12070	Sap-r	no phenotype
51130	CG12070	Sap-r	no phenotype
51237	CG8577	PGRP-SC1b	no phenotype
51240	CG5619	trk	no phenotype
51272	CG9429	Calr	no phenotype
51438	CG4226	GluRIIC	no phenotype
51459	CG18660	Nckx30C	no phenotype
51479	CG2125	ci	no phenotype
51526	CG5657	Scgbeta	no phenotype
51584	CG7509	CG7509	no phenotype
51719	CG33531	Ddr	no phenotype
51855	CG3966	ninaA	no phenotype
51939	CG9023	Drip	no phenotype
51977	CG10580	fng	no phenotype
51979	CG10564	Ac78C	no phenotype
52435	CG8622	Acp53Ea	no phenotype
52457	CG16944	sesB	no phenotype
100010	CG7595	ck	no phenotype
100018	CG2380	Nfl	no phenotype
100021	CG4389	Mtpalpha	no phenotype
100032	CG14925	Osi21	no phenotype
100036	CG11527	Tig	no phenotype
100038	CG5958	CG5958	no phenotype
100039	CG17348	drl	no phenotype
100046	CG31121	CG31121	no phenotype
100078	CG5490	TI	no phenotype
100079	CG11853	to	no phenotype
100084	CG4790	fs(1)M3	no phenotype
100085	CG11910	alrm	no phenotype
100090	CG5842	nan	no phenotype
100093	CG17929	CG17929	no phenotype
100100	CG17028	CG17028	no phenotype
100105	CG8799	l(2)03659	no phenotype
100112	CG8654	CG8654	no phenotype
100113	CG42679	Lmpt	no phenotype
100120	CG5372	alphaPS5	no phenotype
100134	CG5820	Gp150	no phenotype
100141	CG7631	CG7631	no phenotype
100142	CG7309	CG7309	no phenotype
100149	CG17839	CG17839	no phenotype
100173	CG32476	mthl14	no phenotype
100174	CG1153	Osi7	no phenotype
100181	CG34143	Ir10a	no phenotype

100193	CG9512	CG9512	no phenotype
100194	CG9649	CG9649	no phenotype
100199	CG33522	scaf6	no phenotype
100200	CG1697	rho-4	no phenotype
100202	CG4465	CG4465	no phenotype
100210	CG15188	Osi20	no phenotype
100219	CG1887	CG1887	no phenotype
100240	CG15591	Osi8	no phenotype
100246	CG32475	mthl8	no phenotype
100252	CG10345	CG10345	no phenotype
100253	CG3853	Glut3	no phenotype
100268	CG32146	dlp	no phenotype
100281	CG9390	AcCoAS	no phenotype
100321	CG15661	Ugt49C1	no phenotype
100325	CG33282	CG33282	no phenotype
100334	CG5507	T48	no phenotype
100345	CG31718	Ir31a	no phenotype
100348	CG3382	Oatp58Db	no phenotype
100351	CG9981	CG9981	no phenotype
100354	CG4409	CG4409	no phenotype
100357	CG5700	prc	no phenotype
100372	CG3476	CG3476	no phenotype
100376	CG34127	CG34127	no phenotype
100378	CG17646	CG17646	no phenotype
100391	CG7228	pes	no phenotype
100404	CG2969	Atet	no phenotype
100407	CG17382	Ir94h	no phenotype
100411	CG9009	pdgy	no phenotype
100416	CG6499	CG6499	no phenotype
100422	CG15732	Ir11a	no phenotype
100424	CG8091	Dronc	no phenotype
100456	CG7936	mex1	no phenotype
100464	CG31911	Ent2	no phenotype
100472	CG8908	CG8908	no phenotype
100476	CG42318	app	no phenotype
100479	CG31561	Osi16	no phenotype
100481	CG1629	yellow-h	no phenotype
100487	CG3212	Sr-CIV	no phenotype
100498	CG15326	Ir7b	no phenotype
100517	CG7409	CG7409	no phenotype
100560	CG2194	su©	no phenotype
100566	CG6378	SPARC	no phenotype
100579	CG5403	retn	no phenotype

100582	CG7954	CG7954	no phenotype
100593	CG9238	Gbs-70E	no phenotype
100600	CG5002	CG5002	no phenotype
100603	CG14214	Sec61gamma	no phenotype
100608	CG3139	Syt1	no phenotype
100613	CG11781	CG11781	no phenotype
100624	CG13521	robo	no phenotype
100641	CG9507	Nep15	no phenotype
100642	CG5803	Fas3	no phenotype
100643	CG9499	ppk7	no phenotype
100654	CG42275	alpha-Man-I	no phenotype
100656	CG17036	CG17036	no phenotype
100658	CG31676	CG31676	no phenotype
100660	CG11898	CG11898	no phenotype
100662	CG13225	Or47a	no phenotype
100667	CG14376	Ir87a	no phenotype
100670	CG8837	CG8837	no phenotype
100680	CG8399	CG8399	no phenotype
100685	CG32717	sdt	no phenotype
100698	CG3926	Spat	no phenotype
100716	CG42679	CG42679	no phenotype
100721	CG11326	Tsp	no phenotype
100739	CG8846	Thor	no phenotype
100742	CG11328	Nhe3	no phenotype
100745	CG32675	Tango5	no phenotype
100749	CG8639	Cirl	no phenotype
100756	CG32538	gfA	no phenotype
100760	CG42301	CCKLR-17D1	no phenotype
100770	CG9623	if	no phenotype
100780	CG6205	por	no phenotype
100795	CG32687	CG32687	no phenotype
100803	CG2675	Csat	no phenotype
100809	CG5014	Vap-33-1	no phenotype
100819	CG8075	Vang	no phenotype
100825	CG10609	Orco	no phenotype
100829	CG17061	mthl10	no phenotype
100834	CG8546	CG8546	no phenotype
100837	CG42315	Ir93a	no phenotype
100840	CG10521	NetB	no phenotype
100842	CG10702	CG10702	no phenotype
100852	CG16727	CG16727	no phenotype
100866	CG9880	Or23a	no phenotype
100882	CG17922	CG17922	no phenotype

100883	CG11155	CG11155	no phenotype
100885	CG15325	Ir7g	no phenotype
100897	CG9196	spz6	no phenotype
100901	CG2507	sas	no phenotype
100903	CG14606	CG14606	no phenotype
100909	CG3592	CG3592	no phenotype
100912	CG42352	Ir40a	no phenotype
100928	CG8856	Sr-CII	no phenotype
100930	CG6868	tld	no phenotype
100931	CG14690	tomboy20	no phenotype
100932	CG31445	CG31445	no phenotype
100933	CG5998	Adgf-B	no phenotype
100935	CG9976	Lectin-galC1	no phenotype
100936	CG12945	CG12945	no phenotype
100944	CG11064	Rfabg	no phenotype
100946	CG4805	ppk28	no phenotype
100949	CG8095	scb	no phenotype
100950	CG6067	CG6067	no phenotype
100953	CG5404	CG5404	no phenotype
100957	CG5559	Syalpha	no phenotype
100961	CG6627	Dnz1	no phenotype
100966	CG13124	CG13124	no phenotype
100967	CG31423	Ir94c	no phenotype
100976	CG9550	CG9550	no phenotype
100977	CG5154	Idgf5	no phenotype
100980	CG34366	Shaw1	no phenotype
100995	CG17797	Acp29AB	no phenotype
100997	CG13360	CG13360	no phenotype
101003	CG5348	CG5348	no phenotype
101004	CG14856	CG14856	no phenotype
101019	CG13762	brv3	no phenotype
101021	CG3206	Or2a	no phenotype
101031	CG10006	CG10006	no phenotype
101041	CG14153	CG14153	no phenotype
101044	CG12843	Tsp42Ei	no phenotype
101065	CG2187	CG2187	no phenotype
101080	CG11069	CG11069	no phenotype
101081	CG11415	Tsp2A	no phenotype
101082	CG8098	Picot	no phenotype
101083	CG3897	blot	no phenotype
101084	CG7627	CG7627	no phenotype
101086	CG15020	CG15020	no phenotype
101091	CG11209	ppk6	no phenotype

101093	CG43901	CG43901	no phenotype
101100	CG3234	tim	no phenotype
101110	CG12783	CG12783	no phenotype
101115	CG9918	Pk1r	no phenotype
101125	CG9559	fog	no phenotype
101128	CG8925	CG8925	no phenotype
101136	CG7422	Snmp2	no phenotype
101137	CG16960	Or33a	no phenotype
101145	CG9317	CG9317	no phenotype
101153	CG9138	uif	no phenotype
101154	CG1389	tor	no phenotype
101166	CG12283	kek1	no phenotype
101174	CG10369	Irk3	no phenotype
101175	CG31247	tinc	no phenotype
101180	CG4226	GluRIIC	no phenotype
101204	CG14630	CG14630	no phenotype
101220	CG15538	Osi23	no phenotype
101221	CG14709	Mrp4	no phenotype
101238	CG10101	Ir84a	no phenotype
101242	CG18734	Fur2	no phenotype
101249	CG13253	cmpy	no phenotype
101254	CG4630	CG4630	no phenotype
101261	CG13592	Ir60e	no phenotype
101282	CG11101	pwn	no phenotype
101289	CG12594	CG12594	no phenotype
101290	CG12866	CG12866	no phenotype
101298	CG9681	PGRP-SB1	no phenotype
101348	CG8111	CG8111	no phenotype
101379	CG18803	Psn	no phenotype
101396	CG32220	Csas	no phenotype
101406	CG5643	wdb	no phenotype
101408	CG18177	Naa60	no phenotype
101411	CG6120	Tsp96F	no phenotype
101426	CG4080	CG4080	no phenotype
101428	CG42311	grh	no phenotype
101449	CG1417	slgA	no phenotype
101453	CG1358	CG1358	no phenotype
101466	CG13827	CG13827	no phenotype
101473	CG9093	Tsp26A	no phenotype
101476	CG7470	CG7470	no phenotype
101477	CG17228	pros	no phenotype
101483	CG43155	CG43155	no phenotype
101505	CG4859	Mmp1	no phenotype

101518	CG32183	Ccn	no phenotype
101520	CG32183	Ccn	no phenotype
101525	CG18361	DISHEVELLED	no phenotype
101540	CG7499	Rh50	no phenotype
101557	CG3971	Baldspot	no phenotype
101563	CG13116	CG13116	no phenotype
101569	CG10353	CG10353	no phenotype
101571	CG4128	nAcRalpha-30D	no phenotype
101573	CG1889	CG1889	no phenotype
101574	CG11589	VhaM9.7-c	no phenotype
101575	CG8602	CG8602	no phenotype
101584	CG17632	bw	no phenotype
101590	CG42584	Ir76a	no phenotype
101593	CG6965	mth15	no phenotype
101596	CG6509	Dlg5	no phenotype
101600	CG42269	CG42269	no phenotype
101610	CG18788	CG18788	no phenotype
101618	CG31673	CG31673	no phenotype
101621	CG6407	Wnt5	no phenotype
101633	CG8916	CG8916	no phenotype
101636	CG4432	PGRP-LC	no phenotype
101642	CG7100	CadN	no phenotype
101643	CG10175	CG10175	no phenotype
101645	CG33957	Plp	no phenotype
101649	CG6234	CG6234	no phenotype
101659	CG42829	CadN2	no phenotype
101662	CG7644	beat-Ib	no phenotype
101664	CG33289	CG33289	no phenotype
101679	CG9722	CG9722	no phenotype
101682	CG42642	Ir75c	no phenotype
101684	CG1214	ru	no phenotype
101686	CG6992	GluRIIA	no phenotype
101687	CG42345	stw	no phenotype
101695	CG34405	NaCP60E	no phenotype
101700	CG34120	CG34120	no phenotype
101701	CG17610	grk	no phenotype
101705	CG15520	capa	no phenotype
101708	CG9668	Rh4	no phenotype
101725	CG42352	Ir40a	no phenotype
101729	CG43657	Myo10A	no phenotype
101736	CG6017	Hip14	no phenotype
101740	CG10851	B52	no phenotype
101742	CG5594	kcc	no phenotype

101743	CG42314	PMCA	no phenotype
101745	CG42701	Cng	no phenotype
101752	CG33198	pen-2	no phenotype
101757	CG7540	M6	no phenotype
101759	CG9533	rut	no phenotype
101765	CG4070	Tis11	no phenotype
101768	CG43066	CG43066	no phenotype
101778	CG15595	Osi13	no phenotype
101779	CG6588	Fas1	no phenotype
101786	CG6788	CG6788	no phenotype
101790	CG7333	CG7333	no phenotype
101808	CG33349	ppk25	no phenotype
101811	CG42628	rad	no phenotype
101817	CG1157	Osi15	no phenotype
101820	CG32975	nAcRalpha-34E	no phenotype
101844	CG17364	CG17364	no phenotype
101855	CG33970	CG33970	no phenotype
101866	CG6356	CG6356	no phenotype
101867	CG34100	mld	no phenotype
101888	CG8642	CG8642	no phenotype
101915	CG16876	nimC4	no phenotype
101918	CG9280	Glt	no phenotype
101920	CG15685	Ir92a	no phenotype
101924	CG8012	CG8012	no phenotype
101945	CG32136	Tsp68C	no phenotype
101947	CG1698	CG1698	no phenotype
101948	CG6096	E(spl)m5-HLH	no phenotype
101949	CG4250	CG4250	no phenotype
101982	CG13747	CG13747	no phenotype
102001	CG33203	CG33203	no phenotype
102014	CG14808	Scgdelta	no phenotype
102018	CG34413	NKAIN	no phenotype
102019	CG5855	cni	no phenotype
102043	CG13687	Ptth	no phenotype
102046	CG4591	Tsp86D	no phenotype
102047	CG1079	Fie	no phenotype
102058	CG1128	alpha-Est9	no phenotype
102072	CG13780	Pvf2	no phenotype
102087	CG4716	CG4716	no phenotype
102097	CG31689	CG31689	no phenotype
102101	CG3218	fs(1)K10	no phenotype
102105	CG1056	5-HT2	no phenotype
102107	CG14691	CG14691	no phenotype

102110	CG13252	CG13252	no phenotype
102132	CG13427	CG13427	no phenotype
102136	CG15551	CtrlC	no phenotype
102158	CG8167	Ilp2	no phenotype
102166	CG15013	dyl	no phenotype
102175	CG10788	ng3	no phenotype
102182	CG13432	qsm	no phenotype
102183	CG7091	CG7091	no phenotype
102201	CG14935	Mal-B2	no phenotype
102204	CG13419	burs	no phenotype
102206	CG11303	TM4SF	no phenotype
102214	CG2611	CG2611	no phenotype
102218	CG43128	Shab	no phenotype
102220	CG5835	CG5835	no phenotype
102236	CG7448	CG7448	no phenotype
102247	CG1318	Hexo1	no phenotype
102252	CG11422	Obp83b	no phenotype
102253	CG13503	Vrp1	no phenotype
102255	CG9355	dy	no phenotype
102257	CG14375	CCHa2	no phenotype
102269	CG9057	Lsd-2	no phenotype
102270	CG7084	CG7084	no phenotype
102277	CG32042	PGRP-LA	no phenotype
102281	CG4710	Pino	no phenotype
102292	CG12370	Dh44-R2	no phenotype
102294	CG12841	Tsp42Ek	no phenotype
102295	CG12175	tth	no phenotype
102299	CG8630	CG8630	no phenotype
102303	CG6936	mth	no phenotype
102317	CG8028	CG8028	no phenotype
102319	CG12781	nahoda	no phenotype
102329	CG42242	beat-VII	no phenotype
102339	CG4626	fz4	no phenotype
102344	CG8788	CG8788	no phenotype
102351	CG9935	CG9935	no phenotype
102352	CG9614	pip	no phenotype
102357	CG4920	ea	no phenotype
102359	CG11637	NijB	no phenotype
102363	CG1139	CG1139	no phenotype
102389	CG9972	spz5	no phenotype
102392	CG15590	Osi5	no phenotype
102396	CG42234	Dbx	no phenotype
102398	CG15717	CG15717	no phenotype

102411	CG43395	Cngl	no phenotype
102424	CG17637	CG17637	no phenotype
102438	CG2082	CG2082	no phenotype
102441	CG12443	ths	no phenotype
102443	CG5955	CG5955	no phenotype
102445	CG16886	Vajk1	no phenotype
102461	CG9366	CG9366	no phenotype
102463	CG34366	Shaw1	no phenotype
102465	CG14049	Ilp6	no phenotype
102466	CG2715	Syx4	no phenotype
102476	CG32632	Tango13	no phenotype
102488	CG7105	Proct	no phenotype
102505	CG31778	CG31778	no phenotype
102516	CG13796	CG13796	no phenotype
102518	CG10287	Gasp	no phenotype
102533	CG1683	Ant2	no phenotype
102534	CG31764	vir-1	no phenotype
102543	CG2781	CG2781	no phenotype
102570	CG7589	CG7589	no phenotype
102588	CG7478	Act79B	no phenotype
102602	CG9211	ihog	no phenotype
102612	CG7740	prominin-like	no phenotype
102615	CG10675	CHKov2	no phenotype
102619	CG10303	Osi4	no phenotype
102631	CG31974	CG31974	no phenotype
102635	CG13248	CG13248	no phenotype
102639	CG42555	tweek	no phenotype
102643	CG7431	TyrR	no phenotype
102644	CG18321	miple2	no phenotype
102647	CG32206	CG32206	no phenotype
102648	CG14741	CG14741	no phenotype
102662	CG2191	Smvt	no phenotype
102670	CG10359	CG10359	no phenotype
102672	CG2736	CG2736	no phenotype
102676	CG34139	CG34139	no phenotype
102678	CG32695	CG32695	no phenotype
102679	CG33177	CG33177	no phenotype
102684	CG44325	CG44325	no phenotype
102687	CG4605	Acp32CD	no phenotype
102690	CG15284	pburs	no phenotype
102698	CG10134	beat-Va	no phenotype
102699	CG7103	Pvf1	no phenotype
102701	CG4960	CG4960	no phenotype

102707	CG42253	Ndae1	no phenotype
102728	CG8226	Tom7	no phenotype
102735	CG14919	Ast-C	no phenotype
102739	CG2374	lbm	no phenotype
102745	CG8860	CG8860	no phenotype
102750	CG8740	CG8740	no phenotype
102758	CG32632	Tango13	no phenotype
102762	CG16743	CG16743	no phenotype
102772	CG45017	IP3K2	no phenotype
102783	CG42701	Cng	no phenotype
102805	CG15189	Osi19	no phenotype
102811	CG7476	mthl7	no phenotype
102823	CG42613	CG42613	no phenotype
102826	CG11575	Ir100a	no phenotype
102850	CG9902	CG9902	no phenotype
102859	CG32669	CG32669	no phenotype
102861	CG15293	CG15293	no phenotype
102865	CG31720	mthl15	no phenotype
102880	CG9812	CG9812	no phenotype
102900	CG17218	crok	no phenotype
102908	CG16756	CG16756	no phenotype
102919	CG42677	wb	no phenotype
102923	CG15555	CG15555	no phenotype
102954	CG42248	CG42248	no phenotype
102979	CG1155	Osi14	no phenotype
102983	CG42315	Ir93a	no phenotype
102985	CG45049	CG45049	no phenotype
102995	CG33344	CcapR	no phenotype
103023	CG7514	CG7514	no phenotype
103032	CG33968	drd	no phenotype
103037	CG11425	CG11425	no phenotype
103040	CG15642	CG15642	no phenotype
103041	CG12045	Cpr100A	no phenotype
103044	CG9619	Gbs-76A	no phenotype
103045	CG30035	Tret1-1	no phenotype
103047	CG30040	jeb	no phenotype
103101	CG17271	CG17271	no phenotype
103142	CG33181	CG33181	no phenotype
103171	CG41106	CG41106	no phenotype
103193	CG10693	slo	no phenotype
103215	CG13633	Ast	no phenotype
103222	CG12838	Tsp42Eo	no phenotype
103234	CG32694	CG32694	no phenotype

103256	CG2977	Inx7	no phenotype
103263	CG3994	ZnT35C	no phenotype
103270	CG17027	CG17027	no phenotype
103271	CG12344	CG12344	no phenotype
103285	CG42235	CG42235	no phenotype
103296	CG13664	Cad96Cb	no phenotype
103298	CG42338	Ten-a	no phenotype
103327	CG4722	bib	no phenotype
103345	CG42333	Sytbeta	no phenotype
103354	CG7115	CG7115	no phenotype
103359	CG1907	CG1907	no phenotype
103363	CG9262	Shal	no phenotype
103382	CG44015	Hph	no phenotype
103398	CG31860	CG31860	no phenotype
103411	CG33106	mask	no phenotype
103415	CG7962	CdsA	no phenotype
103420	CG8594	ClC-b	no phenotype
103427	CG43081	vas	no phenotype
103452	CG8805	wun2	no phenotype
103457	CG11516	Ptp99A	no phenotype
103492	CG3829	CG3829	no phenotype
103494	CG18314	DopEcR	no phenotype
103506	CG11801	Elo68beta	no phenotype
103544	CG11909	tobi	no phenotype
103553	CG30421	Usp15-31	no phenotype
103556	CG3770	CG3770	no phenotype
103565	CG31694	CG31694	no phenotype
103570	CG11194	Hey	no phenotype
103586	CG8394	VGAT	no phenotype
103592	CG30483	Prosap	no phenotype
103604	CG12130	Pal1	no phenotype
103605	CG12121	CG12121	no phenotype
103611	CG17657	fritz	no phenotype
103621	CG3359	mfas	no phenotype
103629	CG3054	l(2)k05819	no phenotype
103630	CG7980	RabX5	no phenotype
103645	CG10743	Liprin-beta	no phenotype
103651	CG3328	CG3328	no phenotype
103652	CG30345	CG30345	no phenotype
103661	CG42611	mgl	no phenotype
103662	CG14734	Tk	no phenotype
103702	CG9258	nrv1	no phenotype
103705	CG31678	CG31678	no phenotype

103707	CG10470	CG10470	no phenotype
103713	CG33174	inaE	no phenotype
103715	CG1664	sbr	no phenotype
103717	CG7127	CG7127	no phenotype
103736	CG11144	mGluRA	no phenotype
103750	CG4928	CG4928	no phenotype
103754	CG1517	na	no phenotype
103764	CG1311	CG1311	no phenotype
103766	CG6910	CG6910	no phenotype
103770	CG14646	CG14646	no phenotype
103780	CG10413	CG10413	no phenotype
103790	CG5085	CG5085	no phenotype
103807	CG3665	Fas2	no phenotype
103812	CG6210	wls	no phenotype
103817	CG10334	spi	no phenotype
103821	CG4677	lmd	no phenotype
103822	CG8784	CG8784	no phenotype
103825	CG5791	BomBc3	no phenotype
103861	CG34398	CG34398	no phenotype
103925	CG6812	CG6812	no phenotype
103931	CG11516	Ptp99A	no phenotype
103941	CG11537	CG11537	no phenotype
103950	CG4743	CG4743	no phenotype
103956	CG15096	CG15096	no phenotype
103962	CG3722	shg	no phenotype
103966	CG9780	Nep111	no phenotype
103969	CG17928	CG17928	no phenotype
103970	CG9864	CG9864	no phenotype
103973	CG5811	NepYr	no phenotype
103981	CG2346	Fmrf	no phenotype
103985	CG10706	SK	no phenotype
103992	CG12825	CG12825	no phenotype
104015	CG5805	CG5805	no phenotype
104020	CG4969	Wnt6	no phenotype
104033	CG6530	mth13	no phenotype
104050	CG33976	Octbeta2R	no phenotype
104067	CG17662	CG17662	no phenotype
104072	CG33528	Vmat	no phenotype
104079	CG14936	Tsp33B	no phenotype
104098	CG8850	CG8850	no phenotype
104099	CG11592	CG11592	no phenotype
104112	CG14021	fusl	no phenotype
104118	CG5455	CG5455	no phenotype

104126	CG2310	CG2310	no phenotype
104145	CG4288	CG4288	no phenotype
104152	CG4323	Dic2	no phenotype
104168	CG43368	cac	no phenotype
104172	CG33991	nuf	no phenotype
104174	CG3331	e	no phenotype
104177	CG8451	CG8451	no phenotype
104180	CG6816	Cyp18a1	no phenotype
104181	CG2913	yin	no phenotype
104198	CG5006	Or33c	no phenotype
104206	CG13801	CG13801	no phenotype
104208	CG3533	uzip	no phenotype
104209	CG31146	Nlg1	no phenotype
104214	CG3095	hfw	no phenotype
104215	CG31213	CG31213	no phenotype
104241	CG5772	Sur	no phenotype
104254	CG7526	frac	no phenotype
104272	CG10560	CG10560	no phenotype
104278	CG9394	CG9394	no phenotype
104279	CG12676	ed	no phenotype
104295	CG43079	nrm	no phenotype
104301	CG31106	CG31106	no phenotype
104315	CG1268	VhaM9.7-a	no phenotype
104321	CG8507	CG8507	no phenotype
104324	CG9887	Vglut	no phenotype
104326	CG9904	Seipin	no phenotype
104336	CG12025	CG12025	no phenotype
104337	CG17754	CG17754	no phenotype
104338	CG1916	Wnt2	no phenotype
104350	CG5887	desat1	no phenotype
104368	CG5634	dsd	no phenotype
104371	CG3159	Eaat2	no phenotype
104397	CG43658	CG43658	no phenotype
104408	CG6321	CG6321	no phenotype
104414	CG10157	GILT2	no phenotype
104430	CG4999	Tsp66E	no phenotype
104432	CG10225	RanBP3	no phenotype
104438	CG44193	Cdep	no phenotype
104445	CG1869	Cht7	no phenotype
104450	CG18345	trpl	no phenotype
104454	CG32079	CG32079	no phenotype
104472	CG31637	CG31637	no phenotype
104474	CG12348	Sh	no phenotype

104503	CG6659	CG6659	no phenotype
104505	CG18405	Sema-1a	no phenotype
104514	CG15553	CG15553	no phenotype
104515	CG14032	Cyp4ac1	no phenotype
104521	CG42340	CG42340	no phenotype
104523	CG4005	yki	no phenotype
104524	CG33976	Octbeta2R	no phenotype
104529	CG9444	CG9444	no phenotype
104536	CG4145	Cg25C	no phenotype
104538	CG10176	CG10176	no phenotype
104543	CG42351	Jabba	no phenotype
104557	CG14704	PGRP-LB	no phenotype
104572	CG7206	CG7206	no phenotype
104578	CG14745	PGRP-SC2	no phenotype
104589	CG42274	RhoGAP18B	no phenotype
104590	CG1169	Osi18	no phenotype
104613	CG32356	ImpE1	no phenotype
104623	CG1221	miple	no phenotype
104662	CG15361	Nplp4	no phenotype
104668	CG4482	mol	no phenotype
104671	CG4698	Wnt4	no phenotype
104683	CG9347	ninaB	no phenotype
104689	CG33484	zormin	no phenotype
104697	CG31431	CG31431	no phenotype
104698	CG3182	sei	no phenotype
104703	CG17579	sca	no phenotype
104716	CG3019	su(w[a])	no phenotype
104719	CG32513	bves	no phenotype
104726	CG7486	Dredd	no phenotype
104729	CG11597	CG11597	no phenotype
104735	CG2397	Cyp6a13	no phenotype
104736	CG31619	nolo	no phenotype
104744	CG14160	CG14160	no phenotype
104748	CG31832	CG31832	no phenotype
104752	CG14487	Ir54a	no phenotype
104762	CG3649	CG3649	no phenotype
104763	CG10251	prt	no phenotype
104771	CG31973	Cda5	no phenotype
104773	CG2902	Nmdar1	no phenotype
104775	CG9907	para	no phenotype
104789	CG5685	Calx	no phenotype
104790	CG10326	CG10326	no phenotype
104795	CG7736	Syx6	no phenotype

104804	CG12073	5-HT7	no phenotype
104814	CG12484	CG12484	no phenotype
104874	CG34394	GramD1B	no phenotype
104883	CG1615	Ork1	no phenotype
104888	CG7345	Sox21a	no phenotype
104892	CG33532	lectin-37Da	no phenotype
104906	CG16705	SPE	no phenotype
104908	CG16844	BomS3	no phenotype
104929	CG15211	CG15211	no phenotype
104935	CG4135	beat-lib	no phenotype
104943	CG8663	nrv3	no phenotype
104950	CG12837	Tsp42Er	no phenotype
104952	CG34369	CG34369	no phenotype
104956	CG16704	CG16704	no phenotype
104964	CG8956	AhcyL2	no phenotype
104974	CG14358	CCHa1	no phenotype
104983	CG8714	sut1	no phenotype
104986	CG9336	CG9336	no phenotype
104993	CG6151	fwe	no phenotype
105004	CG33273	Ilp5	no phenotype
105008	CG34378	Pvf3	no phenotype
105010	CG14624	CG14624	no phenotype
105016	CG14871	Trissin	no phenotype
105017	CG6134	spz	no phenotype
105024	CG13317	Ilp7	no phenotype
105036	CG11405	Atf3	no phenotype
105037	CG42338	Ten-a	no phenotype
105046	CG42340	CG42340	no phenotype
105055	CG3327	E23	no phenotype
105063	CG1171	Akh	no phenotype
105067	CG16713	CG16713	no phenotype
105071	CG42611	mgl	no phenotype
105077	CG15406	CG15406	no phenotype
105105	CG9723	CG9723	no phenotype
105108	CG9450	tud	no phenotype
105121	CG3845	NAT1	no phenotype
105144	CG9098	CG9098	no phenotype
105145	CG17723	ZnT63C	no phenotype
105155	CG10626	Lkr	no phenotype
105174	CG11897	CG11897	no phenotype
105183	CG13920	CG13920	no phenotype
105191	CG12143	Tsp42Ej	no phenotype
105193	CG6981	Ssk	no phenotype

105194	CG6231	CG6231	no phenotype
105202	CG40494	RhoGAP1A	no phenotype
105252	CG32239	RhoGEF64C	no phenotype
105280	CG5996	Trpgamma	no phenotype
105281	CG8444	VhaM8.9	no phenotype
105286	CG7655	CG7655	no phenotype
105288	CG9947	CG9947	no phenotype
105290	CG8331	CG8331	no phenotype
105301	CG32180	Eip74EF	no phenotype
105307	CG30460	CG30460	no phenotype
105308	CG5581	Ote	no phenotype
105309	CG16987	daw	no phenotype
105314	CG10382	wrapper	no phenotype
105330	CG11347	DOR	no phenotype
105360	CG8930	rk	no phenotype
105372	CG8907	CG8907	no phenotype
105373	CG14767	CG14767	no phenotype
105398	CG10627	nst	no phenotype
105400	CG12891	whd	no phenotype
105410	CG9620	nac	no phenotype
105412	CG43398	scrib	no phenotype
105418	CG1275	CG1275	no phenotype
105419	CG6214	MRP	no phenotype
105422	CG9148	scf	no phenotype
105429	CG12286	kar	no phenotype
105439	CG4484	Slc45-1	no phenotype
105446	CG1791	CG1791	no phenotype
105453	CG7157	Acp36DE	no phenotype
105462	CG8428	spin	no phenotype
105463	CG1058	rpk	no phenotype
105472	CG32982	CG32982	no phenotype
105477	CG32000	CG32000	no phenotype
105486	CG33197	mbl	no phenotype
105493	CG17697	fz	no phenotype
105495	CG7437	mub	no phenotype
105509	CG1803	regucalcin	no phenotype
105516	CG6736	Ilp4	no phenotype
105518	CG1443	wat	no phenotype
105526	CG13077	CG13077	no phenotype
105528	CG9593	CG9593	no phenotype
105530	CG7068	Tep3	no phenotype
105546	CG32853	mthl12	no phenotype
105549	CG3837	CG3837	no phenotype

105555	CG11136	Lrt	no phenotype
105556	CG14575	capaR	no phenotype
105558	CG31693	CG31693	no phenotype
105560	CG5427	Oatp33Ea	no phenotype
105562	CG3244	slf	no phenotype
105566	CG4462	CG4462	no phenotype
105570	CG33124	CG33124	no phenotype
105576	CG7881	CG7881	no phenotype
105579	CG11020	nompC	no phenotype
105581	CG7234	GluRIIB	no phenotype
105584	CG13061	Nplp3	no phenotype
105586	CG1154	Osi12	no phenotype
105595	CG13417	Gr93a	no phenotype
105600	CG4231	Or22b	no phenotype
105608	CG1718	CG1718	no phenotype
105611	CG4335	CG4335	no phenotype
105645	CG42672	CG42672	no phenotype
105646	CG3156	CG3156	no phenotype
105647	CG9431	kek4	no phenotype
105656	CG4435	FucTB	no phenotype
105677	CG1607	CG1607	no phenotype
105681	CG8026	CG8026	no phenotype
105693	CG5532	CG5532	no phenotype
105697	CG31732	yuri	no phenotype
105724	CG15592	Osi9	no phenotype
105754	CG7535	GluClalpha	no phenotype
105756	CG32632	Tango13	no phenotype
105767	CG2520	lap	no phenotype
105771	CG12531	CG12531	no phenotype
105780	CG6034	CG6034	no phenotype
105784	CG15546	CG15546	no phenotype
105785	CG11956	SP1029	no phenotype
105794	CG18330	Peyt2	no phenotype
105798	CG14064	beat-VI	no phenotype
105799	CG8942	nimC1	no phenotype
105821	CG31743	CG31743	no phenotype
105839	CG9494	Tsp29Fa	no phenotype
105841	CG30069	CG30069	no phenotype
105847	CG12846	TSP42ED	no phenotype
105848	CG43729	Stacl	no phenotype
105850	CG15596	Osi11	no phenotype
105852	CG8815	Sin3A	no phenotype
105853	CG9224	sog	no phenotype

105859	CG11411	fs(1)N	no phenotype
105868	CG9825	CG9825	no phenotype
105870	CG8681	clumsy	no phenotype
105877	CG4683	Tengl4	no phenotype
105880	CG14743	CG14743	no phenotype
105883	CG1987	Rbp1-like	no phenotype
105885	CG42665	Exn	no phenotype
105893	CG34413	NKAIN	no phenotype
105895	CG13576	Ir60a	no phenotype
105896	CG18110	CG18110	no phenotype
105901	CG6977	Cad87A	no phenotype
105910	CG15221	CG15221	no phenotype
105911	CG31547	CG31547	no phenotype
105913	CG7449	hbs	no phenotype
105915	CG15593	Osi10	no phenotype
105920	CG11262	CG11262	no phenotype
105922	CG4822	CG4822	no phenotype
105928	CG15121	Ir56b	no phenotype
105947	CG33350	CheB42c	no phenotype
105969	CG7510	CG7510	no phenotype
105987	CG31729	CG31729	no phenotype
106006	CG3597	CG3597	no phenotype
106020	CG33348	CheB42a	no phenotype
106027	CG3252	NAAT1	no phenotype
106039	CG7955	ABCB7	no phenotype
106046	CG3423	SA	no phenotype
106053	CG9256	Nhe2	no phenotype
106056	CG17559	dnt	no phenotype
106064	CG10550	CG10550	no phenotype
106068	CG3757	y	no phenotype
106077	CG8249	CG8249	no phenotype
106080	CG9704	Nrt	no phenotype
106090	CG3593	r-l	no phenotype
106092	CG8224	babo	no phenotype
106094	CG16720	5-HT1A	no phenotype
106097	CG3143	CG3143	no phenotype
106115	CG14909	VhaM9.7-d	no phenotype
106122	CG31999	CG31999	no phenotype
106135	CG9361	Task7	no phenotype
106142	CG8817	lilli	no phenotype
106149	CG7919	fan	no phenotype
106207	CG15094	MFS15	no phenotype
106225	CG42289	Ir60b	no phenotype

106254	CG6453	GCS2beta	no phenotype
106255	CG7125	PKD	no phenotype
106284	CG1092	CG1092	no phenotype
106286	CG14076	Ir75d	no phenotype
106293	CG31769	CG31769	no phenotype
106298	CG43078	CG43078	no phenotype
106307	CG3488	Hydr2	no phenotype
106314	CG17273	AdSS	no phenotype
106334	CG8086	CG8086	no phenotype
106338	CG43225	axo	no phenotype
106354	CG10842	Cyp4p1	no phenotype
106355	CG5023	CG5023	no phenotype
106377	CG30277	Oatp58Da	no phenotype
106381	CG13758	Pdfr	no phenotype
106384	CG31105	CG31105	no phenotype
106392	CG33115	nimB4	no phenotype
106397	CG7334	Sug	no phenotype
106399	CG33207	pxb	no phenotype
106405	CG31352	Unc-115a	no phenotype
106408	CG31262	CG31262	no phenotype
106410	CG17923	Jyalpha	no phenotype
106433	CG33261	Trl	no phenotype
106449	CG2272	slpr	no phenotype
106455	CG14996	Chd64	no phenotype
106464	CG7447	slow	no phenotype
106468	CG8865	Rgl	no phenotype
106470	CG2789	Tspo	no phenotype
106479	CG6186	Tsf1	no phenotype
106484	CG15112	ena	no phenotype
106488	CG42318	app	no phenotype
106490	CG4678	CG4678	no phenotype
106494	CG2264	magu	no phenotype
106502	CG31298	beat-Vb	no phenotype
106504	CG45051	sima	no phenotype
106507	CG33967	kibra	no phenotype
106511	CG3856	Oamb	no phenotype
106512	CG14167	Ilp3	no phenotype
106513	CG6006	CG6006	no phenotype
106525	CG42636	Gyc76C	no phenotype
106531	CG8116	CG8116	no phenotype
106538	CG9697	PGRP-SB2	no phenotype
106540	CG5326	CG5326	no phenotype
106548	CG31509	TotA	no phenotype

106555	CG7442	CG7442	no phenotype
106559	CG42333	Sytbeta	no phenotype
106570	CG11348	nAcRbeta-64B	no phenotype
106575	CG18087	sgs7	no phenotype
106577	CG43443	hts	no phenotype
106606	CG6040	CG6040	no phenotype
106610	CG43313	CG43313	no phenotype
106618	CG30265	CG30265	no phenotype
106628	CG1464	ey	no phenotype
106655	CG33135	KCNQ	no phenotype
106656	CG1500	fw	no phenotype
106668	CG9485	CG9485	no phenotype
106669	CG33134	debel	no phenotype
106673	CG4615	CG4615	no phenotype
106679	CG8434	lbk	no phenotype
106681	CG13610	Orct2	no phenotype
106683	CG5410	Miro	no phenotype
106690	CG2179	Xe7	no phenotype
106698	CG13384	CG13384	no phenotype
106723	CG15624	hoe2	no phenotype
106729	CG10207	NaPi-T	no phenotype
106731	CG15627	Ir25a	no phenotype
106737	CG10553	CG10553	no phenotype
106738	CG6052	CG6052	no phenotype
106749	CG9977	AhcyL1	no phenotype
106781	CG7714	CG7714	no phenotype
106785	CG4334	CG4334	no phenotype
106787	CG17752	CG17752	no phenotype
106790	CG1545	CG1545	no phenotype
106839	CG9220	CG9220	no phenotype
106844	CG5284	Clc-c	no phenotype
106846	CG11525	CycG	no phenotype
106862	CG33526	PNUTS	no phenotype
106869	CG33542	upd3	no phenotype
106870	CG30344	CG30344	no phenotype
106873	CG8527	ppk23	no phenotype
106876	CG3302	Crz	no phenotype
106888	CG13568	ppk29	no phenotype
106907	CG6945	sstn	no phenotype
106909	CG5541	CG5541	no phenotype
106911	CG9023	Drip	no phenotype
106926	CG33131	SCAP	no phenotype
106935	CG1824	CG1824	no phenotype

106961	CG8380	DAT	no phenotype
106973	CG14616	l(1)G0196	no phenotype
106975	CG4562	CG4562	no phenotype
106982	CG1063	Itp-r83A	no phenotype
106983	CG14621	CG14621	no phenotype
106992	CG30147	Hil	no phenotype
107004	CG11081	plexA	no phenotype
107006	CG17896	CG17896	no phenotype
107008	CG10444	CG10444	no phenotype
107022	CG4459	CG4459	no phenotype
107023	CG32081	CG32081	no phenotype
107029	CG18250	Dg	no phenotype
107030	CG5535	CG5535	no phenotype
107036	CG7147	kuz	no phenotype
107043	CG8811	muskelin	no phenotype
107051	CG30011	gem	no phenotype
107058	CG9652	DopR	no phenotype
107061	CG42702	Oaz	no phenotype
107066	CG42273	mnb	no phenotype
107071	CG7904	put	no phenotype
107080	CG1407	CG1407	no phenotype
107083	CG8250	Alk	no phenotype
107088	CG6042	Cyp12a4	no phenotype
107102	CG14430	bou	no phenotype
107110	CG11140	Aldh-III	no phenotype
107116	CG3441	Nplp1	no phenotype
107122	CG34417	CG34417	no phenotype
107130	CG10079	Egfr	no phenotype
107135	CG31731	CG31731	no phenotype
107136	CG9628	CG9628	no phenotype
107146	CG3090	Sox14	no phenotype
107155	CG33116	CG33116	no phenotype
107169	CG10514	CG10514	no phenotype
107174	CG31706	CG31706	no phenotype
107183	CG42768	Msp-300	no phenotype
107194	CG5893	D	no phenotype
107195	CG17119	CG17119	no phenotype
107199	CG9850	sona	no phenotype
107213	CG15151	rdo	no phenotype
107214	CG32054	CG32054	no phenotype
107215	CG2857	Tpc2	no phenotype
107219	CG4607	CG4607	no phenotype
107225	CG32053	CG32053	no phenotype

107233	CG6446	Sema-1b	no phenotype
107236	CG32091	CG32091	no phenotype
107237	CG31792	CG31792	no phenotype
107243	CG8588	pst	no phenotype
107258	CG3903	Gli	no phenotype
107275	CG31753	ham	no phenotype
107292	CG5583	Ets98B	no phenotype
107307	CG34126	CG34126	no phenotype
107309	CG9428	ZIP1	no phenotype
107319	CG42543	mp	no phenotype
107320	CG10497	Sdc	no phenotype
107325	CG1753	Cbs	no phenotype
107339	CG13907	CG13907	no phenotype
107342	CG2316	CG2316	no phenotype
107343	CG11049	sv	no phenotype
107350	CG9432	l(2)01289	no phenotype
107355	CG14020	CG14020	no phenotype
107361	CG9657	CG9657	no phenotype
107363	CG7411	ort	no phenotype
107366	CG7021	Elal	no phenotype
107370	CG3701	CG3701	no phenotype
107371	CG31147	mthl1	no phenotype
107374	CG3308	CG3308	no phenotype
107388	CG6672	CG6672	no phenotype
107403	CG44328	Neto	no phenotype
107418	CG18445	oys	no phenotype
107434	CG4313	CG4313	no phenotype
107435	CG11335	lox	no phenotype
107437	CG10872	CG31926	no phenotype
107451	CG3937	cher	no phenotype
107452	CG10026	CG10026	no phenotype
107455	CG1136	CG1136	no phenotype
107457	CG4680	Gagr	no phenotype
107459	CG31762	bru1	no phenotype
107469	CG31770	He	no phenotype
107488	CG4521	mthl1	no phenotype
107491	CG43225	axo	no phenotype
107496	CG14629	CG14629	no phenotype
107502	CG1004	rho	no phenotype
107505	CG13999	CG13999	no phenotype
107521	CG33179	beat-IIIb	no phenotype
107527	CG12038	CG12038	no phenotype
107534	CG3541	pio	no phenotype

107536	CG9024	Acp26Ab	no phenotype
107537	CG34123	TrpM	no phenotype
107538	CG12840	Tsp42E1	no phenotype
107544	CG9990	CG9990	no phenotype
107559	CG2915	CG2915	no phenotype
107567	CG33533	lectin-37Db	no phenotype
107597	CG31092	LpR2	no phenotype
107604	CG30438	CG30438	no phenotype
107610	CG11407	CG11407	no phenotype
107629	CG10645	lama	no phenotype
107633	CG15122	Ir56c	no phenotype
107641	CG3050	Cyp6d5	no phenotype
107646	CG6398	CG6398	no phenotype
107648	CG14396	Ret	no phenotype
107656	CG4726	MFS3	no phenotype
107662	CG42235	CG42235	no phenotype
107719	CG6845	CG6845	no phenotype
107727	CG8458	wntD	no phenotype
107734	CG31164	Ir94a	no phenotype
107739	CG14666	Tim17a2	no phenotype
107741	CG34058	ppk11	no phenotype
107752	CG9552	rost	no phenotype
107768	CG12023	GV1	no phenotype
107771	CG6371	hug	no phenotype
107776	CG8666	Tsp39D	no phenotype
107798	CG2155	v	no phenotype
107816	CG3874	frc	no phenotype
107822	CG2679	gol	no phenotype
107830	CG42275	alpha-Man-I	no phenotype
107840	CG32775	GlcAT-I	no phenotype
107842	CG10505	CG10505	no phenotype
107843	CG13003	CG13003	no phenotype
107846	CG9932	CG9932	no phenotype
107857	CG1146	CG1146	no phenotype
107858	CG10864	CG10864	no phenotype
107870	CG17142	pyx	no phenotype
107875	CG14511	CG14511	no phenotype
107883	CG11280	trn	no phenotype
107892	CG12048	ppk21	no phenotype
107894	CG6125	CG6125	no phenotype
107896	CG42235	CG42235	no phenotype
107901	CG17381	Ir94g	no phenotype
107903	CG10486	CG10486	no phenotype

107911	CG12755	l(3)mbn	no phenotype
107921	CG32058	Ir67c	no phenotype
107931	CG11163	CG11163	no phenotype
107939	CG42256	Dscam2	no phenotype
107948	CG42253	Ndae1	no phenotype
107955	CG7414	CG7414	no phenotype
107962	CG15890	CG15890	no phenotype
107967	CG32498	dnc	no phenotype
107980	CG4019	CG4019	no phenotype
107991	CG1634	Nrg	no phenotype
108005	CG33103	Ppn	no phenotype
108019	CG8442	GluRIA	no phenotype
108020	CG42677	wb	no phenotype
108034	CG1149	MstProx	no phenotype
108042	CG7454	Or85a	no phenotype
108045	CG4330	MFS10	no phenotype
108047	CG6185	Ir68a	no phenotype
108048	CG16992	mthl6	no phenotype
108049	CG10348	CG10348	no phenotype
108053	CG1744	chp	no phenotype
108054	CG12092	Npc1b	no phenotype
108059	CG7227	CG7227	no phenotype
108101	CG11804	ced-6	no phenotype
108103	CG16947	Rchyl	no phenotype
108127	CG43286	cnc	no phenotype
108135	CG9820	Or59a	no phenotype
108142	CG33114	Gyc32E	no phenotype
108150	CG4587	CG4587	no phenotype
108159	CG1886	ATP7	no phenotype
108160	CG6649	Ugt35B1	no phenotype
108171	CG12663	Ir7a	no phenotype
108179	CG30379	CG30379	no phenotype
108196	CG10226	CG10226	no phenotype
108198	CG4962	CG4962	no phenotype
108203	CG14979	Gr63a	no phenotype
108217	CG4402	lox2	no phenotype
108223	CG3790	CG3790	no phenotype
108234	CG6698	NtR	no phenotype
108262	CG15110	botv	no phenotype
108265	CG32796	boi	no phenotype
108274	CG4434	bb8	no phenotype
108281	CG7860	CG7860	no phenotype
108295	CG9134	tfc	no phenotype

108312	CG7727	Appl	no phenotype
108313	CG4437	PGRP-LF	no phenotype
108323	CG32250	CG32250	no phenotype
108327	CG3879	Mdr49	no phenotype
108330	CG43340	CG43340	no phenotype
108337	CG11340	CG11340	no phenotype
108347	CG42610	Fhos	no phenotype
108348	CG6127	Ser	no phenotype
108353	CG4096	CG4096	no phenotype
108354	CG10420	CG10420	no phenotype
108359	CG6578	phm	no phenotype
108364	CG8062	out	no phenotype
108373	CG9613	Coq2	no phenotype
108374	CG5249	Blimp-1	no phenotype
108375	CG6120	Tsp96F	no phenotype
108378	CG3798	Nmda1	no phenotype
108388	CG10237	CG10237	no phenotype
108419	CG4991	CG4991	no phenotype
108426	CG10311	CG10311	no phenotype
108427	CG5588	Mtl	no phenotype
108430	CG12142	Tsp42Eg	no phenotype
108445	CG6822	ergic53	no phenotype
108455	CG4316	Sb	no phenotype
108470	CG3666	Tsf3	no phenotype
108473	CG8348	Dh44	no phenotype
108500	CG3036	CG3036	no phenotype
108506	CG10698	GRHRII	no phenotype
108508	CG43867	CG43867	no phenotype
108509	CG12317	JhI-21	no phenotype
108515	CG4471	Tsp42Ep	no phenotype
108551	CG30281	CG30281	no phenotype
108569	CG12295	stj	no phenotype
108577	CG18657	NetA	no phenotype
108591	CG42265	OtopLc	no phenotype
108594	CG34404	CG34404	no phenotype
108604	CG15629	CG15629	no phenotype
108612	CG7851	Scgalpha	no phenotype
108629	CG8909	Lrp4	no phenotype
108635	CG10069	MFS16	no phenotype
108652	CG8032	CG8032	no phenotype
108667	CG12773	CG12773	no phenotype
108670	CG8085	RN-tre	no phenotype
108683	CG3478	ppk	no phenotype

108697	CG14744	CG14744	no phenotype
108709	CG8864	Cyp28a5	no phenotype
108713	CG34139	CG34139	no phenotype
108714	CG14963	CG14963	no phenotype
108733	CG1599	CG1599	no phenotype
108739	CG5977	spas	no phenotype
108746	CG15427	tutl	no phenotype
108750	CG1502	tsg	no phenotype
108755	CG15917	Gbp	no phenotype
108758	CG9194	CG9194	no phenotype
108759	CG15279	CG15279	no phenotype
108766	CG9438	Cyp6a2	no phenotype
108770	CG7458	CG7458	no phenotype
108772	CG10342	npf	no phenotype
108782	CG2196	salt	no phenotype
108785	CG31358	CG31358	no phenotype
108814	CG12919	egr	no phenotype
108815	CG31326	CG31326	no phenotype
108825	CG7452	Syx17	no phenotype
108835	CG17800	Dscam	no phenotype
108863	CG3352	ft	no phenotype
108867	CG9413	CG9413	no phenotype
108877	CG4225	Hmt-1	no phenotype
108894	CG42576	NT1	no phenotype
108907	CG7250	Toll-6	no phenotype
108912	CG17930	CG17930	no phenotype
108929	CG8632	CG8632	no phenotype
108944	CG6202	Surf4	no phenotype
108953	CG16718	CG16718	no phenotype
108963	CG32055	CG32055	no phenotype
108967	CG17084	mthl9	no phenotype
108980	CG33111	CG33111	no phenotype
108990	CG42748	CG42748	no phenotype
108998	CG9739	fz2	no phenotype
109001	CG10277	CG10277	no phenotype
109013	CG12201	CG12201	no phenotype
109015	CG15138	beat-IIIc	no phenotype
109016	CG12730	CG12730	no phenotype
109022	CG5381	CG5381	no phenotype
109023	CG42768	Msp-300	no phenotype
109025	CG4096	CG4096	no phenotype
109071	CG44244	Gyg	no phenotype
109084	CG6998	CTP	no phenotype

109109	CG33270	CG33270	no phenotype
109111	CG11100	Mes2	no phenotype
109141	CG12505	Arc1	no phenotype
109148	CG40005	CR40005	no phenotype
109152	CG11765	Prx2540-2	no phenotype
109175	CG17673	Acp70A	no phenotype
109179	CG33105	p24-2	no phenotype
109180	CG12896	CG12896	no phenotype
109186	CG42671	CG42671	no phenotype
109188	CG42314	PMCA	no phenotype
109193	CG12559	rl	no phenotype
109198	CG8629	Acbp4	no phenotype
109200	CG12559	rl	no phenotype
109278	CG34069	mt:CoII	no phenotype
109283	CG14995	CG14995	no phenotype
109287	CG12194	CG12194	no phenotype
109289	CG10939	CG10939	no phenotype
109291	CG8596	CG8596	no phenotype
109314	CG12251	AQP	no phenotype
109317	CG3767	JhI-26	no phenotype
109324	CG14584	Ir20a	no phenotype
109325	CG42390	CG42390	no phenotype
109401	CG3747	Eaat1	no phenotype
109418	CG3576	schlank	no phenotype
109427	CG6281	Timp	no phenotype
109432	CG2448	FucT6	no phenotype
109433	CG4324	CG4324	no phenotype
109434	CG3671	Mvl	no phenotype
109437	CG10491	vn	no phenotype
109442	CG33141	sns	no phenotype
109450	CG6798	nAcRbeta-96A	no phenotype
109462	CG12303	Ir67b	no phenotype
109481	CG6484	CG6484	no phenotype
109485	CG15324	Ir7c	no phenotype
109501	CG1200	CG1200	no phenotype
109502	CG14981	mge	no phenotype
109504	CG1467	Syx16	no phenotype
109556	CG14266	ng2	no phenotype
109558	CG12370	Dh44-R2	no phenotype
109559	CG40160	CG40160	no phenotype
109570	CG40263	MFS17	no phenotype
109573	CG12559	rl	no phenotype
109580	CG12926	CG12926	no phenotype

109585	CG3653	kirre	no phenotype
109586	CG31719	RluA-1	no phenotype
109594	CG8177	Ae2	no phenotype
109600	CG6323	Tsp97E	no phenotype
109601	CG4322	moody	no phenotype
109605	CG33087	LRP1	no phenotype
109606	CG17336	Lcch3	no phenotype
109608	CG1771	mew	no phenotype
109620	CG1021	CG1021	no phenotype
109624	CG4332	CG4332	no phenotype
109625	CG12908	Ndg	no phenotype
109629	CG6512	CG6512	no phenotype
109631	CG10844	Rya-r44F	no phenotype
109635	CG5528	Toll-9	no phenotype
109663	CG17342	Lk6	no phenotype
109677	CG4476	CG4476	no phenotype
109678	CG3777	CG3777	no phenotype
109681	CG1804	kek6	no phenotype
109685	CG34369	CG34369	no phenotype
109690	CG42601	Cad86C	no phenotype
109691	CG30125	Ir56a	no phenotype
109705	CG7121	Tehao	no phenotype
109717	CG5398	CG5398	no phenotype
109763	CG18617	Vha100-2	no phenotype
109772	CG33492	Ir41a	no phenotype
109777	CG17853	Or43b	no phenotype
109783	CG16827	alphaPS4	no phenotype
109785	CG9270	CG9270	no phenotype
109791	CG15088	List	no phenotype
109793	CG4314	st	no phenotype
109819	CG3279	Vti1	no phenotype
109838	CG4385	S	no phenotype
109849	CG42599	Pif1A	no phenotype
109857	CG16857	CG16857	no phenotype
109863	CG2040	hig	no phenotype
109871	CG12581	CG12581	no phenotype
109885	CG11907	Ent1	no phenotype
109888	CG33080	CG33080	no phenotype
109889	CG14468	Tsp42A	no phenotype
109892	CG31163	SKIP	no phenotype
109895	CG10671	CG10671	no phenotype
109897	CG31176	CG31176	no phenotype
109901	CG43897	CG43897	no phenotype

109908	CG5840	P5cr-2	no phenotype
109914	CG10197	kn	no phenotype
109918	CG7882	CG7882	no phenotype
109927	CG13278	CG13278	no phenotype
109929	CG15113	5-HT1B	no phenotype
109937	CG44162	Strn-Mlck	no phenotype
109949	CG8433	Ext2	no phenotype
109970	CG1220	Kaz1-ORFB	no phenotype
109997	CG13606	CG13606	no phenotype
110008	CG17136	Rbp1	no phenotype
110016	CG10806	Nha1	no phenotype
110018	CG1702	GstT3	no phenotype
110043	CG1462	Aph-4	no phenotype
110047	CG9430	CG9430	no phenotype
110050	CG4104	Tps1	no phenotype
110068	CG12664	fend	no phenotype
110084	CG33508	ppk13	no phenotype
110085	CG42329	CG42329	no phenotype
110117	CG7217	Prx5	no phenotype
110137	CG43770	Sxl	no phenotype
110139	CG11659	CG11659	no phenotype
110155	CG8166	unc-5	no phenotype
110157	CG14869	CG14869	no phenotype
110184	CG7766	CG7766	no phenotype
110188	CG4893	CG4893	no phenotype
110201	CG3822	CG3822	no phenotype
110205	CG12178	Nhe1	no phenotype
110213	CG32555	RhoGAPp190	no phenotype
110217	CG3297	mnd	no phenotype
110223	CG10185	CG10185	no phenotype
110226	CG44240	Trpm	no phenotype
110229	CG1673	CG1673	no phenotype
110237	CG3811	Oatp30B	no phenotype
110241	CG12132	c11.1	no phenotype
110246	CG43693	CG43693	no phenotype
110248	CG34378	Pvf3	no phenotype
110257	CG10152	beat-IV	no phenotype
110268	CG6706	GABA-B-R2	no phenotype
110270	CG9089	wus	no phenotype
110274	CG8585	Ih	no phenotype
110277	CG32134	btI	no phenotype
110291	CG6707	CG6707	no phenotype
110312	CG18599	CG18599	no phenotype

110319	CG31751	CG31751	no phenotype
110322	CG17660	CG17660	no phenotype
110344	CG32701	l(1)G0320	no phenotype
110353	CG11186	toy	no phenotype
110358	CG7188	BI-1	no phenotype
110371	CG6016	bbc	no phenotype
110373	CG12787	hoe1	no phenotype
110374	CG32082	IRSp53	no phenotype
110375	CG9655	nes	no phenotype
110390	CG7749	kug	no phenotype
110406	CG9520	C1GalTA	no phenotype
110431	CG1693	tty	no phenotype
110443	CG1817	Ptp10D	no phenotype
110448	CG1511	Eph	no phenotype
110464	CG12582	beta-Man	no phenotype
110473	CG5760	rtet	no phenotype
110480	CG9066	MSBP	no phenotype
110487	CG34345	CG34345	no phenotype
110488	CG17943	comm	no phenotype
110489	CG5592	CG5592	no phenotype
110490	CG9621	Adgf-D	no phenotype
110492	CG13458	CG13458	no phenotype
110494	CG33950	trol	no phenotype
110495	CG42576	NT1	no phenotype
110518	CG32062	Rbfox1	no phenotype
110523	CG8547	CG8547	no phenotype
110574	CG1167	Ras64B	no phenotype
110577	CG9635	RhoGEF2	no phenotype
110588	CG31665	wry	no phenotype
110589	CG2822	Shaw	no phenotype
110590	CG43867	CG43867	no phenotype
110595	CG31795	IA-2	no phenotype
110603	CG44533	Nna1	no phenotype
110619	CG6692	Cp1	no phenotype
110638	CG1830	PhKgamma	no phenotype
110650	CG7450	CrebA	no phenotype
110661	CG3705	aay	no phenotype
110663	CG17370	SppL	no phenotype
110668	CG14040	CG14040	no phenotype
110671	CG1471	Cdase	no phenotype
110674	CG12858	CG12858	no phenotype
110676	CG16833	TLL4A	no phenotype
110684	CG6638	CG6638	no phenotype

110686	CG42555	tweek	no phenotype
110698	CG12703	Pmp70	no phenotype
110723	CG10037	vvl	no phenotype
110737	CG12125	CG12125	no phenotype
110739	CG7285	star1	no phenotype
110766	CG3048	Traf4	no phenotype
110784	CG1449	zfh2	no phenotype
110804	CG9930	E5	no phenotype

KEY RESOURCE TABLE

Fly stocks:

Abbreviation	Genotype	Identifier
QUAS-6xGFP, UAS-mtdTomato-3xHA	y[1]w[*]; Pbac{y[+mDint2] w[+mC]=10XQUAS-6XGFP}VK00018, P{w[+mC]=UAS-mtdTomato-3xHA}2; +	BDSC_66479
OK371-QF2	w[*]; Vglut[OK371-QF2]; +	BDSC_66473
repo-Gal4	w[1118]; +; repo-Gal4/ TM3, Sb[1]	BDSC_7415
Vglut-QF2	w[*]; Mi{Trojan-QF2.2} Vglut[MI04979-TQF2.2]/CyO; +	BDSC_60315
QUAS-mCD8::GFP	y[1] w[1118]; P{w[+mC]=QUAS-mCD8-GFP.P}5J; +	BDSC_30002
UAS-Dronc::GFP	w[*]; P{w[+mC]=UAS-Dronc.EGFP}2; +	BDSC_56759
UAS-dark	w[*]; +; P{w[+mC]=UAS-dark ^{WT} }	Akdemir et al., 2006
UAS-Reaper	w[1118]; P{w[+mC]=UAS-rpr.C}14; +	BDSC_5824
UAS-lacZ(III)	w[1118]; +; P{w[+mC]=UAS-lacZ.NZ}J312	BDSC_3956
UAS-lacZ(II)	w[1118]; +; P{w[+mC]=UAS-lacZ.NZ}20b	BDSC_3955
QUAS-Wld ^S	w[1118]; +; P{w[+mC]=5XQUAS-Wld ^S }9	Lassetter et al. 2022
w ¹¹¹⁸	w[1118]; +; +	VDRG_60000
nrv2-GFP		Stork et al. 2008
nrv2-Gal4	w[*]; +; P{w[+mC]=nrv2-GAL4.S}8	BDSC_6799
UAS-mCherry-NLS	w[*]; +; P{w[+mC]=UAS-mCherry-NLS}3	BDSC_38424
babo-Gal4 [3xP3-RFP] removed	y[1] w[*]; TI{RFP[3xP3.PB]=T-GEM.1}babo[CR00274-TG4.1]/SM6a; +	Modified from: BDSC_83164
UAS-babo ^{DN}	P{w[+mC]=UAS-babo.A.DeltaI}1, y[1] w[*]; +; +	BDSC_64423
babo ^{RNAi-2}	y[1]v[1]; P{y[+t7.7] v[+t1.8]=TriP.HMS02033}attP40; +	BDSC_40866
Smox ^{RNAi-2}	y[1]sc[*]v[1]sev[21]; P{y[+t7.7]v[+t1.8]=TriP.HMS02203}attP40; +	BDSC_41670
tubP-Gal80 ^{ts}	w[*]; P{w[+mC]=tubP-GAL80[ts]}20; TM2/TM6B, Tb[1]	BDSC_7019
UAS-Lamin::GFP	y[1]w[*]; P{w[+mC]=UAS-Lam.GFP}3-3; +	BDSC_7376
UAS-myr::tdTomato	w[*]; P{y[+t7.7] w[+mC]=10XUAS-IVS-myr::tdTomato}attP40; +	BDSC_32222
IT.0117-VP16AD	w[1118]; +; Pbac{w[+mC]=IT.GAL4VP16AD}0117-G4	Modified from: BDSC_62647 Corty et al., 2021
nrv2-DBD	w[1118]; +; P{w[+mC]=nrv2-GAL4DBD}	Corty et al., 2021
UAS-p35	w[*]; P{w[+mC]=UAS-p35.H}BH1; +	BDSC_5072
UAS-CD8::GFP	w[*]; UAS-CD8::GFP; UAS-CD8::GFP	
UAS-iATPsnFR	w[*]; UAS-iATPsnFR; +	Lobas et al., 2019
UAS-mito-roGFP.Grx1	w[1118]; P{w[+mC]=UAS-mito-roGFP2-Grx1}9; +	BDSC_67664
srl-OE	y[1] w[67c23]; +; P{y[+mDint2] w[+mC]=EPgy2}srl[EY05931]	BDSC_20009
Mitf-RNAi	y[1] v[1]; P{y[+t7.7] v[+t1.8]=TRiP.HMS02857}attP40	BDSC_44561
cnc-RNAi	y[1] v[1]; P{y[+t7.7] v[+t1.8]=TRiP.HMS02021}attP40	BDSC_40854

Genotypes corresponding to main figures:

Figure 1:	-	-
B	control:	w*/(w[1118]); OK371-QF2, 10XQUAS-6xGFP, UAS-mtdTomato-3xHA/+; repo-Gal4/+
C	control:	w*/(w[1118]); Vglut-QF2[MI04979-TQF2.2], QUAS-mCD8::GFP/+; repo-Gal4/+
Figure 2:		
	Nrv2-Gal4	w*; UAS-lamin::GFP, UAS-mtdTomato-3xHA/+; nrv2-Gal4/+

	WG Split-Gal4	w*; UAS-lamin::GFP, UAS-mtdTomato-3xHA/+; WG Split-Gal4/+
Figure 3:		
A		w*; OK371-QF2, 10XQUAS-6xGFP, UAS-mtdTomato-3xHA/UAS-reaper; WG split-Gal4/+
B		w*/(w[1118]); Vglut-QF2[MI04979-TQF2.2], QUAS-mCD8::GFP/[VDRC_3825]; repo-Gal4/+
Figure 4:		
A, D-E	control:	w*/(w[1118]); OK371-QF2, 10XQUAS-6xGFP, UAS-mtdTomato-3xHA/+; WG split-Gal4/UAS-lacZ
B, D-E	ablation:	w*; OK371-QF2, 10XQUAS-6xGFP, UAS-mtdTomato-3xHA/UAS-Dronc::GFP; WG split-Gal4/UAS-Dark
C-E	ablation:	w*; OK371-QF2, 10XQUAS-6xGFP, UAS-mtdTomato-3xHA/UAS-reaper; WG split-Gal4/+
Figure 5:	-	-
A	-WldS	w*/(w[1118]); Vglut-QF2[MI04979-TQF2.2], QUAS-mCD8::GFP/+; repo-Gal4/+
	+WldS	w*/(w[1118]); Vglut-QF2[MI04979-TQF2.2], QUAS-mCD8::GFP/+; repo-Gal4, QUAS-WldS/+
B	control:	w*/(w[1118]); OK371-QF2, 10XQUAS-6xGFP, UAS-mtdTomato-3xHA/UAS-lacZ; WG split-Gal4/QUAS-WldS
	ablation:	w*; OK371-QF2, 10XQUAS-6xGFP, UAS-mtdTomato-3xHA/UAS-reaper; WG split-Gal4/QUAS-WldS
Figure 6:		
A	control:	w*/w[1118]; Vglut-QF2[MI04979-TQF2.2], QUAS-mCD8::GFP/+; repo-Gal4, QUAS-WldS/+
	RNAi:	w*/w[1118]; Vglut-QF2[MI04979-TQF2.2], QUAS-mCD8::GFP/(VDRC RNAi); repo-Gal4, QUAS-WldS/(VDRC RNAi)
Figure 7 & 8:	-	-
B/C	control:	w*/(w[1118]); Vglut-QF2[MI04979-TQF2.2], QUAS-mCD8::GFP/+; repo-Gal4, QUAS-WldS/+
	RNAi (VDRC):	w*/(w[1118]); Vglut-QF2[MI04979-TQF2.2], QUAS-mCD8::GFP/(VDRC RNAi); repo-Gal4, QUAS-WldS/(VDRC RNAi)
	RNAi (Bloomington):	w*/(y[1]sc*v[1]sev[21]); Vglut-QF2[MI04979-TQF2.2], QUAS-mCD8::GFP/(BDSC RNAi); repo-Gal4, QUAS-WldS/(BDSC RNAi)
Figure 9:	-	-
A/B	control:	w*/(w[1118]); Vglut-QF2[MI04979-TQF2.2], QUAS-mCD8::GFP/+; repo-Gal4/+
	RNAi (VDRC):	w*/(w[1118]); Vglut-QF2[MI04979-TQF2.2], QUAS-mCD8::GFP/+; repo-Gal4/baboRNAi[VDRC_3825]
C	control:	w*/(w[1118]); Vglut-QF2[MI04979-TQF2.2], QUAS-mCD8::GFP/+; repo-Gal4/+
	babo RNAi 1 (VDRC):	w*/(w[1118]); Vglut-QF2[MI04979-TQF2.2], QUAS-mCD8::GFP/+; repo-Gal4/baboRNAi[VDRC_3825]
	babo RNAi 2 (Bloomington):	w*/(y[1]v[1]); Vglut-QF2[MI04979-TQF2.2], QUAS-mCD8::GFP/baboRNAi[BDSC_40866]; repo-Gal4/+

	Smox RNAi 1 (VDRC):	w*/(w[1118]); Vglut-QF2[MI04979-TQF2.2], QUAS-mCD8::GFP/SmoxRNAi[VDRC_105687]; repo-Gal4/+
	Smox RNAi 2 (Bloomington):	w*/(y[1]sc*v[1]sev[21]); Vglut-QF2[MI04979-TQF2.2], QUAS-mCD8::GFP/SmoxRNAi[BDSC_41670]; repo-Gal4/+
D	control:	w*/w[1118]; Vglut-QF2[MI04979-TQF2.2], QUAS-mCD8::GFP/+; repo-Gal4/+
	babo ^{DN} :	w*/UAS-babo.A.DeltaI, y[1]w*; Vglut-QF2[MI04979-TQF2.2], QUAS-mCD8::GFP/+; repo-Gal4/+
E	control:	w*/(w[1118]); Vglut-QF2[MI04979-TQF2.2], QUAS-mCD8::GFP, tubP-Gal80ts/+; repo-Gal4/+
	RNAi:	w*/(w[1118]); Vglut-QF2[MI04979-TQF2.2], QUAS-mCD8::GFP, tubP-Gal80ts/(VDRC RNAi); repo-Gal4/(VDRC RNAi)
Figure 10:	-	-
		w*/(y[1]w*); babo-Gal4[CR00274-TG4.1]/UAS-lamin::GFP; +
Figure 11:		
A/B	control:	w*; nrv2-GFP/+; UAS-mCherry.NLS/nrv2-Gal4
	babo-Gal4:	w*/(y[1]w*); nrv2-GFP/babo-Gal4[CR00274-TG4.1]; UAS-mCherry.NLS/+
C		w*/(y[1]w*); Vglut-QF2[MI04979-TQF2.2], QUAS-mCD8::GFP/babo-Gal4[CR00274-TG4.1]; UAS-mCherry.NLS/+
Figure 12:	-	-
A	4-28	w*/(y[1]w*); nrv2-GFP/babo-Gal4[CR00274-TG4.1]; UAS-mCherry.NLS/+
B		w*/(y[1]w*); UAS-CD8::GFP/3xP3-RFP, babo-Gal4[CR00274-TG4.1]; UAS-CD8::GFP/+
C/D		w*/(y[1]w*); Vglut-QF2[MI04979-TQF2.2], QUAS-mCD8::GFP/3xP3-RFP, babo-Gal4[CR00274-TG4.1]; UAS-mCherry.NLS/+
Figure 13:	-	-
	control (nrv2>):	w*/(w[1118]); UAS-lamin::GFP, UAS-mtdTomato-3xHA/+; nrv2-Gal4/+
	control (nrv2>lacZ):	w*/(w[1118]); UAS-lamin::GFP, UAS-mtdTomato-3xHA/UAS-lacZ.NZ[20b]; nrv2-Gal4/+
	baboRNAi:	w*/(w[1118]); UAS-lamin::GFP, UAS-mtdTomato-3xHA/+; nrv2-Gal4/[VDRC_3825]
	SmoxRNAi:	w*/(w[1118]); UAS-lamin::GFP, UAS-mtdTomato-3xHA/[VDRC_105687]; nrv2-Gal4/+
Figure 14:		
A/B	control (nrv2>):	w*/(w[1118]); UAS-lamin::GFP, UAS-mtdTomato-3xHA/+; nrv2-Gal4/+
	control (nrv2>lacZ):	w*/(w[1118]); UAS-lamin::GFP, UAS-mtdTomato-3xHA/UAS-lacZ.NZ[20b]; nrv2-Gal4/+
	baboRNAi:	w*/(w[1118]); UAS-lamin::GFP, UAS-mtdTomato-3xHA/+; nrv2-Gal4/[VDRC_3825]

	P35:	w*; UAS-lamin::GFP, UAS-mtdTomato-3xHA/UAS-p35.H[BH1]; nrv2-Gal4/+
C	control:	w*/(w[1118]); Vglut-QF2[MI04979-TQF2.2], QUAS-mCD8::GFP/+; repo-Gal4/+
	baboRNAi:	w*/(w[1118]); Vglut-QF2[MI04979-TQF2.2], QUAS-mCD8::GFP/+; repo-Gal4/[VDRC_3825]
	P35:	w*/(w[1118]); Vglut-QF2[MI04979-TQF2.2], QUAS-mCD8::GFP/UAS-p35.H[BH1]; repo-Gal4/+
Figure 15:		
A/B	control:	w*; OK371-QF2, 10XQUAS-6xGFP, UAS-mtdTomato-3xHA/+; repo-Gal4/+
	RNAi:	w*; OK371-QF2, 10XQUAS-6xGFP, UAS-mtdTomato-3xHA/(VDRC RNAi); repo-Gal4/(VDRC RNAi)
C/D	control:	w*; OK371-QF2, 10XQUAS-6xGFP, UAS-mtdTomato-3xHA/+; nrv2-Gal4/+
	RNAi:	w*; OK371-QF2, 10XQUAS-6xGFP, UAS-mtdTomato-3xHA/(VDRC RNAi); nrv2-Gal4/(VDRC RNAi)
Figure 16:	-	-
	control:	w*/(w[1118]); Vglut-QF2[MI04979-TQF2.2], QUAS-mCD8::GFP/+; repo-Gal4/+
	baboRNAi:	w*/(w[1118]); Vglut-QF2[MI04979-TQF2.2], QUAS-mCD8::GFP/+; repo-Gal4/[VDRC_3825]
	SmoxRNAi:	w*/(w[1118]); Vglut-QF2[MI04979-TQF2.2], QUAS-mCD8::GFP/[VDRC_105687]; repo-Gal4/+
Figure 17:		
A-C	control - Wlds:	w*/(w[1118]); Vglut-QF2[MI04979-TQF2.2], QUAS-mCD8::GFP/+; repo-Gal4/+
	control + Wlds:	w*/(w[1118]); Vglut-QF2[MI04979-TQF2.2], QUAS-mCD8::GFP/+; repo-Gal4, QUAS-Wlds/+
	baboRNAi - Wlds:	w*/(w[1118]); Vglut-QF2[MI04979-TQF2.2], QUAS-mCD8::GFP/+; repo-Gal4/baboRNAi[VDRC_3825]
	baboRNAi + Wlds:	w*/(w[1118]); Vglut-QF2[MI04979-TQF2.2], QUAS-mCD8::GFP/+; repo-Gal4, QUAS-Wlds/baboRNAi[VDRC_3825]
Figure 18:	-	-
A-C	control - P35:	w*/(w[1118]); Vglut-QF2[MI04979-TQF2.2], QUAS-mCD8::GFP/+; repo-Gal4/+
	control + P35:	w*/(w[1118]); Vglut-QF2[MI04979-TQF2.2], QUAS-mCD8::GFP/QUAS-p35; repo-Gal4/+
	baboRNAi - P35:	w*/(w[1118]); Vglut-QF2[MI04979-TQF2.2], QUAS-mCD8::GFP/+; repo-Gal4/baboRNAi[VDRC_3825]
	baboRNAi + P35:	w*/(w[1118]); Vglut-QF2[MI04979-TQF2.2], QUAS-mCD8::GFP/QUAS-p35; repo-Gal4/baboRNAi[VDRC_3825]
Figure 19:		
	control:	w*/(w[1118]); UAS-iATPsnFR/+; nrv2-Gal4/UAS-lacZ.NZ[J312]
	baboRNAi:	w*/(w[1118]); UAS-iATPsnFR/+; nrv2-Gal4/[VDRC_3825]

	SmoxRNAi:	w*/(w[1118]); UAS-iATPsnFR/[VDRC_105687]; nrv2-Gal4/+
	srl[OE]:	w*/(y[1]w[67c23]); UAS-iATPsnFR/+; nrv2-Gal4/P{y[+mDint2] w[+mC]=EPgy2}srl[EY05931]
	cncRNAi:	w*/(y[1] v[1]); UAS-iATPsnFR/BL40854; nrv2-Gal4/+
	MitfRNAi:	w*/(y[1] v[1]); UAS-iATPsnFR/BL44561; nrv2-Gal4/+
	BsgRNAi:	w*/(y[1]v[1]); UAS-iATPsnFR/BL52110; nrv2-Gal4/+
Figure 20:		
A/B	control:	w*; UAS-mito-roGFP.Grx1/+; repo-Gal4/UAS-lacZ.NZ
	baboRNAi:	w*; UAS-mito-roGFP.Grx1/+; repo-Gal4/[VDRC_3825]
	SmoxRNAi:	w*; UAS-mito-roGFP.Grx1/[VDRC_105687]; repo-Gal4/+
	srl[OE]:	w*/(y[1]w[67c23]); UAS-mito-roGFP.Grx1/+; repo-Gal4/P{y[+mDint2] w[+mC]=EPgy2}srl[EY05931]
	cncRNAi:	w*/(y[1] v[1]); UAS-mito-roGFP.Grx1/BL40854; repo-Gal4/+
	MitfRNAi:	w*/(y[1] v[1]); UAS-mito-roGFP.Grx1/BL44561; repo-Gal4/+
	BsgRNAi:	w*/(y[1] v[1]); UAS-mito-roGFP.Grx1/BL52110; repo-Gal4/+
C	control:	w*; OK371-QF2, 10XQUAS-6xGFP, UAS-mtdTomato-3xHA/+; nrv2-Gal4/+
	srl[OE]:	w*/(y[1]w[67c23]); OK371-QF2, 10XQUAS-6xGFP, UAS-mtdTomato-3xHA/+; nrv2-Gal4/ P{y[+mDint2] w[+mC]=EPgy2}srl[EY05931]
	BsgRNAi:	w*; OK371-QF2, 10XQUAS-6xGFP, UAS-mtdTomato-3xHA/BL52110; nrv2-Gal4/+
Figure 22:		
		w[1118]
Figure 23:		
	<1 & 5 dpe	w[1118]
	28 dpe	w*; +; nrv2-Gal4, UAS-mCD8::GFP

Antibodies:

Abbreviation	Identifier
Ms ∞ repo	DSHB #8D12
Rb ∞ oaz	Lassetter et al. 2022 & Corty et al. 2021
A647-Gt ∞ HRP	Jackson Labs #123-605-021
Ch ∞ GFP	ab13970
A488-Dk ∞ Ch	Jackson Labs #703-545-155
Red-X-Dk ∞ Rb	Jackson Labs #711-295-152
Dy405-Dk ∞ Ms	Jackson Labs #715-475-150
A647- Dk ∞ Ms	Jackson Labs #715-605-150

REFERENCES:

- Adalbert, R., Gillingwater, T. H., Haley, J. E., Bridge, K., Beirowski, B., Berek, L., Wagner, D., Grumme, D., Thomson, D., Celik, A., Addicks, K., Ribchester, R. R., & Coleman, M. P. (2005). A rat model of slow Wallerian degeneration (WldS) with improved preservation of neuromuscular synapses. *European Journal of Neuroscience*, *21*(1), 271–277. <https://doi.org/10.1111/J.1460-9568.2004.03833.X>
- Adalbert, R., Nógrádi, A., Szabó, A., & Coleman, M. P. (2006). The slow Wallerian degeneration gene in vivo protects motor axons but not their cell bodies after avulsion and neonatal axotomy. *European Journal of Neuroscience*, *24*(8), 2163–2168. <https://doi.org/10.1111/J.1460-9568.2006.05103.X>
- Adlkofer, K., Martini, R., Aguzzi, A., Zielasek, J., Toyka, K. v., & Suter, U. (1995). Hypermyelination and demyelinating peripheral neuropathy in Pmp22-deficient mice. *Nature Genetics*, *11*(3), 274–280. <https://doi.org/10.1038/ng1195-274>
- Akdemir, F., Farkaš, R., Chen, P., Juhasz, G., Medved'ova, L., Sass, M., Wang, L., Wang, X., Chittaranjan, S., Gorski, S. M., Rodriguez, A., & Abrams, J. M. (2006). Autophagy occurs upstream or parallel to the apoptosome during histolytic cell death. *Development*, *133*(8), 1457–1465. <https://doi.org/10.1242/dev.02332>
- Albrecht, S. C., Barata, A. G., Großhans, J., Telemán, A. A., & Dick, T. P. (2011). In vivo mapping of hydrogen peroxide and oxidized glutathione reveals chemical and regional specificity of redox homeostasis. *Cell Metabolism*, *14*(6), 819–829. <https://doi.org/10.1016/J.CMET.2011.10.010/ATTACHMENT/8D585F5A-F250-4260-A22C-8C60B728EA5E/MMC1.PDF>

- Allen, N. J., & Barres, B. A. (2009). Glia — more than just brain glue. *Nature* 2009 457:7230, 457(7230), 675–677. <https://doi.org/10.1038/457675a>
- Alvarez, J. I., Cayrol, R., & Prat, A. (2011). Disruption of central nervous system barriers in multiple sclerosis. *Biochimica et Biophysica Acta (BBA) - Molecular Basis of Disease*, 1812(2), 252–264. <https://doi.org/10.1016/J.BBADIS.2010.06.017>
- Ames, A. (2000). CNS energy metabolism as related to function. *Brain Research Reviews*, 34(1–2), 42–68. [https://doi.org/10.1016/S0165-0173\(00\)00038-2](https://doi.org/10.1016/S0165-0173(00)00038-2)
- Angeletti, R. H., Angeletti, P. U., & Levi-Montalcini, R. (1972). Selective accumulation of [125I] labelled nerve growth factor in sympathetic ganglia. *Brain Research*, 46(C), 421–425. [https://doi.org/10.1016/0006-8993\(72\)90033-9](https://doi.org/10.1016/0006-8993(72)90033-9)
- Araki, T., Sasaki, Y., & Milbrandt, J. (2004). Increased nuclear NAD biosynthesis and SIRT1 activation prevent axonal degeneration. *Science*, 305(5686), 1010–1013. https://doi.org/10.1126/SCIENCE.1098014/SUPPL_FILE/ARAKI_SOM.PDF
- Attwell, D., Buchan, A. M., Charpak, S., Lauritzen, M., MacVicar, B. A., & Newman, E. A. (2010). Glial and neuronal control of brain blood flow. *Nature* 2010 468:7321, 468(7321), 232–243. <https://doi.org/10.1038/nature09613>
- Attwell, D., & Laughlin, S. B. (2001). An energy budget for signaling in the grey matter of the brain. *Journal of Cerebral Blood Flow and Metabolism*, 21(10), 1133–1145. <https://doi.org/10.1097/00004647-200110000-00001>

- Avery, M. A., Sheehan, A. E., Kerr, K. S., Wang, J., & Freeman, M. R. (2009). WldS requires Nmnat1 enzymatic activity and N16–VCP interactions to suppress Wallerian degeneration. *The Journal of Cell Biology*, *184*(4), 501. <https://doi.org/10.1083/JCB.200808042>
- Baba, M., Nakajo, S., Tu, P. H., Tomita, T., Nakaya, K., Lee, V. M. Y., Trojanowski, J. Q., & Iwatsubo, T. (1998). Aggregation of alpha-synuclein in Lewy bodies of sporadic Parkinson's disease and dementia with Lewy bodies. *The American Journal of Pathology*, *152*(4), 879. [/pmc/articles/PMC1858234/?report=abstract](https://pubmed.ncbi.nlm.nih.gov/1158234/)
- Baldwin, K. R., Godena, V. K., Hewitt, V. L., & Whitworth, A. J. (2016). Axonal transport defects are a common phenotype in *Drosophila* models of ALS. *Human Molecular Genetics*, *25*(12), ddw105. <https://doi.org/10.1093/hmg/ddw105>
- Baloh, R. H. (2008). Mitochondrial dynamics and peripheral neuropathy. *Neuroscientist*, *14*(1), 12–18. <https://doi.org/10.1177/1073858407307354>
- Beirowski, B. (2013). Concepts for regulation of axon integrity by enwrapping glia. *Frontiers in Cellular Neuroscience*, *7*. <https://doi.org/10.3389/fncel.2013.00256>
- Beirowski, B., Babetto, E., Coleman, M. P., & Martin, K. R. (2008). The WldS gene delays axonal but not somatic degeneration in a rat glaucoma model. *European Journal of Neuroscience*, *28*(6), 1166–1179. <https://doi.org/10.1111/J.1460-9568.2008.06426.X>
- Besse, F., Mertel, S., Kittel, R. J., Wichmann, C., Rasse, T. M., Sigrist, S. J., & Ephrussi, A. (2007). The Ig cell adhesion molecule Basigin controls compartmentalization and

- vesicle release at *Drosophila melanogaster* synapses. *Journal of Cell Biology*, 177(5), 843–855. <https://doi.org/10.1083/JCB.200701111>
- Black, J. A., Kocsis, J. D., & Waxman, S. G. (1990). Ion channel organization of the myelinated fiber. *Trends in Neurosciences*, 13(2), 48–54. [https://doi.org/10.1016/0166-2236\(90\)90068-L](https://doi.org/10.1016/0166-2236(90)90068-L)
- Brand, A. H., & Dormand, E. L. (1995). The GAL4 system as a tool for unravelling the mysteries of the *Drosophila* nervous system. *Current Opinion in Neurobiology*, 5(5), 572–578. [https://doi.org/10.1016/0959-4388\(95\)80061-1](https://doi.org/10.1016/0959-4388(95)80061-1)
- Brennan, K. M., Bai, Y., & Shy, M. E. (2015). Demyelinating CMT—what’s known, what’s new and what’s in store? *Neuroscience Letters*, 596, 14–26. <https://doi.org/10.1016/J.NEULET.2015.01.059>
- Brummel, T., Abdollah, S., Haerry, T. E., Shimell, M. J., Merriam, J., Raftery, L., Wrana, J. L., & O’Connor, M. B. (1999). The *Drosophila* Activin receptor Baboon signals through dSmad2 and controls cell proliferation but not patterning during larval development. *Genes & Development*, 13(1), 98–111. <https://doi.org/10.1101/gad.13.1.98>
- Buckmaster, E. A., Perry, V. H., & Brown, M. C. (1995). The Rate of Wallerian Degeneration in Cultured Neurons from Wild Type and C57BL/WldS Mice Depends on Time in Culture and may be Extended in the Presence of Elevated K⁺ Levels. *European Journal of Neuroscience*, 7(7), 1596–1602. <https://doi.org/10.1111/J.1460-9568.1995.TB01155.X>

Cajal, S. R. y, May, R. M., DeFelipe, J., & Jones, E. G. (1991). *Cajal's Degeneration and Regeneration of the Nervous System* (P. Corsi, E. G. Jones, & G. M. Shepherd, Eds.). Oxford University Press.

<https://doi.org/10.1093/acprof:oso/9780195065169.001.0001>

Campenot, R. B. (2009). NGF Uptake and Retrograde Signaling Mechanisms in Sympathetic Neurons in Compartmented Cultures. *Results and Problems in Cell Differentiation*, 48, 141–158. https://doi.org/10.1007/400_2009_7

Cole, E. S., & Palka, J. (1982). The pattern of campaniform sensilla on the wing and haltere of *Drosophila melanogaster* and several of its homeotic mutants. *J. Embryol. Exp. Morph.*, 71, 41–61. <https://doi.org/10.1.1.983.8201>

Coleman, M. P., Conforti, L., Anne Buckmaster, E., Tarlton, A., Ewing, R. M., Brown, M. C., Lyon ¶, M. F., & Perry, V. H. (1998). An 85-kb tandem triplication in the slow Wallerian degeneration (Wld s) mouse. *Genetics*, 95, 9985–9990.

www.pnas.org.

Coleman, M. P., & Freeman, M. R. (2010). Wallerian Degeneration, Wld S, and Nmnat. *Annual Review of Neuroscience*, 33(1), 245–267. <https://doi.org/10.1146/annurev-neuro-060909-153248>

Coleman, M. P., & Höke, A. (2020). Programmed axon degeneration: from mouse to mechanism to medicine. *Nature Reviews Neuroscience* 2020 21:4, 21(4), 183–196. <https://doi.org/10.1038/S41583-020-0269-3>

- Colonna, M., & Butovsky, O. (2017). Microglia Function in the Central Nervous System During Health and Neurodegeneration. *Annual Review of Immunology*, 35, 441. <https://doi.org/10.1146/ANNUREV-IMMUNOL-051116-052358>
- Compston, A., & Coles, A. (2008). Multiple sclerosis. *The Lancet*, 372(9648), 1502–1517. [https://doi.org/10.1016/S0140-6736\(08\)61620-7](https://doi.org/10.1016/S0140-6736(08)61620-7)
- Conforti, L., Fang, G., Beirowski, B., Wang, M. S., Sorci, L., Asress, S., Adalbert, R., Silva, A., Bridge, K., Huang, X. P., Magni, G., Glass, J. D., & Coleman, M. P. (2006). NAD⁺ and axon degeneration revisited: Nmnat1 cannot substitute for WldS to delay Wallerian degeneration. *Cell Death & Differentiation* 2007 14:1, 14(1), 116–127. <https://doi.org/10.1038/sj.cdd.4401944>
- Conforti, L., Fang, G., Beirowski, B., Wang, M. S., Sorci, L., Asress, S., Adalbert, R., Silva, A., Bridge, K., Huang, X. P., Magni, G., Glass, J. D., & Coleman, M. P. (2007). NAD⁺ and axon degeneration revisited: Nmnat1 cannot substitute for WldS to delay Wallerian degeneration. *Cell Death and Differentiation*, 14(1), 116–127. <https://doi.org/10.1038/sj.cdd.4401944>
- Conforti, L., Tarlton, A., Mack, T. G. A., Mi, W., Buckmaster, E. A., Wagner, D., Perry, V. H., & Coleman, M. P. (2000). A Ufd2/D4Cole1e chimeric protein and overexpression of Rbp7 in the slow Wallerian degeneration (WldS) mouse. *Proceedings of the National Academy of Sciences*, 97(21), 11377–11382. <https://doi.org/10.1073/PNAS.97.21.11377>

- Corty, M. M., Lassetter, A. P., Hill, J. Q., Sheehan, A. E., Bernardo-Garcia, F. J., Davis, G. W., Aicher, S. A., & Freeman, M. R. (2021). Discoidin domain receptor regulates ensheathment, survival, and caliber of peripheral axons. *BioRxiv*, 2021.09.21.461270. <https://doi.org/10.1101/2021.09.21.461270>
- Coutinho-Budd, J. C., Sheehan, A. E., & Freeman, M. R. (2017). The secreted neurotrophin Spätzle 3 promotes glial morphogenesis and supports neuronal survival and function. *Genes & Development*, 31(20), 2023–2038. <https://doi.org/10.1101/gad.305888.117>
- Cunningham, R. L., & Monk, K. R. (2018). Transmission Electron Microscopy for Zebrafish Larvae and Adult Lateral Line Nerve. *Methods in Molecular Biology*, 1739, 385–400. https://doi.org/10.1007/978-1-4939-7649-2_26
- Czopka, T., & Lyons, D. A. (2011). Dissecting Mechanisms of Myelinated Axon Formation Using Zebrafish. In *Methods in Cell Biology* (Vol. 105, pp. 25–62). Academic Press Inc. <https://doi.org/10.1016/B978-0-12-381320-6.00002-3>
- D’Antonio, M., Droggiti, A., Feltri, M. L., Roes, J., Wrabetz, L., Mirsky, R., & Jessen, K. R. (2006). TGF β type II receptor signaling controls schwann cell death and proliferation in developing nerves. *Journal of Neuroscience*, 26(33), 8417–8427. <https://doi.org/10.1523/JNEUROSCI.1578-06.2006>
- Deckwerth, T. L., & Johnson, E. M. (1994). Neurites Can Remain Viable after Destruction of the Neuronal Soma by Programmed Cell Death (Apoptosis). *Developmental Biology*, 165(1), 63–72. <https://doi.org/10.1006/DBIO.1994.1234>

- Delgado, M. G., Oliva, C., López, E., Ibacache, A., Galaz, A., Delgado, R., Barros, L. F., & Sierralta, J. (2018). Chaski, a novel *Drosophila* lactate/pyruvate transporter required in glia cells for survival under nutritional stress. *Scientific Reports*, *8*(1), 1186. <https://doi.org/10.1038/s41598-018-19595-5>
- di Stefano, M., Nascimento-Ferreira, I., Orsomando, G., Mori, V., Gilley, J., Brown, R., Janeckova, L., Vargas, M. E., Worrell, L. A., Loreto, A., Tickle, J., Patrick, J., Webster, J. R. M., Marangoni, M., Carpi, F. M., Pucciarelli, S., Rossi, F., Meng, W., Sagasti, A., ... Conforti, L. (2014). A rise in NAD precursor nicotinamide mononucleotide (NMN) after injury promotes axon degeneration. *Cell Death & Differentiation* *2015 22:5*, *22*(5), 731–742. <https://doi.org/10.1038/cdd.2014.164>
- Diao, F., Ironfield, H., Luan, H., Diao, F., Shropshire, W. C., Ewer, J., Marr, E., Potter, C. J., Landgraf, M., & H., W. B. (2015). Plug-and-Play Genetic Access to *Drosophila* Cell Types using Exchangeable Exon Cassettes. *Cell Reports*, *10*(8), 1410–1421. <https://doi.org/10.1016/J.CELREP.2015.01.059>
- Dominy, J. E., & Puigserver, P. (2013). Mitochondrial Biogenesis through Activation of Nuclear Signaling Proteins. *Cold Spring Harbor Perspectives in Biology*, *5*(7), a015008. <https://doi.org/10.1101/CSHPERSPECT.A015008>
- Dorstyn, L., Colussi, P. A., Quinn, L. M., Richardson, H., & Kumar, S. (1999). DRONC, an ecdysone-inducible *Drosophila* caspase. *Proceedings of the National Academy of Sciences of the United States of America*, *96*(8), 4307–4312. <https://doi.org/10.1073/pnas.96.8.4307>

- Dutta, R., McDonough, J., Yin, X., Peterson, J., Chang, A., Torres, T., Gudz, T., Macklin, W. B., Lewis, D. A., Fox, R. J., Rudick, R., Mirnics, K., & Trapp, B. D. (2006). Mitochondrial dysfunction as a cause of axonal degeneration in multiple sclerosis patients. *Annals of Neurology*, *59*(3), 478–489. <https://doi.org/10.1002/ana.20736>
- Dyrna, F., Hanske, S., Krueger, M., & Bechmann, I. (2013). The blood-brain barrier. *Journal of Neuroimmune Pharmacology*, *8*(4), 763–773. <https://doi.org/10.1007/S11481-013-9473-5/FIGURES/5>
- Edgar, J. M., McLaughlin, M., Yool, D., Zhang, S.-C., Fowler, J. H., Montague, P., Barrie, J. A., McCulloch, M. C., Duncan, I. D., Garbern, J., Nave, K. A., & Griffiths, I. R. (2004). Oligodendroglial modulation of fast axonal transport in a mouse model of hereditary spastic paraplegia. *The Journal of Cell Biology*, *166*(1), 121–131. <https://doi.org/10.1083/jcb.200312012>
- Engl, E., & Attwell, D. (2015). Non-signalling energy use in the brain. *The Journal of Physiology*, *593*(16), 3417–3429. <https://doi.org/10.1113/jphysiol.2014.282517>
- Essuman, K., Summers, D. W., Sasaki, Y., Mao, X., DiAntonio, A., & Milbrandt, J. (2017). The SARM1 Toll/Interleukin-1 Receptor Domain Possesses Intrinsic NAD + Cleavage Activity that Promotes Pathological Axonal Degeneration. *Neuron*, *93*(6), 1334-1343.e5. <https://doi.org/10.1016/j.neuron.2017.02.022>
- Farley, J. E., Burdett, T. C., Barria, R., Neukomm, L. J., Kenna, K. P., Landers, J. E., & Freeman, M. R. (2018). Transcription factor Pebbled/RREB1 regulates injury-

- induced axon degeneration. *Proceedings of the National Academy of Sciences*, 115(6), 1358–1363. <https://doi.org/10.1073/pnas.1715837115>
- Feng, X. H., & Derynck, R. (2005). SPECIFICITY AND VERSATILITY IN TGF- β SIGNALING THROUGH SMADS. <Http://Dx.Doi.Org.Liboff.Ohsu.Edu/10.1146/Annurev.Cellbio.21.022404.142018>, 21, 659–693. <https://doi.org/10.1146/ANNUREV.CELLBIO.21.022404.142018>
- Fernandes, K. A., Mitchell, K. L., Patel, A., Marola, O. J., Shrager, P., Zack, D. J., Libby, R. T., & Welsbie, D. S. (2018). Role of SARM1 and DR6 in retinal ganglion cell axonal and somal degeneration following axonal injury. *Experimental Eye Research*, 171, 54–61. <https://doi.org/10.1016/J.EXER.2018.03.007>
- Fernyhough, P., Chowdhury, S. K. R., & Schmidt, R. E. (2010). Mitochondrial stress and the pathogenesis of diabetic neuropathy. *Expert Review of Endocrinology & Metabolism*, 5(1), 39. <https://doi.org/10.1586/eem.09.55>
- Ferri, A., Sanes, J. R., Coleman, M. P., Cunningham, J. M., & Kato, A. C. (2003). Inhibiting Axon Degeneration and Synapse Loss Attenuates Apoptosis and Disease Progression in a Mouse Model of Motoneuron Disease. *Current Biology*, 13(8), 669–673. [https://doi.org/10.1016/S0960-9822\(03\)00206-9](https://doi.org/10.1016/S0960-9822(03)00206-9)
- Finn, J. T., Weil, M., Archer, F., Siman, R., Srinivasan, A., & Raff, M. C. (2000). Evidence That Wallerian Degeneration and Localized Axon Degeneration Induced by Local Neurotrophin Deprivation Do Not Involve Caspases. *Journal of*

Neuroscience, 20(4), 1333–1341. <https://doi.org/10.1523/JNEUROSCI.20-04-01333.2000>

Fischer, L. R., Culver, D. G., Davis, A. A., Tennant, P., Wang, M., Coleman, M., Asress, S., Adalbert, R., Alexander, G. M., & Glass, J. D. (2005). The WldS gene modestly prolongs survival in the SOD1G93A fALS mouse. *Neurobiology of Disease*, 19(1–2), 293–300. <https://doi.org/10.1016/J.NBD.2005.01.008>

Fiz, C., Apprato, G., Ricca, C., Aillon, A., Bergandi, L., & Silvagno, F. (2021). TGF Beta Induces Vitamin D Receptor and Modulates Mitochondrial Activity of Human Pancreatic Cancer Cells. *Cancers 2021, Vol. 13, Page 2932, 13(12)*, 2932. <https://doi.org/10.3390/CANCERS13122932>

Fünfschilling, U., Supplie, L. M., Mahad, D., Boretius, S., Saab, A. S., Edgar, J., Brinkmann, B. G., Kassmann, C. M., Tzvetanova, I. D., Möbius, W., Diaz, F., Meijer, D., Suter, U., Hamprecht, B., Sereda, M. W., Moraes, C. T., Frahm, J., Goebbels, S., & Nave, K. A. (2012). Glycolytic oligodendrocytes maintain myelin and long-term axonal integrity. *Nature*, 485(7399), 517–521. <https://doi.org/10.1038/nature11007>

Geisler, S., Doan, R. A., Strickland, A., Huang, X., Milbrandt, J., & DiAntonio, A. (2016). Prevention of vincristine-induced peripheral neuropathy by genetic deletion of SARM1 in mice. *Brain*, 139(12), 3092–3108. <https://doi.org/10.1093/BRAIN/AWW251>

- Gerdts, J., Brace, E. J., Sasaki, Y., DiAntonio, A., & Milbrandt, J. (2015). SARM1 activation triggers axon degeneration locally via NAD⁺ destruction. *Science*, *348*(6233), 453–457. <https://doi.org/10.1126/science.1258366>
- Ghosh, A. C., & O'Connor, M. B. (2014). Systemic Activin signaling independently regulates sugar homeostasis, cellular metabolism, and pH balance in *Drosophila melanogaster*. *Proceedings of the National Academy of Sciences*, *111*(15), 5729–5734. <https://doi.org/10.1073/PNAS.1319116111>
- Giangrande, A. (1994). Glia in the fly wing are clonally related to epithelial cells and use the nerve as a pathway for migration. *Development*, *120*(3), 523–534. <https://doi.org/10.1242/DEV.120.3.523>
- Glass, J. D., & Griffin, J. W. (1991). Neurofilament redistribution in transected nerves: Evidence for bidirectional transport of neurofilaments. *Journal of Neuroscience*, *11*(10), 3146–3154. <https://doi.org/10.1523/jneurosci.11-10-03146.1991>
- Gohl, D. M., Silies, M. A., Gao, X. J., Bhalerao, S., Luongo, F. J., Lin, C. C., Potter, C. J., & Clandinin, T. R. (2011). A versatile *in vivo* system for directed dissection of gene expression patterns. *Nature Methods*, *8*(3), 231–237. <https://doi.org/10.1038/nmeth.1561>
- Gonçalves, N. P., Jager, S. E., Richner, M., Murray, S. S., Mohseni, S., Jensen, T. S., & Vægter, C. B. (2020). Schwann cell p75 neurotrophin receptor modulates small fiber degeneration in diabetic neuropathy. *Glia*, *68*(12), 2725–2743. <https://doi.org/10.1002/GLIA.23881>

- Grafstein, B., & Forman, D. S. (1980). Intracellular transport in neurons. *Physiological Reviews*, *60*(4), 1167–1283. <https://doi.org/10.1152/physrev.1980.60.4.1167>
- Halestrap, A. P., & Wilson, M. C. (2012). The monocarboxylate transporter family—
Role and regulation. *IUBMB Life*, *64*(2), 109–119. <https://doi.org/10.1002/IUB.572>
- Harris, J. J., Jolivet, R., & Attwell, D. (2012). Synaptic Energy Use and Supply. *Neuron*, *75*(5), 762–777. <https://doi.org/10.1016/J.NEURON.2012.08.019>
- Hartenstein, V., & Posakony, J. W. (1989). Development of adult sensilla on the wing and notum of *Drosophila melanogaster*. *Development*, *107*(2), 389–405. <https://doi.org/10.1242/DEV.107.2.389>
- Harty, B. L., & Monk, K. R. (2017). Unwrapping the unappreciated: recent progress in Remak Schwann cell biology. *Current Opinion in Neurobiology*, *47*, 131–137. <https://doi.org/10.1016/J.CONB.2017.10.003>
- Hay, B. A., Wolff, T., & Rubin, G. M. (1994). Expression of baculovirus P35 prevents cell death in *Drosophila*. *Development*, *120*(8), 2121–2129. <https://doi.org/10.1242/dev.120.8.2121>
- Henninger, N., Bouley, J., Sikoglu, E. M., An, J., Moore, C. M., King, J. A., Bowser, R., Freeman, M. R., & Brown, R. H. (2016a). Attenuated traumatic axonal injury and improved functional outcome after traumatic brain injury in mice lacking Sarm1. *Brain*, *139*, 1094–1105. <https://doi.org/10.1093/brain/aww001>

- Henninger, N., Bouley, J., Sikoglu, E. M., An, J., Moore, C. M., King, J. A., Bowser, R., Freeman, M. R., & Brown, R. H. (2016b). Attenuated traumatic axonal injury and improved functional outcome after traumatic brain injury in mice lacking Sarm1. *Brain*, *139*(4), 1094–1105. <https://doi.org/10.1093/BRAIN/AWW001>
- Hollenbeck, P. J., & Saxton, W. M. (2005). The axonal transport of mitochondria. *Journal of Cell Science*, *118*(23), 5411–5419. <https://doi.org/10.1242/JCS.02745>
- Hoopfer, E. D., McLaughlin, T., Watts, R. J., Schuldiner, O., O’Leary, D. D. M., & Luo, L. (2006a). Wlds Protection Distinguishes Axon Degeneration following Injury from Naturally Occurring Developmental Pruning. *Neuron*, *50*(6), 883–895. <https://doi.org/10.1016/j.neuron.2006.05.013>
- Hoopfer, E. D., McLaughlin, T., Watts, R. J., Schuldiner, O., O’Leary, D. D. M., & Luo, L. (2006b). Wlds Protection Distinguishes Axon Degeneration following Injury from Naturally Occurring Developmental Pruning. *Neuron*, *50*(6), 883–895. <https://doi.org/10.1016/J.NEURON.2006.05.013>
- Hsu, J. M., Kang, Y., Corty, M. M., Mathieson, D., Peters, O. M., & Freeman, M. R. (2021). Injury-Induced Inhibition of Bystander Neurons Requires dSarm and Signaling from Glia. *Neuron*, *109*(3), 473-487.e5. <https://doi.org/10.1016/J.NEURON.2020.11.012/ATTACHMENT/B1F5EF60-364F-410B-AF1D-58F81D5D3421/MMC1.PDF>

- Jang, C. W., Chen, C. H., Chen, C. C., Chen, J. Y., Su, Y. H., & Chen, R. H. (2001). TGF- β induces apoptosis through Smad-mediated expression of DAP-kinase. *Nature Cell Biology* 2001 4:1, 4(1), 51–58. <https://doi.org/10.1038/ncb731>
- Jessen, K. R., & Mirsky, R. (2005). *THE ORIGIN AND DEVELOPMENT OF GLIAL CELLS IN PERIPHERAL NERVES*. 6(September), 671–682. <https://doi.org/10.1038/nrn1746>
- Kirk, P., Wilson, M. C., Heddle, C., Brown, M. H., Barclay, A. N., & Halestrap, A. P. (2000). CD147 is tightly associated with lactate transporters MCT1 and MCT4 and facilitates their cell surface expression. *The EMBO Journal*, 19(15), 3896–3904. <https://doi.org/10.1093/EMBOJ/19.15.3896>
- Koch, J. C., Bitow, F., Haack, J., d’Hedouville, Z., Zhang, J.-N., Tönges, L., Michel, U., Oliveira, L. M. A., Jovin, T. M., Liman, J., Tatenhorst, L., Bähr, M., & Lingor, P. (2015). Alpha-Synuclein affects neurite morphology, autophagy, vesicle transport and axonal degeneration in CNS neurons. *Cell Death & Disease*, 6(7), e1811–e1811. <https://doi.org/10.1038/cddis.2015.169>
- Kordower, J. H., Chu, Y., Hauser, R. A., Freeman, T. B., & Olanow, C. W. (2008). Lewy body-like pathology in long-term embryonic nigral transplants in Parkinson’s disease. *Nature Medicine* 2008 14:5, 14(5), 504–506. <https://doi.org/10.1038/nm1747>
- Kottmeier, R., Bittern, J., Schoofs, A., Scheiwe, F., Matzat, T., Pankratz, M., & Klämbt, C. (2020). Wrapping glia regulates neuronal signaling speed and precision in the

peripheral nervous system of *Drosophila*. *Nature Communications*, *11*(1), 1–17.
<https://doi.org/10.1038/s41467-020-18291-1>

Kuo, C. T., Zhu, S., Younger, S., Jan, L. Y., & Jan, Y. N. (2006). Identification of E2/E3 Ubiquitinating Enzymes and Caspase Activity Regulating *Drosophila* Sensory Neuron Dendrite Pruning. *Neuron*, *51*(3), 283–290.
<https://doi.org/10.1016/J.NEURON.2006.07.014/ATTACHMENT/02A85620-67D3-47DB-B7EB-53A6B5EACB32/MMC1.PDF>

Lee, P.-T., Zirin, J., Kanca, O., Lin, W.-W., Schulze, K. L., Li-Kroeger, D., Tao, R., Devereaux, C., Hu, Y., Chung, V., Fang, Y., He, Y., Pan, H., Ge, M., Zuo, Z., Housden, B. E., Mohr, S. E., Yamamoto, S., Levis, R. W., ... Bellen, H. J. (2018). A gene-specific T2A-GAL4 library for *drosophila*. *ELife*, *7*.
<https://doi.org/10.7554/eLife.35574>

Lee, Y., Morrison, B. M., Li, Y., Lengacher, S., Farah, M. H., Hoffman, P. N., Liu, Y., Tsingalia, A., Jin, L., Zhang, P. W., Pellerin, L., Magistretti, P. J., & Rothstein, J. D. (2012). Oligodendroglia metabolically support axons and contribute to neurodegeneration. *Nature*, *487*(7408), 443–448.
<https://doi.org/10.1038/nature11314>

Leiserson, W. M., Forbush, B., & Keshishian, H. (2011). *Drosophila* glia use a conserved cotransporter mechanism to regulate extracellular volume. *Glia*, *59*(2), 320–332.
<https://doi.org/10.1002/glia.21103>

- Levi-Montalcini, R., Caramia, F., & Angeletti, P. U. (1969). Alterations in the fine structure of nucleoli in sympathetic neurons following NGF-antiserum treatment. *Brain Research*, *12*(1), 54–73. [https://doi.org/10.1016/0006-8993\(69\)90055-9](https://doi.org/10.1016/0006-8993(69)90055-9)
- Levi-Montalcini, R., Caramia, F., Luse, S. A., & Angeletti, P. U. (1968). In vitro effects of the nerve growth factor on the fine structure of the sensory nerve cells. *Brain Research*, *8*(2), 347–362. [https://doi.org/10.1016/0006-8993\(68\)90054-1](https://doi.org/10.1016/0006-8993(68)90054-1)
- Li, J. Y., Englund, E., Holton, J. L., Soulet, D., Hagell, P., Lees, A. J., Lashley, T., Quinn, N. P., Rehncrona, S., Björklund, A., Widner, H., Revesz, T., Lindvall, O., & Brundin, P. (2008). Lewy bodies in grafted neurons in subjects with Parkinson's disease suggest host-to-graft disease propagation. *Nature Medicine* *2008* *14*:5, *14*(5), 501–503. <https://doi.org/10.1038/nm1746>
- Liddelow, S. A., Guttenplan, K. A., Clarke, L. E., Bennett, F. C., Bohlen, C. J., Schirmer, L., Bennett, M. L., Münch, A. E., Chung, W. S., Peterson, T. C., Wilton, D. K., Frouin, A., Napier, B. A., Panicker, N., Kumar, M., Buckwalter, M. S., Rowitch, D. H., Dawson, V. L., Dawson, T. M., ... Barres, B. A. (2017). Neurotoxic reactive astrocytes are induced by activated microglia. *Nature* *2017* *541*:7638, *541*(7638), 481–487. <https://doi.org/10.1038/nature21029>
- Lobas, M. A., Tao, R., Nagai, J., Kronschläger, M. T., Borden, P. M., Marvin, J. S., Looger, L. L., & Khakh, B. S. (2019). A genetically encoded single-wavelength sensor for imaging cytosolic and cell surface ATP. *Nature Communications* *2019* *10*:1, *10*(1), 1–13. <https://doi.org/10.1038/s41467-019-08441-5>

- Luan, H., Peabody, N. C., Vinson, C. R. R., & White, B. H. (2006). Refined Spatial Manipulation of Neuronal Function by Combinatorial Restriction of Transgene Expression. *Neuron*, 52(3), 425–436. <https://doi.org/10.1016/j.neuron.2006.08.028>
- Lunn, E., Perry, V., Brown, M., Rosen, H., & Gordon, S. (1989). Absence of Wallerian Degeneration Does not Hinder Regeneration in Peripheral Nerve. *European Journal of Neuroscience*, 1(1), 27–33.
- MacDonald, J. M., Beach, M. G., Porpiglia, E., Sheehan, A. E., Watts, R. J., & Freeman, M. R. (2006). The Drosophila Cell Corpse Engulfment Receptor Draper Mediates Glial Clearance of Severed Axons. *Neuron*, 50(6), 869–881. <https://doi.org/10.1016/j.neuron.2006.04.028>
- Marshall-Phelps, K. L. H., Kegel, L., Baraban, M., Ruhwedel, T., Almeida, R. G., Rubio-Brotons, M., Klingseisen, A., Benito-Kwiecinski, S. K., Early, J. J., Bin, J. M., Suminaite, D., Livesey, M. R., Möbius, W., Poole, R. J., & Lyons, D. A. (2020). Neuronal activity disrupts myelinated axon integrity in the absence of NKCC1b. *Journal of Cell Biology*, 219(7). <https://doi.org/10.1083/JCB.201909022>
- Martini, R. (2001). The effect of myelinating Schwann cells on axons. *Muscle & Nerve*, 24(4), 456–466. <https://doi.org/10.1002/MUS.1027>
- Massagué, J. (2008). TGF β in Cancer. *Cell*, 134(2), 215–230. <https://doi.org/10.1016/J.CELL.2008.07.001>
- Matzat, T., Sieglitz, F., Kottmeier, R., Babatz, F., Engelen, D., & Klambt, C. (2015). Axonal wrapping in the Drosophila PNS is controlled by glia-derived neuregulin

homolog Vein. *Development*, 142(7), 1336–1345.

<https://doi.org/10.1242/dev.116616>

Matzat, T., Sieglitz, F., Kottmeier, R., Babatz, F., Engelen, D., & Klämbt, C. (2015).

Axonal wrapping in the *Drosophila* PNS is controlled by glia-derived neuregulin homolog Vein. *Development (Cambridge)*, 142(7), 1336–1345.

<https://doi.org/10.1242/dev.116616>

Mishra, A., Reynolds, J. P., Chen, Y., Gourine, A. v., Rusakov, D. A., & Attwell, D.

(2016). Astrocytes mediate neurovascular signaling to capillary pericytes but not to arterioles. *Nature Neuroscience* 2016 19:12, 19(12), 1619–1627.

<https://doi.org/10.1038/nn.4428>

Mukherjee, C., Kling, T., Russo, B., Miebach, K., Kess, E., Schifferer, M., Pedro, L. D.,

Weikert, U., Fard, M. K., Kannaiyan, N., Rossner, M., Aicher, M. L., Goebbels, S., Nave, K. A., Krämer-Albers, E. M., Schneider, A., & Simons, M. (2020).

Oligodendrocytes Provide Antioxidant Defense Function for Neurons by Secreting Ferritin Heavy Chain. *Cell Metabolism*, 32(2), 259-272.e10.

<https://doi.org/10.1016/j.cmet.2020.05.019>

Mullins, M. C., Hammerschmidt, M., Kane, D. A., Odenthal, J., Brand, M., van Eeden, F.

J., Furutani-Seiki, M., Granato, M., Haffter, P., Heisenberg, C. P., Jiang, Y. J., Kelsh, R. N., & Nusslein-Volhard, C. (1996). Genes establishing dorsoventral pattern formation in the zebrafish embryo: the ventral specifying genes.

Development, 123(1), 81–93. <https://doi.org/10.1242/dev.123.1.81>

- Nam, H., Kundu, A., Karki, S., Brinkley, G. J., Chandrashekar, D. S., Kirkman, R. L., Liu, J., Liberti, M. v., Locasale, J. W., Mitchell, T., Varambally, S., & Sudarshan, S. (2021). The TGF- β /HDAC7 axis suppresses TCA cycle metabolism in renal cancer. *JCI Insight*, 6(22). <https://doi.org/10.1172/JCI.INSIGHT.148438>
- Nave, K. A. (2010). Myelination and the trophic support of long axons. *Nat Rev Neurosci*, 11, 275–283. <https://doi.org/10.1038/nrn2797>
- Neukomm, L. J., Burdett, T. C., Gonzalez, M. a, Züchner, S., & Freeman, M. R. (2014). Rapid in vivo forward genetic approach for identifying axon death genes in *Drosophila*. *Proceedings of the National Academy of Sciences of the United States of America*, 111(27), 9965–9970. <https://doi.org/10.1073/pnas.1406230111>
- Neukomm, L. J., Burdett, T. C., Seeds, A. M., Hampel, S., Coutinho-Budd, J. C., Farley, J. E., Wong, J., Karadeniz, Y. B., Osterloh, J. M., Sheehan, A. E., & Freeman, M. R. (2017). Axon Death Pathways Converge on Axundead to Promote Functional and Structural Axon Disassembly. *Neuron*, 95(1), 78-91.e5. <https://doi.org/10.1016/j.neuron.2017.06.031>
- Neul, J. L., & Ferguson, E. L. (1998). Spatially Restricted Activation of the SAX Receptor by SCW Modulates DPP/TKV Signaling in *Drosophila* Dorsal–Ventral Patterning. *Cell*, 95(4), 483–494. [https://doi.org/10.1016/S0092-8674\(00\)81616-5](https://doi.org/10.1016/S0092-8674(00)81616-5)
- Niemann, A., Berger, P., & Suter, U. (2006). Pathomechanisms of mutant proteins in charcot-marie-tooth disease. In *NeuroMolecular Medicine* (Vol. 8, Issues 1–2, pp. 217–241). Humana Press Inc. <https://doi.org/10.1385/NMM:8:1-2:217>

- Nikolaev, A., McLaughlin, T., O’Leary, D. D. M., & Tessier-Lavigne, M. (2009). APP binds DR6 to trigger axon pruning and neuron death via distinct caspases. *Nature* 2009 457:7232, 457(7232), 981–989. <https://doi.org/10.1038/nature07767>
- Niu, J., Tsai, H., Hoi, K. K., Huang, N., Yu, G., Kim, K., Baranzini, S. E., Xiao, L., Chan, J. R., & Fancy, S. P. J. (2019). Aberrant oligodendroglial–vascular interactions disrupt the blood–brain barrier, triggering CNS inflammation. *Nature Neuroscience*, 22(5), 709–718. <https://doi.org/10.1038/s41593-019-0369-4>
- Obermeier, B., Daneman, R., & Ransohoff, R. M. (2013). Development, maintenance and disruption of the blood-brain barrier. *Nature Medicine* 2013 19:12, 19(12), 1584–1596. <https://doi.org/10.1038/nm.3407>
- Ochoa, J., & Mair, W. G. P. (1969). The Normal Sural Nerve in Man * I. Ultrastructure and Numbers of Fibres and Cells. *Acta Neuropath. (Berl.)*, 13, 197–216.
- Osterloh, J. M., Yang, J., Rooney, T. M., Fox, A. N., Adalbert, R., Powell, E. H., Sheehan, A. E., Avery, M. A., Hackett, R., Logan, M. A., MacDonald, J. M., Ziegenfuss, J. S., Milde, S., Hou, Y.-J., Nathan, C., Ding, A., Brown, R. H., Conforti, L., Coleman, M., ... Freeman, M. R. (2012). dSarm/Sarm1 Is Required for Activation of an Injury-Induced Axon Death Pathway. *Science*, 337(6093), 481–484. <https://doi.org/10.1126/science.1223899>
- Palka, J., Schubiger, M., & Ellison, R. L. (1983). The polarity of axon growth in the wings of *Drosophila melanogaster*. *Developmental Biology*, 98(2), 481–492. [https://doi.org/10.1016/0012-1606\(83\)90377-9](https://doi.org/10.1016/0012-1606(83)90377-9)

Parkinson, D. B., Dong, Z., Bunting, H., Whitfield, J., Meier, C., Marie, H., Mirsky, R., & Jessen, K. R. (2001). Transforming Growth Factor β (TGF β) Mediates Schwann Cell Death *In Vitro* and *In Vivo* : Examination of c-Jun Activation, Interactions with Survival Signals, and the Relationship of TGF β -Mediated Death to Schwann Cell Differentiation. *The Journal of Neuroscience*, *21*(21), 8572–8585.
<https://doi.org/10.1523/JNEUROSCI.21-21-08572.2001>

Pellerin, L., & Magistretti, P. J. (1994). Glutamate uptake into astrocytes stimulates aerobic glycolysis: a mechanism coupling neuronal activity to glucose utilization. *Proceedings of the National Academy of Sciences*, *91*(22), 10625–10629.
<https://doi.org/10.1073/pnas.91.22.10625>

Peppiatt, C. M., Howarth, C., Mobbs, P., & Attwell, D. (2006). Bidirectional control of CNS capillary diameter by pericytes. *Nature* *2006 443:7112*, *443*(7112), 700–704.
<https://doi.org/10.1038/nature05193>

Pérez-Escuredo, J., van Hée, V. F., Sboarina, M., Falces, J., Payen, V. L., & Pellerin, L. (2016). Monocarboxylate transporters in the brain and in cancer. *Biochimica et Biophysica Acta (BBA) - Molecular Cell Research*, *1863*(10), 2481–2497.
<https://doi.org/10.1016/J.BBAMCR.2016.03.013>

Perlman, R., Schiemann, W. P., Brooks, M. W., Lodish, H. F., & Weinberg, R. A. (2001). TGF- β -induced apoptosis is mediated by the adapter protein Daxx that facilitates JNK activation. *Nature Cell Biology* *2001 3:8*, *3*(8), 708–714.
<https://doi.org/10.1038/35087019>

- Perrimon, N., Ni, J. Q., & Perkins, L. (2010). In vivo RNAi: today and tomorrow. In *Cold Spring Harbor perspectives in biology* (Vol. 2, Issue 8, p. a003640). Cold Spring Harbor Laboratory Press. <https://doi.org/10.1101/cshperspect.a003640>
- Peters, O. M., Lewis, E. A., Osterloh, J. M., Weiss, A., Salameh, J. S., Metterville, J., Brown, R. H., & Freeman, M. R. (2018). Loss of Sarm1 does not suppress motor neuron degeneration in the SOD1G93A mouse model of amyotrophic lateral sclerosis. *Human Molecular Genetics*, 27(21), 3761–3771. <https://doi.org/10.1093/HMG/DDY260>
- Petley-Ragan, L. M., Ardiel, E. L., Rankin, C. H., & Auld, V. J. (2016). Accumulation of Laminin Monomers in Drosophila Glia Leads to Glial Endoplasmic Reticulum Stress and Disrupted Larval Locomotion. *Journal of Neuroscience*, 36(4), 1151–1164. <https://doi.org/10.1523/JNEUROSCI.1797-15.2016>
- Potter, C. J., Tasic, B., Russler, E. v, Liang, L., & Luo, L. (2010). The Q System: A Repressible Binary System for Transgene Expression, Lineage Tracing, and Mosaic Analysis. *Cell*, 141(3), 536–548. <https://doi.org/10.1016/j.cell.2010.02.025>
- Prinz, M., Erny, D., & Hagemeyer, N. (2017). Ontogeny and homeostasis of CNS myeloid cells. *Nature Immunology* 2017 18:4, 18(4), 385–392. <https://doi.org/10.1038/ni.3703>
- Prior, R., van Helleputte, L., Benoy, V., & van den Bosch, L. (2017). Defective axonal transport: A common pathological mechanism in inherited and acquired peripheral

neuropathies. *Neurobiology of Disease*, 105, 300–320.

<https://doi.org/10.1016/J.NBD.2017.02.009>

Raad, H., Ferveur, J.-F., Ledger, N., Capovilla, M., & Robichon, A. (2016). Functional Gustatory Role of Chemoreceptors in Drosophila Wings. *Cell Reports*, 15(7), 1442–1454. <https://doi.org/10.1016/j.celrep.2016.04.040>

Raftery, L., Brummel, T., Haerry, T. E., O'Connor, M. B., Shimell, M. J., Wrana, J. L., Merriam, J., & Abdollah, S. (2008). The Drosophila Activin receptor Baboon signals through dSmad2 and controls cell proliferation but not patterning during larval development. *Genes & Development*, 13(1), 98–111. <https://doi.org/10.1101/gad.13.1.98>

Ramesh, S., Wildey, G. M., & Howe, P. H. (2009). Transforming growth factor β (TGF β)-induced apoptosis: The rise & fall of Bim. *Cell Cycle (Georgetown, Tex.)*, 8(1), 11. <https://doi.org/10.4161/CC.8.1.7291>

Riabinina, O., Luginbuhl, D., Marr, E., Liu, S., Wu, M. N., Luo, L., & Potter, C. J. (2015). Improved and expanded Q-system reagents for genetic manipulations. *Nature Methods*, 12(3), 219–222. <https://doi.org/10.1038/nmeth.3250>

Rocha, A. G., Franco, A., Krezel, A. M., Rumsey, J. M., Alberti, J. M., Knight, W. C., Biris, N., Zacharioudakis, E., Janetka, J. W., Baloh, R. H., Kitsis, R. N., Mochly-Rosen, D., Townsend, R. R., Gavathiotis, E., & Dorn, G. W. (2018). MFN2 agonists reverse mitochondrial defects in preclinical models of Charcot-Marie-Tooth disease

type 2A. *Science (New York, N.Y.)*, 360(6386), 336–341.

<https://doi.org/10.1126/science.aao1785>

Saab, A. S., Tzvetavona, I. D., Trevisiol, A., Baltan, S., Dibaj, P., Kusch, K., Möbius, W., Goetze, B., Jahn, H. M., Huang, W., Steffens, H., Schomburg, E. D., Pérez-Samartín, A., Pérez-Cerdá, F., Bakhtiari, D., Matute, C., Löwel, S., Griesinger, C., Hirrlinger, J., ... Nave, K.-A. (2016). Oligodendroglial NMDA Receptors Regulate Glucose Import and Axonal Energy Metabolism. *Neuron*, 91(1), 119–132.

<https://doi.org/10.1016/j.neuron.2016.05.016>

Sagot, Y., Dubois-Dauphin, M., Tan, S. A., de Bilbao, F., Aebischer, P., Martinou, J. C., & Kato, A. C. (1995). Bcl-2 overexpression prevents motoneuron cell body loss but not axonal degeneration in a mouse model of a neurodegenerative disease. *Journal of Neuroscience*, 15(11), 7727–7733. <https://doi.org/10.1523/JNEUROSCI.15-11-07727.1995>

Sambashivan, S., & Freeman, M. R. (2021). SARM1 signaling mechanisms in the injured nervous system. *Current Opinion in Neurobiology*, 69, 247–255.

<https://doi.org/10.1016/J.CONB.2021.05.004>

Samsam, M., Mi, W., Wessig, C., Zielasek, J., Toyka, K. v., Coleman, M. P., & Martini, R. (2003). The Wlds Mutation Delays Robust Loss of Motor and Sensory Axons in a Genetic Model for Myelin-Related Axonopathy. *Journal of Neuroscience*, 23(7), 2833–2839. <https://doi.org/10.1523/JNEUROSCI.23-07-02833.2003>

- Sánchez, I., Hassinger, L., Paskevich, P. A., Shine, H. D., & Nixon, R. A. (1996). Oligodendroglia Regulate the Regional Expansion of Axon Caliber and Local Accumulation of Neurofilaments during Development Independently of Myelin Formation. *Journal of Neuroscience*, *16*(16), 5095–5105. <https://doi.org/10.1523/JNEUROSCI.16-16-05095.1996>
- Sánchez-Capelo, A. (2005). Dual role for TGF- β 1 in apoptosis. *Cytokine & Growth Factor Reviews*, *16*(1), 15–34. <https://doi.org/10.1016/J.CYTOGFR.2004.11.002>
- Sasaki, Y., Vohra, B. P. S., Baloh, R. H., & Milbrandt, J. (2009). Transgenic Mice Expressing the Nmnat1 Protein Manifest Robust Delay in Axonal Degeneration In Vivo. *Journal of Neuroscience*, *29*(20), 6526–6534. <https://doi.org/10.1523/JNEUROSCI.1429-09.2009>
- Schmalbruch, H. (1986). Fiber Composition of the Rat Sciatic Nerve. *THE ANATOMICAL RECORD*, *215*, 71–81.
- Schuster, N., & Krieglstein, K. (2002a). Mechanisms of TGF- β -mediated apoptosis. *Cell and Tissue Research* *2001 307:1*, *307*(1), 1–14. <https://doi.org/10.1007/S00441-001-0479-6>
- Schuster, N., & Krieglstein, K. (2002b). Mechanisms of TGF- β -mediated apoptosis. *Cell and Tissue Research* *2001 307:1*, *307*(1), 1–14. <https://doi.org/10.1007/S00441-001-0479-6>

- Sepp, K. J., Schulte, J., & Auld, V. J. (2001). Peripheral glia direct axon guidance across the CNS/PNS transition zone. *Developmental Biology*, 238(1), 47–63.
<https://doi.org/10.1006/dbio.2001.0411>
- Simon, D. J., Weimer, R. M., McLaughlin, T., Kallop, D., Stanger, K., Yang, J., O’Leary, D. D. M., Hannoush, R. N., & Tessier-Lavigne, M. (2012). A Caspase Cascade Regulating Developmental Axon Degeneration. *Journal of Neuroscience*, 32(49), 17540–17553. <https://doi.org/10.1523/JNEUROSCI.3012-12.2012>
- Slattery, K., Woods, E., Zaiatz-Bittencourt, V., Marks, S., Chew, S., Conroy, M., Goggin, C., Maceochagain, C., Kennedy, J., Lucas, S., Finlay, D. K., & Gardiner, C. M. (2021). TGF β drives NK cell metabolic dysfunction in human metastatic breast cancer. *Journal for ImmunoTherapy of Cancer*, 9(2), e002044.
<https://doi.org/10.1136/JITC-2020-002044>
- Sorbara, C. D., Wagner, N. E., Ladwig, A., Nikić, I., Merkler, D., Kleele, T., Marinković, P., Naumann, R., Godinho, L., Bareyre, F. M., Bishop, D., Misgeld, T., & Kerschensteiner, M. (2014). Pervasive axonal transport deficits in multiple sclerosis models. *Neuron*, 84(6), 1183–1190. <https://doi.org/10.1016/j.neuron.2014.11.006>
- Stavoe, A. K. H., & Holzbaur, E. L. F. (2019). Axonal autophagy: Mini-review for autophagy in the CNS. *Neuroscience Letters*, 697, 17–23.
<https://doi.org/10.1016/J.NEULET.2018.03.025>

- Stork, T., Bernardos, R., & Freeman, M. R. (2012). Analysis of glial cell development and function in *Drosophila*. *Cold Spring Harbor Protocols*, 7(1), 1–17.
<https://doi.org/10.1101/pdb.top067587>
- Stork, T., Engelen, D., Krudewig, A., Silies, M., Bainton, R. J., & Klämbt, C. (2008). Organization and Function of the Blood Brain Barrier in *Drosophila*. *Journal of Neuroscience*, 28(3), 587–597. <https://doi.org/10.1523/JNEUROSCI.4367-07.2008>
- Stork, T., Engelen, D., Krudewig, A., Silies, M., Bainton, R. J., & Klämbt, C. (2008). Organization and function of the blood-brain barrier in *Drosophila*. *Journal of Neuroscience*, 28(3), 587–597. <https://doi.org/10.1523/JNEUROSCI.4367-07.2008>
- Toledo, J. B., Gopal, P., Raible, K., Irwin, D. J., Brettschneider, J., Sedor, S., Waits, K., Boluda, S., Grossman, M., van Deerlin, V. M., Lee, E. B., Arnold, S. E., Duda, J. E., Hurtig, H., Lee, V. M. Y., Adler, C. H., Beach, T. G., & Trojanowski, J. Q. (2016). Pathological α -synuclein distribution in subjects with coincident Alzheimer's and Lewy body pathology. *Acta Neuropathologica*, 131(3), 393–409.
<https://doi.org/10.1007/S00401-015-1526-9/FIGURES/6>
- Turkiew, E., Falconer, D., Reed, N., & Höke, A. (2017). Deletion of *Sarm1* gene is neuroprotective in two models of peripheral neuropathy. *Journal of the Peripheral Nervous System*, 22(3), 162–171. <https://doi.org/10.1111/JNS.12219>
- Upadhyay, A., Moss-Taylor, L., Kim, M.-J., Ghosh, A. C., & O'Connor, M. B. (2017). TGF- β Family Signaling in *Drosophila*. *Cold Spring Harbor Perspectives in Biology*, 9(9). <https://doi.org/10.1101/cshperspect.a022152>

- Vale, R. D. (2003). The molecular motor toolbox for intracellular transport. *Cell*, *112*(4), 467–480. [https://doi.org/10.1016/S0092-8674\(03\)00111-9](https://doi.org/10.1016/S0092-8674(03)00111-9)
- Verhamme, C., King, R. H. M., ten Asbroek, A. L. M. A., Muddle, J. R., Nourallah, M., Wolterman, R., Baas, F., & van Schaik, I. N. (2011). Myelin and Axon Pathology in a Long-Term Study of *PMP22* -Overexpressing Mice. *Journal of Neuropathology & Experimental Neurology*, *70*(5), 386–398. <https://doi.org/10.1097/NEN.0b013e318217eba0>
- Viader, A., Golden, J. P., Baloh, R. H., Schmidt, R. E., Hunter, D. A., & Milbrandt, J. (2011). Schwann Cell Mitochondrial Metabolism Supports Long-Term Axonal Survival and Peripheral Nerve Function. *Journal of Neuroscience*, *31*(28), 10128–10140. <https://doi.org/10.1523/JNEUROSCI.0884-11.2011>
- Viader, A., Sasaki, Y., Kim, S., Strickland, A., Workman, C. S., Yang, K., Gross, R. W., & Milbrandt, J. (2013). Aberrant schwann cell lipid metabolism linked to mitochondrial deficits leads to axon degeneration and neuropathy. *Neuron*, *77*(5), 886–898. <https://doi.org/10.1016/J.NEURON.2013.01.012/ATTACHMENT/9A52FEC0-3F39-4C1F-9250-DDAC41115BE7/MMC2.XLSX>
- Volkenhoff, A., Weiler, A., Letzel, M., Stehling, M., Klämbt, C., & Schirmeier, S. (2015). Glial glycolysis is essential for neuronal survival in drosophila. *Cell Metabolism*, *22*(3), 437–447. <https://doi.org/10.1016/j.cmet.2015.07.006>

- Waller, A. (1850). Experiments on the Section of the Glossopharyngeal and Hypoglossal Nerves of the Frog , and Observations of the Alterations Produced Thereby in the Structure of Their Primitive Fibres. *Philosophical Transactions of the Royal Society of London*, 140, 423–429.
- Waller, A. (1852). New Method for the Study of the Nervous System. *London Journal of Medicine*, 4(43), 609. <https://doi.org/10.1136/BMJ.S2-4.43.609>
- Wallin, M. T., Culpepper, W. J., Campbell, J. D., Nelson, L. M., Langer-Gould, A., Marrie, R. A., Cutter, G. R., Kaye, W. E., Wagner, L., Tremlett, H., Buka, S. L., Dilokthornsakul, P., Topol, B., Chen, L. H., & Larocca, N. G. (2019). The prevalence of MS in the United States. *Neurology*, 92(10), e1029–e1040. <https://doi.org/10.1212/WNL.0000000000007035>
- Wang, J., Zhai, Q., Chen, Y., Lin, E., Gu, W., McBurney, M. W., & He, Z. (2005). A local mechanism mediates NAD-dependent protection of axon degeneration. *Journal of Cell Biology*, 170(3), 349–355. <https://doi.org/10.1083/JCB.200504028>
- Wei, Z., Fei, Y., Su, W., & Chen, G. (2019). Emerging role of schwann cells in neuropathic pain: Receptors, glial mediators and myelination. *Frontiers in Cellular Neuroscience*, 13, 116. <https://doi.org/10.3389/FNCEL.2019.00116/BIBTEX>
- Weil, M.-T., Heibeck, S., Töpperwien, M., Tom Dieck, S., Ruhwedel, T., Salditt, T., Rodicio, M. C., Morgan, J. R., Nave, K.-A., Möbius, W., & Werner, H. B. (2018). Axonal Ensheathment in the Nervous System of Lamprey: Implications for the Evolution of Myelinating Glia. *The Journal of Neuroscience : The Official Journal*

of the Society for Neuroscience, 38(29), 6586–6596.

<https://doi.org/10.1523/JNEUROSCI.1034-18.2018>

Weiss, A., & Attisano, L. (2013). The TGFbeta superfamily signaling pathway. *Wiley Interdisciplinary Reviews: Developmental Biology*, 2(1), 47–63.

<https://doi.org/10.1002/wdev.86>

White, K., Grether, M. E., Abrams, J. M., Young, L., Farrell, K., & Steller, H. (1994). Genetic control of programmed cell death in *Drosophila*. *Science*, 264(5159), 677–683. <https://doi.org/10.1126/science.8171319>

Whitmore, A. v., Lindsten, T., Raff, M. C., & Thompson, C. B. (2003). The proapoptotic proteins Bax and Bak are not involved in Wallerian degeneration. *Cell Death & Differentiation* 2003 10:2, 10(2), 260–261. <https://doi.org/10.1038/sj.cdd.4401147>

Williams, D. W., Kondo, S., Krzyzanowska, A., Hiromi, Y., & Truman, J. W. (2006). Local caspase activity directs engulfment of dendrites during pruning. *Nature Neuroscience* 2006 9:10, 9(10), 1234–1236. <https://doi.org/10.1038/nn1774>

Windebank, A. J., Wood, P., Bunge, R. P., Dyck, P. J., E, Y., Kalachikov, S., Spahn, CM., Frank, J., Kandel, ER., Barad, M., & Martin, KC. (1985). Myelination determines the caliber of dorsal root ganglion neurons in culture. *The Journal of Neuroscience : The Official Journal of the Society for Neuroscience*, 5(6), 1563–1569. <https://doi.org/10.1523/jneurosci.2429-08.2008>

Xiong, X., Hao, Y., Sun, K., Li, J., Li, X., Mishra, B., Soppina, P., Wu, C., Hume, R. I., & Collins, C. A. (2012). The Highwire Ubiquitin Ligase Promotes Axonal

- Degeneration by Tuning Levels of Nmnat Protein. *PLoS Biology*, *10*(12), e1001440.
<https://doi.org/10.1371/journal.pbio.1001440>
- Yang, J., Wu, Z., Renier, N., Simon, D. J., Uryu, K., Park, D. S., Greer, P. A., Tournier, C., Davis, R. J., & Tessier-Lavigne, M. (2015). Pathological Axonal Death through a MAPK Cascade that Triggers a Local Energy Deficit. *Cell*, *160*(1–2), 161–176.
<https://doi.org/10.1016/j.cell.2014.11.053>
- Yin, X., Crawford, T. O., Griffin, J. W., Tu, P. H., Lee, V. M. Y., Li, C., Roder, J., & Trapp, B. D. (1998). Myelin-Associated Glycoprotein Is a Myelin Signal that Modulates the Caliber of Myelinated Axons. *Journal of Neuroscience*, *18*(6), 1953–1962. <https://doi.org/10.1523/JNEUROSCI.18-06-01953.1998>
- Yoo, J., Ghiassi, M., Jirmanova, L., Balliet, A. G., Hoffman, B., Fornace, A. J., Liebermann, D. A., Böttinger, E. P., & Roberts, A. B. (2003). Transforming Growth Factor- β -induced Apoptosis Is Mediated by Smad-dependent Expression of GADD45b through p38 Activation *. *Journal of Biological Chemistry*, *278*(44), 43001–43007. <https://doi.org/10.1074/JBC.M307869200>
- Young, J. W., & Crish, S. D. (2014). *Anterograde transport blockade precedes deficits in retrograde transport in the visual projection of the DBA / 2J mouse model of glaucoma*. *8*(September), 1–12. <https://doi.org/10.3389/fnins.2014.00290>
- Yu, J., Zhang, L., Chen, A., Xiang, G., Wang, Y., Wu, J., Mitchelson, K., Cheng, J., & Zhou, Y. (2008). Identification of the gene transcription and apoptosis mediated by

TGF- β -Smad2/3-Smad4 signaling. *Journal of Cellular Physiology*, 215(2), 422–433.
<https://doi.org/10.1002/JCP.21325>

Yu, W. M., Yu, H., Chen, Z. L., & Strickland, S. (2009). Disruption of laminin in the peripheral nervous system impedes nonmyelinating Schwann cell development and impairs nociceptive sensory function. *Glia*, 57(8), 850–859.
<https://doi.org/10.1002/GLIA.20811>

Zhou, L., Song, Z., Tittel, J., & Steller, H. (1999). HAC-1, a *Drosophila* homolog of APAF-1 and CED-4, functions in developmental and radiation-induced apoptosis. *Molecular Cell*, 4(5), 745–755. [https://doi.org/10.1016/S1097-2765\(00\)80385-8](https://doi.org/10.1016/S1097-2765(00)80385-8)